Design and Evaluation of Bispidine-Based SARS-CoV-2 Main Protease Inhibitors

Dmitriy Shcherbakov,[1,2‡] Dmitriy Baev,[3‡] Mikhail Kalinin,[4,5] Alexander Dalinger,[5] Varvara Chirkova,[2] Svetlana Belenkaya,[1,6] Aleksei Khvostov,[5] Dmitry Krut'ko,[5] Aleksei Medved'ko,[4] Ekaterina Volosnikova,[1] Elena Sharlaeva,[2] Daniil Shanshin,[1] Tatyana Tolstikova,[3] Olga Yarovaya,[3*] Rinat Maksyutov,[1] Nariman Salakhutdinov,[3] Sergey Vatsadze[4]

[1]*State Research Center of Virology and Biotechnology VECTOR, Rospotrebnadzor, 630559, Russia, Koltsovo, Novosibirsk Region, Russian Federation*
[2]*Altay State University 656049, Barnaul, Leninski pr., 61 Russian Federation*
[3]*N.N. Vorozhtsov Novosibirsk Institute of Organic chemistry SB RAS, Lavrent'ev av., 630090, Russia, Novosibirsk, Russian Federation*
[4]*N.D. Zelinsky Institute of Organic Chemistry, Russian Academy of Sciences, Leninski pr., 47, 119991 Moscow, Russian Federation*
[5]*Department of Chemistry, M.V. Lomonosov Moscow State University, Leninskie Gory, 1-3, 119991 Moscow, Russian Federation*
[6]*Novosibirsk State University, Novosibirsk Pirogova 1, 630090 Russian Federation*

* Olga Yarovaya E-mail: ooo@nioch.nsc.ru

Contents.

1. Protein extraction and purification

The sequence encoding the major protease SARS-CoV-2 (Mpro or 3CL) of the Wuhan-Hu-1 isolate (GenBank:MN908947) was synthesized on demand (DnA-synthesis LLC, Russia). Prior to ordering, codon sequence optimization was performed using the GeneOptimizer tool (https://www.thermofisher.com/ru/en/home/life-science/cloning/gene-synthesis/geneart-gene-synthesis/geneoptimizer.html) for expression in *E. coli* cells. To ensure the transport of 3CL into the periplasmic space, the GST (glutathione-S-transferase) and 3CL genes were cloned into a single reading frame. For this purpose, the oligonucleotide primers GST-F 5'-aaaaaacatgtccccttactaggtttt-3' and GST3CL-R 5'-aaaaaaggatccttttttggaggatgtcgccac- 3' (GST amplification) and 3CLGST-F 5'-aaaaaaggatccatctcctaggctgttgttttgttgttgttcagcaggttttcgtaaaatggcat-3' and 3CL-R 5'-aaaaaagcgggccgcttaaccgccccctgaccctgctg-3' (3CL amplification). To ensure that the active form of the protease was obtained, homologous proteolysis sites SAVLQSGFR at the N-terminal and TFQSG at the C-terminal were incorporated into the 3CL flanking sequences. After amplification, the two PCR products were simultaneously cloned as part of the pET21 vector. E. coli BL21(DE3) cells were transfected with the resulting plasmid pET21-GST-3CL. Individual E. coli colonies containing recombinant plasmids were cultured overnight on an orbital shaker (Biosan, Latvia) in LB medium (AppliChem, USA) containing 100 μg/ml ampicillin at 37 °C and 180 rpm. The inoculum in a 1/100 ratio was transferred to an Erlenmeyer flask containing LB medium and grown to an absorbance of 0.8 (at λ = 600 nm). The inducer isopropyl-β-D-1-thiogalactopyranoside (IPTG) (Anatrace Products, USA) was added to a final concentration of 1 mM. The culture was additionally cultured on a shaker for 5 h at 37 °C and 180 rpm. The biomass was precipitated by centrifugation (Beckman Coulter, USA) for 20 min at 5000 g and 4 °C. The resulting precipitate was dissolved in buffer: 12mM Tris; 120mM NaCl; 0.1 mM EDTA; 1 mM DTT. The cells were disrupted using a Soniprep 150 Plus ultrasonic homogenizer (MSE, PRC). Purification was performed by sequential chromatography with intermediate dialysis in 20mM Tris-HCl, pH 7.6 on columns with cation-exchange sorbents (SP-Sepharose and Nuvia HR-S) equilibrated with 20mM Tris-HCl, pH 7.6. The target fraction was eluted in a linear gradient of NaCl concentration from 0 to 1 M in 20mM Tris-HCl , pH 7.6 and analyzed by electrophoresis under denaturing conditions in 15% PAH. The final product was dialyzed against 20 mM Tris-HCl, pH 7.6 and subjected to sterilizing filtration through 0.22 μM pore size filters.

2. Activity Measurement

3CL activity was measured using the fluorogenic substrate Dabcyl-VNSTLQSGLRK(FAM)MA (purity over 95%, CPC Scientific Inc., China). Fluorescence intensity was monitored using a CLARIOstar Plus instrument (BMG Labtech, Germany), using wavelengths of - 495 and - 520 nm for excitation and emission, respectively. Reaction mixtures were prepared in a 384-well plate, then incubated at room temperature for 5 min. All measurements were performed at 25°C. Each well contained one reaction mixture. The instrument was calibrated using the peptide solution that underwent complete hydrolysis. The fluorescence value of this mixture was taken as 80%. The reaction mixtures contained 5 µl Tris-HCl buffer (pH 8.0; 50mM Tris; 50mM NaCl), 2 µl substrate (C=33 µg/ml) and inhibitor at different concentration (0.000058594-0.03 mg/ml). The reaction was triggered by adding 3 µL of 3CL (C=0.025 mg/ml). The measurement was performed in kinetic scan mode. Cycle length and number of cyc les were determined individually depending on the number of scanned wells. All experiments were repeated three times (n = 3). The accompanying software MARS Data Analysis (BMG LABTECH, Germany) was used for the calculations. The IC50 value is the concentration of the test substance that reduces the fluorescence level by 50% of the maximum level observed without adding the inhibitor. As a comparison substances used disulfiram and Ebselen, for which earlier[1] was experimentally demonstrated IC50 = 9.35 and 0.67 µM activity for inhibition of SARS-CoV-2 main protease, respectively.

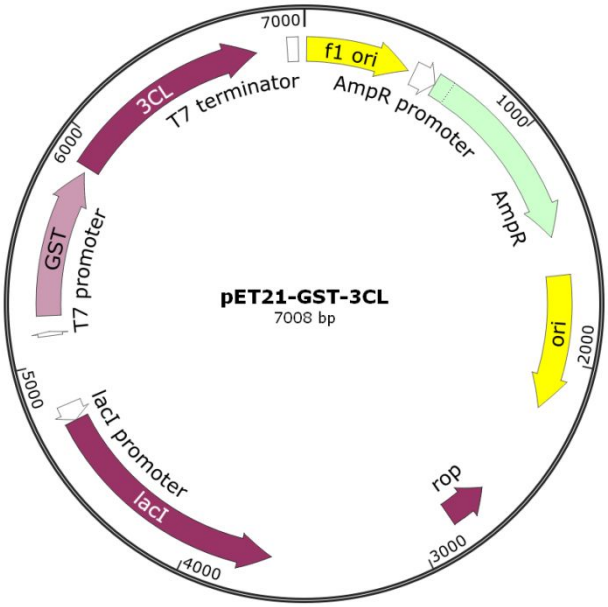

Figure S1. Genetic map of the pET21-GST-3CL plasmid vector.

3. Design strategy for new SARS-CoV-2 main protease inhibitors

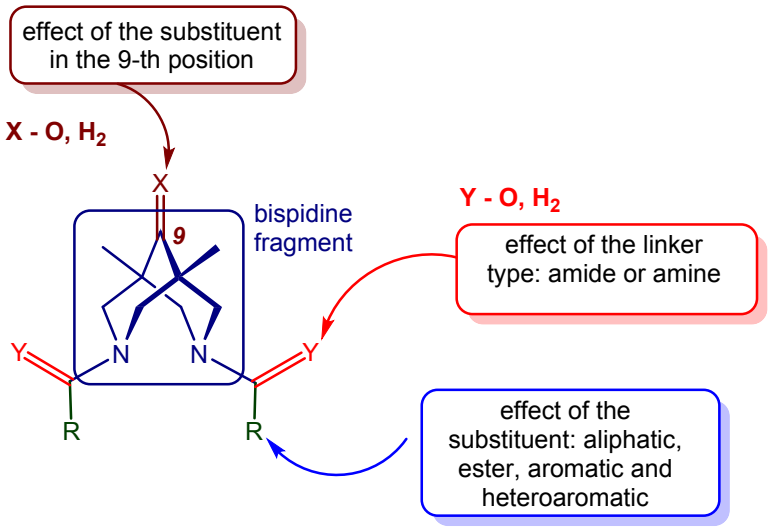

Figure S2. Design strategy for new Bispidine-based SARS-CoV-2 main protease inhibitors

4. Molecular modeling of possible inhibition of SARS-CoV-2 main protease by new bispidine derivatives

4.1. Methods

Molecular modeling was carried out in the Schrodinger Maestro visualization environment using applications from the Schrodinger Small Molecule Drug Discovery Suite 2016-1[2]. The 3D structures of the derivatives were obtained empirically in the LigPrep application using the OPLS3[3] force field. All possible tautomeric forms of the compounds were taken into account, as well as various states of polar protons of molecules in the pH range 7.0 ± 2.0. XRD models of the main protease SARS-CoV-2 co-crystallized with covalent (PDB IDs 6LZE, 6M0K, 6WNP, 6WTK, 6XHM, 6XMK, 6XQS, 6XQT, 6XQU, 6Y2G, 7B3E, 7BE7, 7BQY, 7BUY, 7D3I, 7JPZ) and non-covalent (PDB IDs 6YVF, 7JU7, 7KXS, 7LTJ, 7L14, 7L0D) inhibitors were used for calculations. Pharmacophore models were built and new derivatives screened using the Phase[4] application. To simulate a possible mechanism of non-covalent inhibition of the main protease, molecular docking of compounds was performed into the binding site of the ML188 inhibitor (PDB ID 7L0D[5]) in the Glide[6] application. The search area for docking was selected according to the size of ML188. The XP (extra precision) algorithm was used. Docking was carried out in comparison with the value of the scoring function for ML188 in XRD coordinates (score in place mode). Non-covalent interactions of compounds at the binding site were visualized using Biovia Discovery Studio Visualizer[7]

and Schrodinger Maestro. The covalent binding of the new compounds to the Cys145 amino acid residue was studied using the CovDock[8] application. The search area for docking was selected according to the size of GC373 inhibitor (PDB ID 6WTK[9]). Nucleophilic addition of new compounds to carbonyl groups was considered. The conformations of new compounds that are most favorable for the formation of covalent bond with Cys145 were evaluated. The free energy of the resulting covalent complexes was calculated using the MM/GBSA[10] method.

4.2. Results

Modeling of non-covalent interactions of new bispidine derivatives in the active site of the main protease SARS-CoV-2.

Initially, we created the pharmacophore model of potential inhibitors of the SARS-CoV-2 main protease based on the analysis of Protein Data Bank. XRD models of the main protease SARS-CoV-2 co-crystallized with covalent (PDB IDs 6LZE[11] (T5UX5SKK2S), 6M0K[11] (BDBM420297), 6WNP[12] (boceprevir), 6WTK[9] (GC373), 6XHM[13] (GTPL11250), 6XMK[14] (7j), 6XQS[15] (telaprevir), 6XQT[15] (narlaprevir), 6Y2G[16] (GTPL10720), 7B3E[17] (myricetin), 7BE7[18] (MG-132), 7BQY[19] (N3), 7D3I[20] (MI-23), 7JPZ[21] (MPI1)) and non-covalent (PDB IDs 6YVF[22] (AZD6482), 7JU7[23] (masitinib), 7LTJ[24] (MCULE-5948770040), 7L14[25] (XFD), 7L0D[5] (ML188)) inhibitors were used for calculations (Fig. S3).

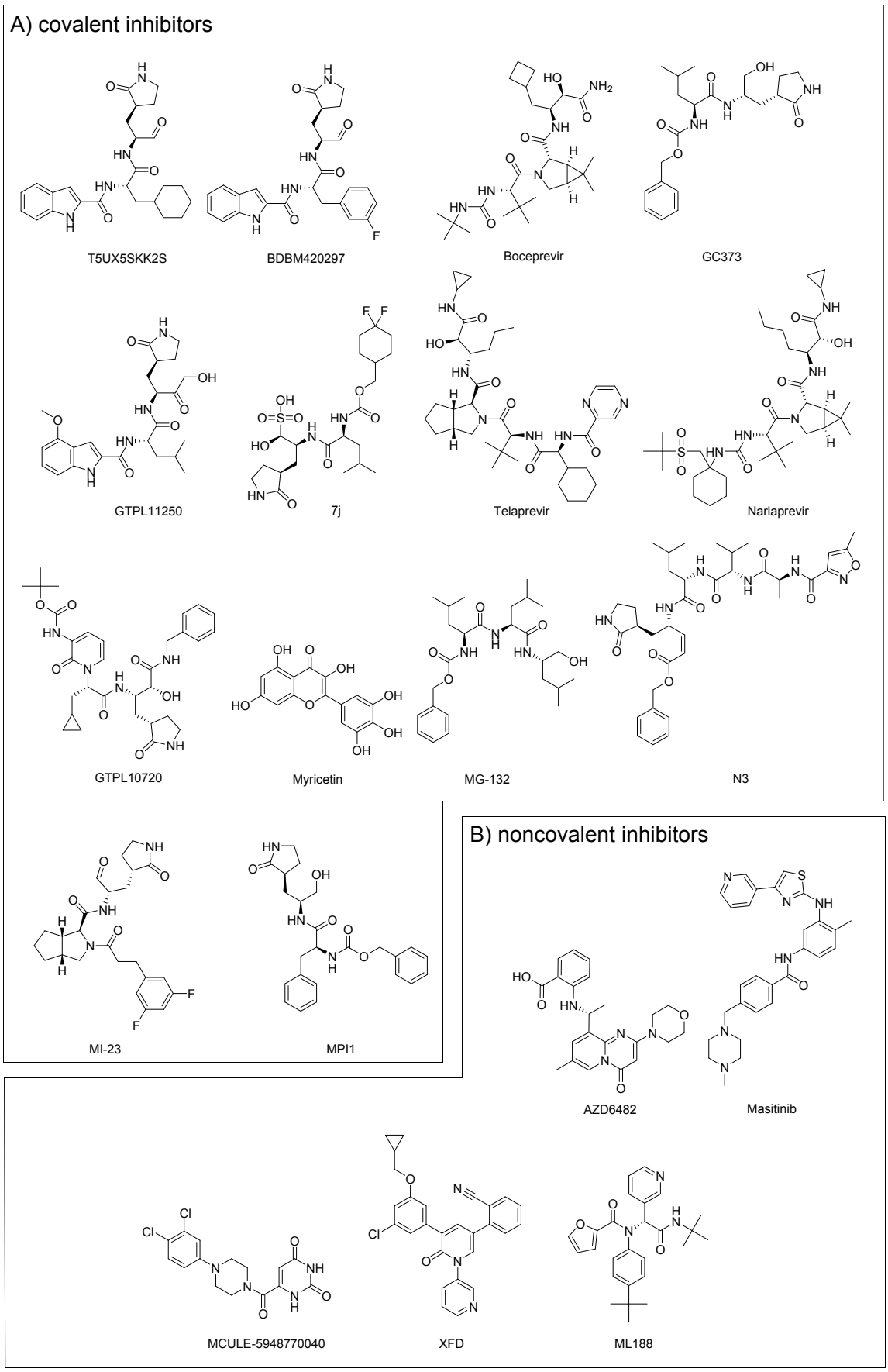

Figure S3. Structures of 3CLpro inhibitors: A) covalent, B) noncovalent.

Analysis of ligands from PDB capable to binding non-covalently shows a wide variety of their chemical structure. In this regard, the pharmacophore hypothesis of non-covalent interaction is represented by only three centers: two acceptors of electron density and one aromatic system (Figure S4).

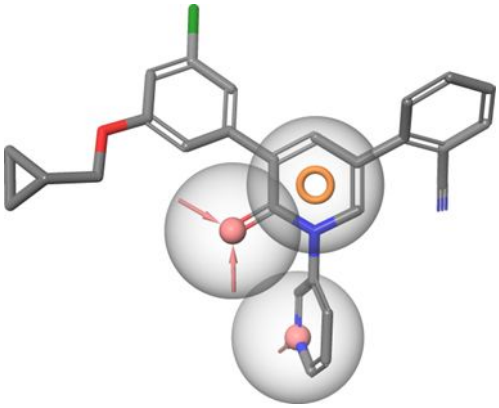

Figure S4. Pharmacophore hypothesis of non-covalent interaction on the example of the inhibitor 2-{3-[3-chloro-5-(cyclopropylmethoxy)phenyl]-2-oxo[2H-[1,3'-bipyridine]]-5-yl}benzonitrile (PDB ID 7L14[25]). Acceptors are shown with red spheres with arrows, and the aromatic system is shown with an orange ring. The gray spheres are the tolerance radii of the hypothesis (2 angstroms).

The assessment of the compliance of new bispidine derivatives with the pharmacophore hypothesis was carried out according to the Phase screen score integral indicator, which includes the sum of estimates of the vector score (from -1 to 1), alignment score (from 0 to 1) and volume score (from 0 to 1). Thus, the Phase screen score ranges from -1 to 3. The reference ligand has a Phase screen score of 3. In the screening process, the rotating bonds of new derivatives were taken into account in order to more closely match the pharmacophore hypothesis. For the new bispidine derivatives, the Phase screen scores indicated in Table S1 were obtained. Compounds absent in the table do not contain scaffolds in their structure that correspond to the pharmacophore hypothesis.

Table S1. Phase screen scores obtained as a result of screening for compliance with the pharmacophore hypothesis of non-covalent interaction of ligands with the active site of the main protease of SARS-CoV-2.

Ligand	Phase screen score
4s	1.832803

2d	1.692387
4t	1.680320
2f	1.504729
2h	1.488712
4p	1.475913
2j	1.461682
4q	1.437867
2i	1.389356
2g	1.387006
4o	1.128681
4r	1.082313
2e	0.886344
3e	0.829824

A superposition of the pharmacophore hypothesis of non-covalent interaction and several new bispidine derivatives is shown in Figure S5.

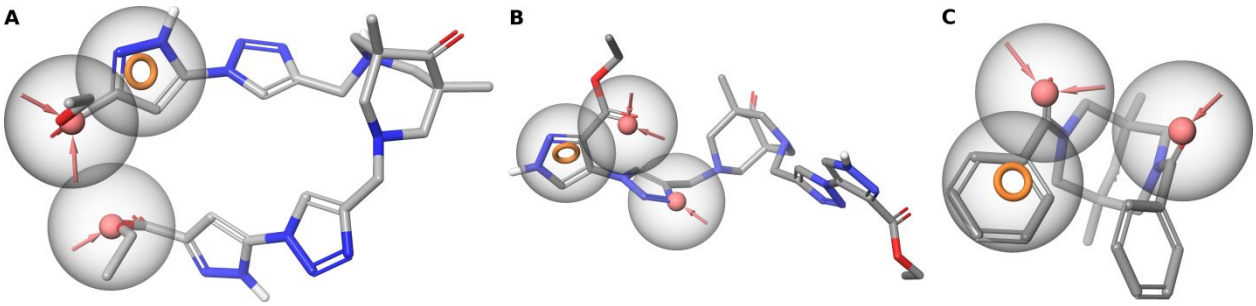

Figure S5. Superposition of the pharmacophore hypothesis of non-covalent interaction and compounds **4t** (A), **4s** (C), **2d** (C). Acceptors are shown with red spheres with arrows, and the aromatic system is shown with an orange ring. The gray spheres are the tolerance radii of the hypothesis (2 angstroms).

Thus, given the significant flexibility of side substituents of new bispidine derivatives carrying a scaffold that satisfies the structure and properties of the pharmacophore of non-covalent interaction with the main protease, it seems possible for these compounds to bind to the active site of the main protease. This hypothesis has been tested using molecular modeling. Molecular docking of new bispidine derivatives into the binding site of the non-

covalent inhibitor of the main protease SARS-CoV-2 (XRD model 7L0D) was performed. The molecular docking results are shown in Table S2.

Table S2. Molecular docking results compared to co-crystallize inhibitor ML188 (XRD model 7L0D).

Ligand	Docking score, kcal/mol
2h	-7.295
2e	-7.093
ML188 (score in place)	-6.810
4s	-6.540
2f	-6.221
2g	-5.528
2d	-5.501
3e	-5.363
4q	-5.303
3a	-5.122
2a	-4.773
4t	-4.713
4r	-4.694
2i	-4.673
4o	-4.650
4l	-4.641
4p	-4.437
3k	-4.375
2b	-4.140
4c	-4.131
4m	-4.125
4d	-4.074
2j	-3.984
2c	-3.926
1	-3.490
4n	-1.940

Comparison of the relative position of the pharmacophore and the conformations of the compounds obtained as a result of docking does not show the coincidence of the pharmacophore centers of non-covalent inhibitors with acceptor groups and aromatic systems of new compounds (Figure S6). This may be due to both the low probability of a non-covalent inhibition mechanism and the high variability of the chemical structures of possible inhibitors.

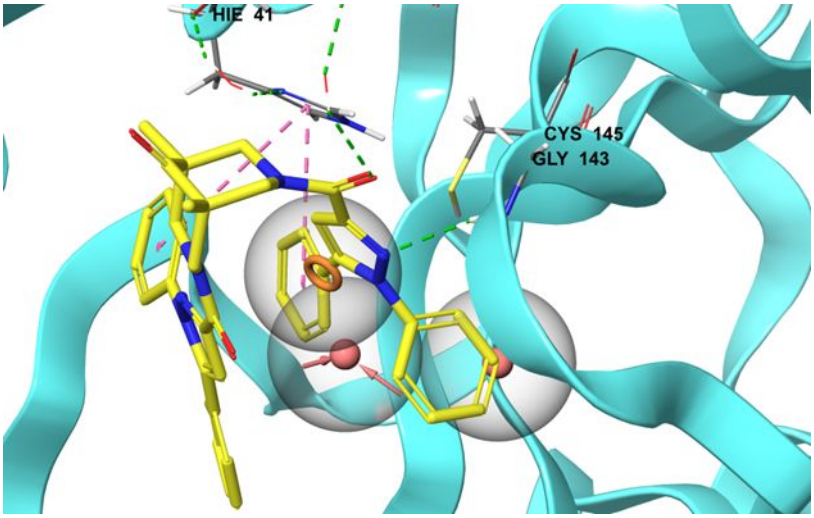

Figure S6. Superposition of the pharmacophore hypothesis of non-covalent binding and conformation of compound **2h**, obtained as a result of non-covalent docking into the active site of the SARS-CoV-2 main protease.

Molecular modeling of covalent binding by new derivatives of the catalytic amino acid residue Cys145 in the active site of the SARS-CoV-2 main protease.

An analysis of the chemical structure of the covalent inhibitors of the main protease published in the literature[9,13–16,20,21,26–28] shows its high conservativity. All inhibitors have in their structure a typical scaffold in which there is an activated carbonyl group subjected to nucleophilic attack by the SH-group of the catalytic amino acid residue Cys145. During bond formation, oxygen of the carbonyl group is converted into a hydroxyl group which forms an additional hydrogen bond with Cys145. The resulting pharmacophore consists of six pharmacophore centers: three electron density acceptors (A1, A2, A3), one donor (D1 (D1)), and two hydrophobic centers (H1, H2) (Figure S7). The carbonyl group undergoing a nucleophilic attack is the pharmacophore center of A1. We assume that the main scaffold required for the interaction of the covalent inhibitor with Cys145 is a chain of electron density acceptors, among which A1 is the attachment center, and the others provide

positioning of the molecule in the binding site by formation of hydrogen bonds. Two hydrophobic centers and an electron density donor provide additional stabilization.

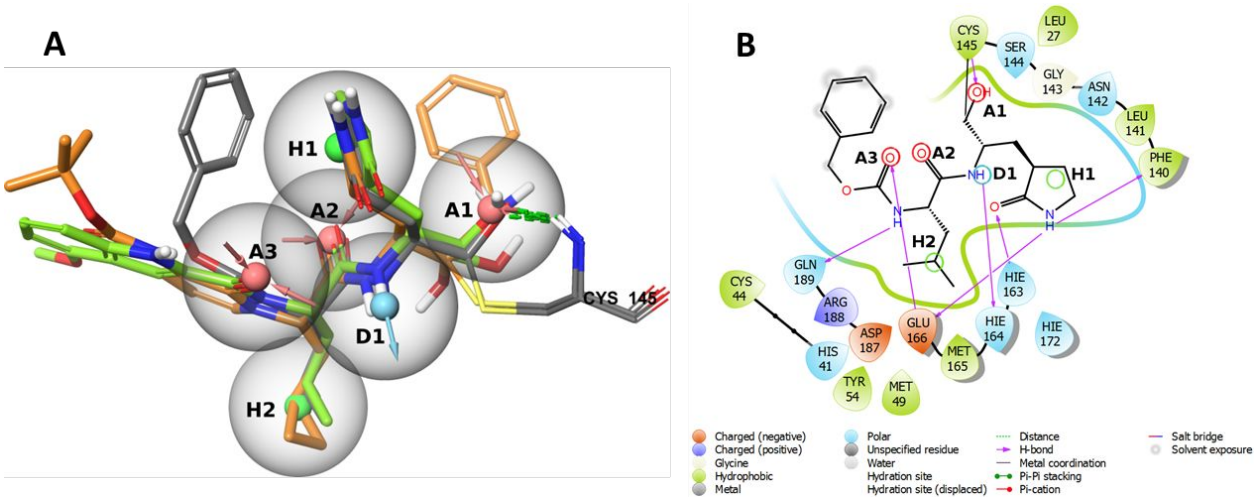

Figure S7. Pharmacophore hypothesis of covalent interaction with Cys145. A is an example of inhibitors: GC373[9] (6WTK) - gray structure, GTPL11250[13] (6XHM) - green structure and GTPL10720[16] (6Y2G) - orange structure. Acceptors are shown by red arrowed spheres, donors by blue arrowed spheres, and hydrophobic centers by green spheres. Gray spheres are tolerance radii of the hypothesis (2 angstroms). B - two-dimensional hypothesis using GC373[9] (6WTK) as an example.

Table S3. Comparison of results of covalent docking, MM/GBSA calculations, FRET assay, conformation analysis and binding sites of new bispidine derivatives.

Ligand	Cdock affinity, kcal/mol	$dG_{complex}$, kcal/mol	$dG_{covalent\ bond}$, kcal/mol	IC_{50}, μM	Conformation*	Binding site**
4q	-6.31	-41.18	5.03	0.83	free	frame
4o	-6.05	-41.75	9.37	5.2	free	side
4s	-6.01	-23.50	2.40	16.3	free	frame
2j	-5.93	-46.68	-0.99	0.75	*anti*	frame
2h	-5.63	-46.53	13.12	1.4	*anti*	side
2b	-5.61	-26.62	3.19	18.5	*syn*	frame
2d	-5.56	-28.85	7.78	3.3	*anti*	frame
2i	-5.43	-5.48	37.11	13.0	*anti*	side

4t	-5.42	-34.47	-0.86	13.6	free	frame
3e	-5.39	-18.62	10.68	46.6	*anti*	side
2g	-5.35	-24.93	18.88	4.99	*anti*	side
4m	-5.09	-13.78	3.80	7.1	free	side
2f	-5.16	-43.99	6.84	1.45	*anti*	frame
2c	-5.11	-25.31	6.34	5.5	*anti*	frame
2e	-4.91	-25.33	1.01	4.8	*anti*	frame
3a	-4.76	-31.26	5.46	17.9	*syn*	side
3k	-4.71	-25.72	2.23	99.6	*anti*	side
4l	-4.68	-28.62	1.49	5.5	free	frame
4o	-4.67	-25.07	6.38	5.2	free	frame
2a	-4.61	-0.36	18.97	5.9	*anti*	side
1	-4.38	-11.68	5.26	2.6	free	frame
4r	-3.89	-29.25	2.66	2.2	free	frame
4c	-3.66	-23.68	3.49	8.8	free	frame
4d	-3.64	-7.89	7.86	0.9	free	frame
4n	-3.05	-17.32	7.08	33.7	free	frame

* “free” means no conformational restrictions (no amide bonds);
“*anti*”:

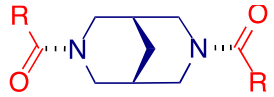

“*syn*”:

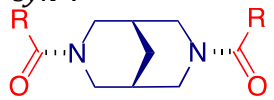

** site of covalent attachment: “frame” - at the carbonyl group of the bispidine backbone, “side” - at the carbonyl group of the side substituent.

In Figs. S8 and S9 are shown, respectively, the 3D and 2D views of superpositions of the pharmacophore hypothesis of covalent binding and conformations of new bispidine derivatives (**2j**, **2i**, **2e**, **3e**, **4r**, **4d**, **3l**, **4o**) obtained as a result of covalent docking.

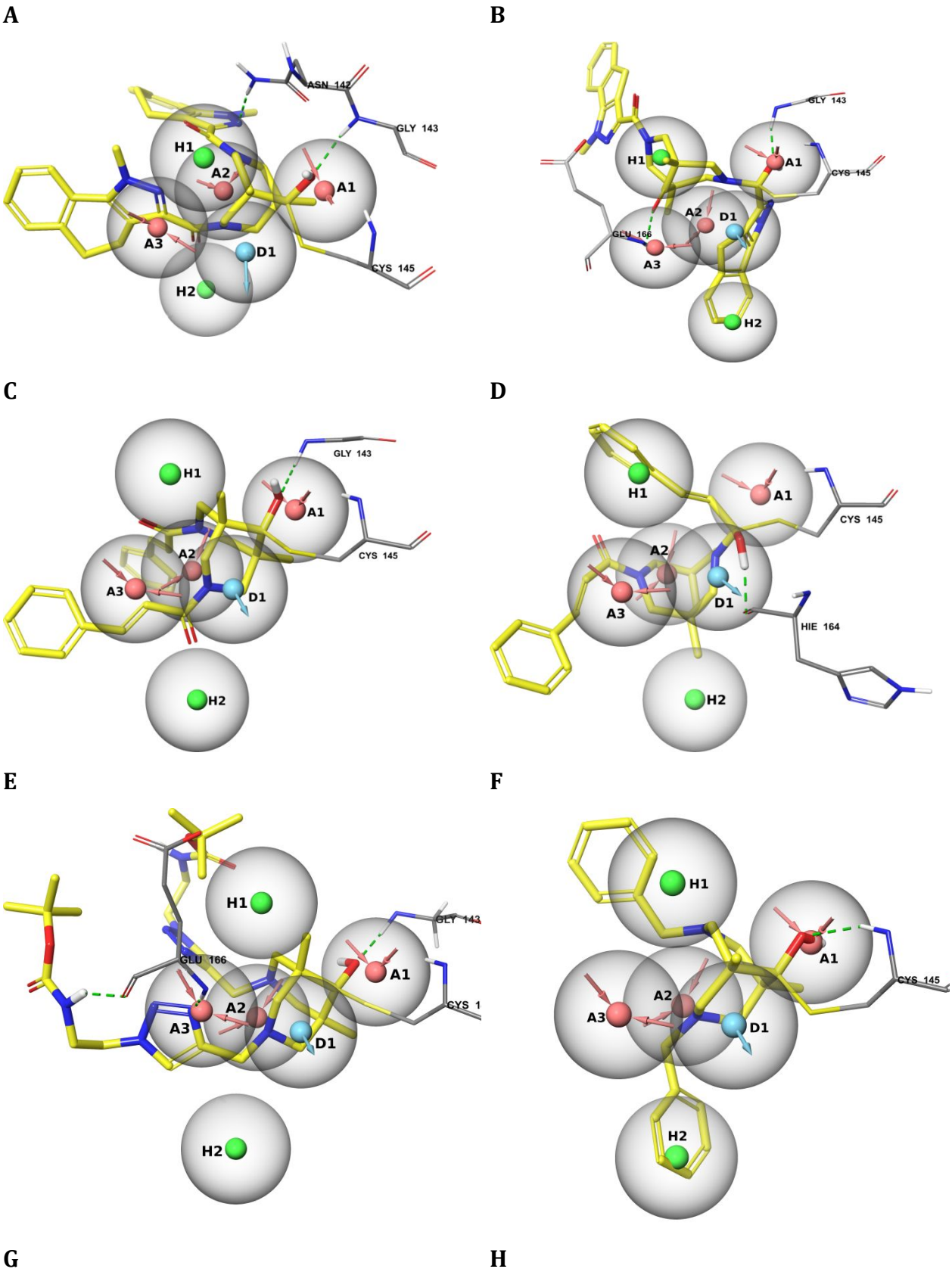
A
ASN 142
GLY 143
H1
A2
A1
A3
D1
CYS 145
H2
B
GLY 143
H1
A1
CYS 145
A2
D1
GLU 166
A3
H2
C
H1
GLY 143
A1
A2
CYS 145
A3
D1
H2
D
H1
A1
CYS 145
A2
A3
D1
HIE 164
H2
E
H1
GLY 143
GLU 166
A1
A2
A3
D1
CYS 1
H2
F
H1
A1
CYS 145
A2
A3
D1
H2
G
H

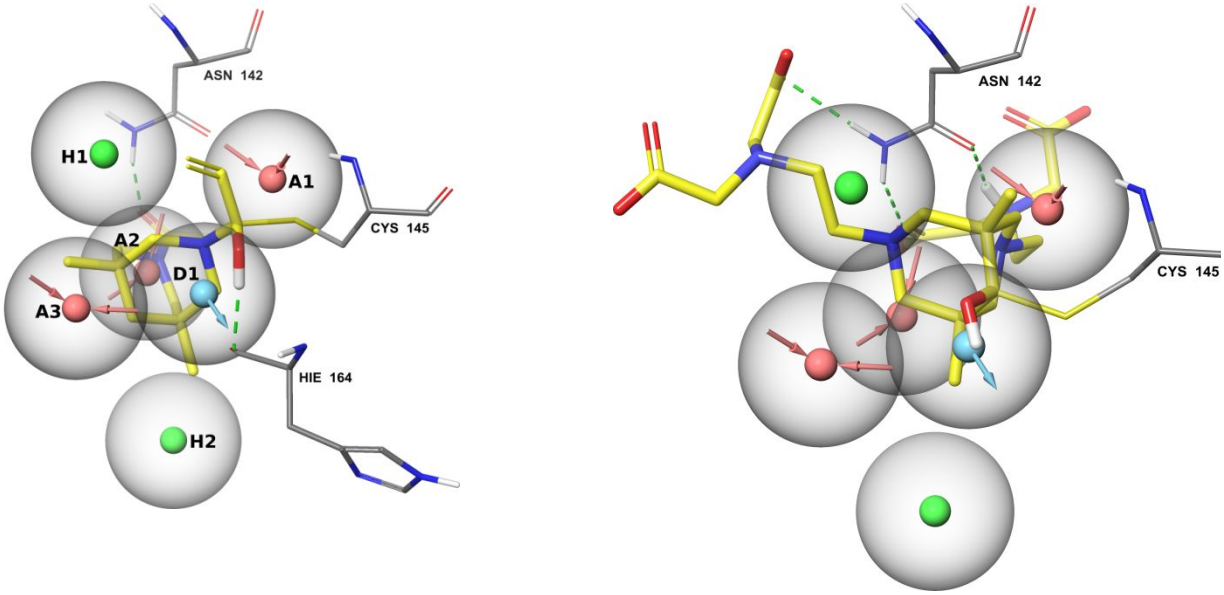

Figure S8. Superpositions of the pharmacophore hypothesis of covalent binding and conformations of new bispidine derivatives obtained as a result of covalent docking: A – **2j**, B – **2i**, C - **2e**, D - **3e**, E – **4q**, F - **4d**, G – **3k**, H - **4n**.

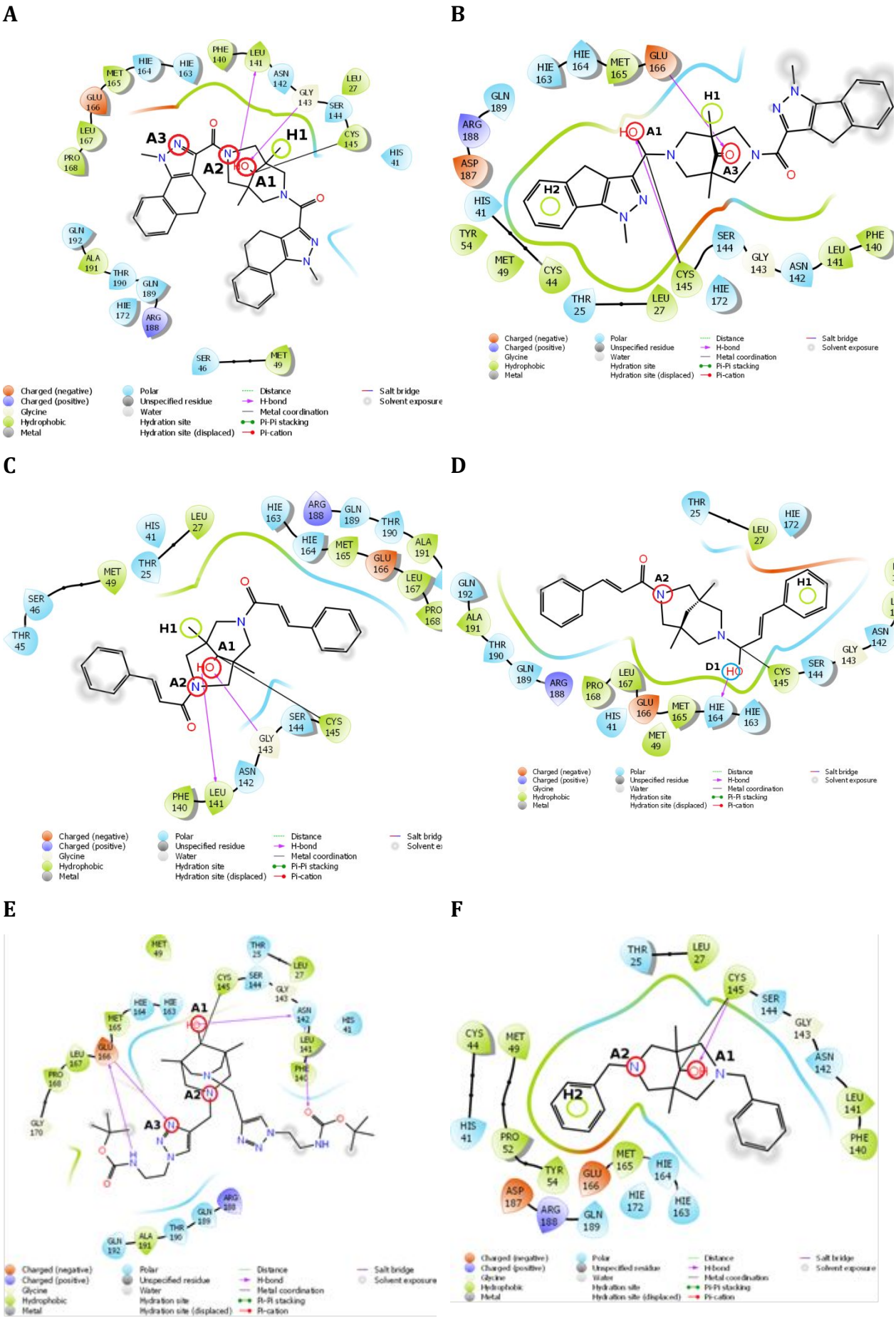
A
B
C
D
E
F
Charged (negative)
Charged (positive)
Glycine
Hydrophobic
Metal
Polar
Unspecified residue
Water
Hydration site
Hydration site (displaced)
Distance
H-bond
Metal coordination
Pi-Pi stacking
Pi-cation
Salt bridge
Solvent exposure

G H

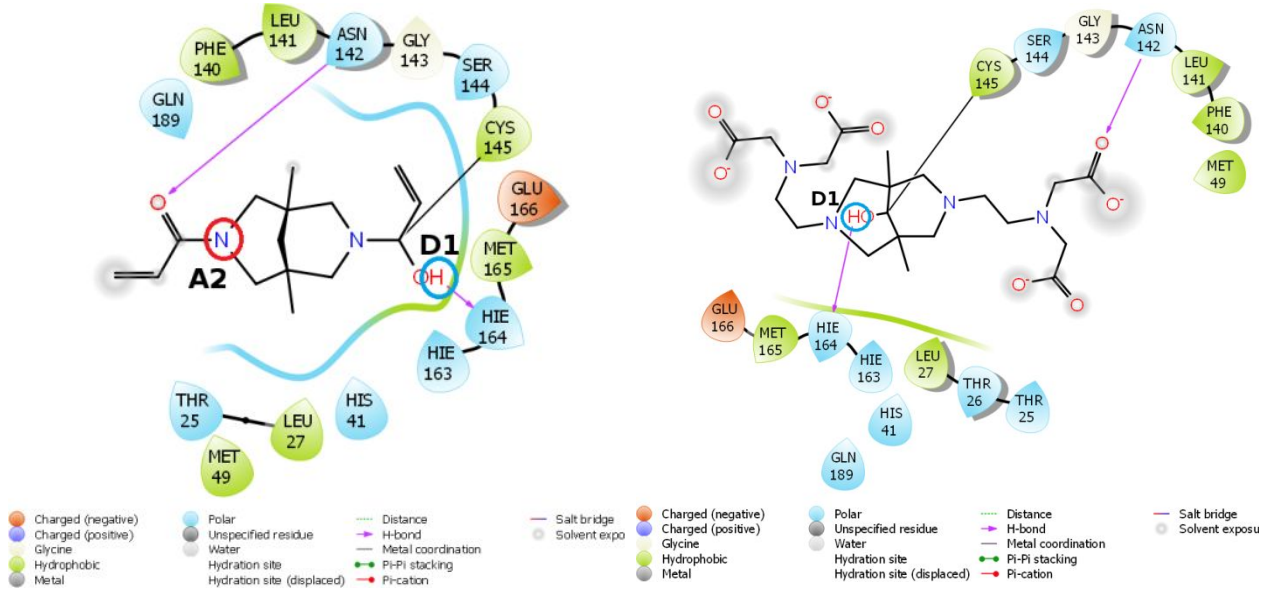

Figure S9. Two-dimensional diagrams of the binding of new bispidine derivatives according to the results of covalent docking and the correspondence of the obtained conformations to the pharmacophore hypothesis: A - **2j**, B - **2i**, C - **2e**, D - **3e**, E – **4q**, F - **4d**, G – **3k**, H – **4n**.

5. ADMET properties

The theoretical ADMET properties were calculated using pkCSM[29] (http://biosig.unimelb.edu.au/pkcsm/) and SwissADME[30] (http://www.swissadme.ch/) web services (Table S4).

Table S4. ADMET properties for studied new bispidine derivatives

Comp	MW	RB/A/D	LogP	LogS	Caco2P	IA	SkinP	BBBP	TC	MTD	LD50	Lipinski	Ghose
1	168.24	0/3/2	-0.2255	-0.069	1.445	87.733	-7.77	-0.187	0.764	0.785	2.329	yes	no
2a	368.47	0/5/0	3.0695	-4.165	1.036	92.2	-7.12	-0.28	0.132	-0.365	2.673	yes	yes
2b	252.31	0/3/0	0.2923	-2.235	1.192	89.286	-8.38	-0.222	0.409	0.606	2.35	yes	no
2c	272.30	0/3/0	-0.4811	-2.263	1.149	86.518	-7.83	-0.152	0.504	0.395	2.266	yes	no
2d	376.45	2/3/0	2.8801	-4.236	1.609	95.304	-6.79	-0.357	0.371	-0.352	2.63	yes	yes
2e	428.53	4/3/0	3.6793	-5.149	1.211	96.118	-6.50	-0.443	0.397	-0.465	3.558	yes	no
2f	536.63	4/7/0	3.6811	-3.805	1.156	94.363	-7.32	-0.825	0.259	0.853	2.864	yes	no
2g	548.69	4/9/0	3.8041	-3.804	1.154	95.116	-7.80	-1.169	0.384	0.745	2.73	yes	no
2h	660.77	6/7/0	6.5855	-2.952	0.996	100	-5.73	-0.283	0.64	0.454	2.909	no	no
2i	560.65	2/7/0	3.4895	-3.689	1.274	100	-7.48	0.039	0.566	0.449	2.953	yes	no
2j	588.71	2/7/0	3.8783	-3.715	1.262	100	-7.22	0.127	0.434	0.375	2.929	yes	no
3a	354.49	0/4/0	3.8905	-4.373	1.323	90.923	-6.18	0.102	0.068	-0.337	2.587	yes	yes
3e	414.54	4/2/0	4.5003	-5.197	1.183	94.926	-5.56	-0.002	0.558	-0.337	3.501	yes	no
3k	262.35	2/2/0	1.4455	-2.692	1.412	96.501	-6.76	-0.038	0.487	0.303	2.401	yes	yes
4c	244.33	2/3/0	0.4657	-1.313	1.494	91.364	-7.40	0.171	0.558	0.343	2.219	yes	yes
4d	348.49	4/3/0	3.5997	-3.144	0.984	92.519	-6.08	0.608	0.595	-0.278	2.769	yes	yes
4l	246.31	2/5/0	0.24646	-1.497	0.763	84.701	-7.88	-0.133	0.328	0.403	2.627	yes	no
4m	284.31	0/7/0	-1.1665	-2.756	0.535	83.053	-8.77	-0.672	1.07	0.35	3.149	yes	no
4n	486.52	14/9/4	-1.8583	-2.892	-0.785	0	-16.62	-2.566	-0.587	0.941	2.482	yes	no
4o	358.44	4/7/0	2.19254	-3.303	1.039	95.218	-7.73	-0.547	0.425	-0.63	2.847	yes	yes
4p	558.68	4/13/0	2.3491	-4.063	-0.018	68.133	-8.51	-0.018	-0.634	-0.392	2.711	no	no
4q	616.76	16/11/2	1.8321	-3.84	0.02	65.586	-9.93	-1.808	-0.309	-0.418	2.308	no	no
4r	510.64	8/9/0	2.8793	-3.615	0.956	95.972	-7.92	-1.074	0.184	0.033	2.628	yes	no
4s	606.64	10/15/2	0.5607	-2.891	1.06	40.819	-10.06	-2.371	0.016	0.491	2.272	no	no
4t	606.64	10/15/2	0.5607	-2.891	0.953	47.812	-9.58	-2.537	0.095	0.538	2.387	no	no

MW – molecular weight; **RB/A/D** – number of rotable bonds/acceptors/donors; **LogP** - partition coefficient; **LogS** - predicted aqueous solubility (log mol/L); **Caco2P** - Caco2 permeability (log 10^{-6} cm/s); **IA** – intestinal absorption (%); **SkinP** - skin permeability (log cm/s); **BBBP** – blood-brain barrier permeability (logBB); **TC** - total clearance (log ml/min/kg); **MTD** – maximum tolerated dose, human (log mg/kg/day); **LD50** – predicted oral rat acute toxicity (mol/kg); **Lipinski** – compliance with Lipinski rule of five (no more than one violation); **Ghose** - compliance with **Ghose** rule (zero violations).

Among the new bispidine derivatives, most of the molecules (21 out of 26) fit well the less strict classical druglikeness Lipinski rule of five[31]. Several compounds with pronounced *in vitro* 3CLpro inhibitory activity have significant molecular weight, excessive flexibility and a large number of acceptors, which can reduce their bioavailability and increase metabolism. When using a stricter Ghose[32] rule, among the new derivatives, only 7 out of 26 molecules fit to it. Among these 7 molecules, 5 (**2d**, **4p**, **2a**, **4c**, **4d**) showed significant inhibitory activity. The combination of theoretically calculated parameters (docking score and druglikeness) and the presence of pronounced *in vitro* 3CLpro inhibitory activity make compound **2d** the most interesting potential inhibitor of SARS-CoV-2 main protease.

Considering the range of values of the octanol-water partition coefficient (LogP) according to the Ghose filter (−0.4 to 5.6), it can be concluded that most of the compounds have medium lipophilicity characteristic of most drugs. Exceptions are bispidine derivatives **2h**, **2i**, **4n**, **2c** and **4o**. Most derivatives have acceptable theoretical absorption parameters. All compounds are insoluble or slightly soluble in water. The value of predicted Caco2 monolayer permeability parameter for most compounds exceeds 0.9, which indicates a high absorption through the intestinal epithelium. It is for this reason that the intestinal absorption index of is high for most compounds. The skin permeability of the new bispidine derivatives seems unlikely due to the low skin permeability coefficient[33] of all compounds. As for the theoretical distribution parameters, most of the new bispidine derivatives poorly penetrate the blood-brain barrier (logBB < 0,3) except derivative **4d**. Apparently, all new bispidine derivatives have an average total clearance (0,23 – 5,81 ml/min/kg). All new compounds are characterized by low theoretical toxicity (for all derivatives predicted LD50 > 2 mol/kg). However, the maximum tolerated dose for human of most compounds (19 of 26) can be considered low (log MTD < 0,477).

6. Synthesis of compounds 1-4

All reagents and solvents used in the work (purity 90.0– 99.9+ %) were purchased from commercial sources (SigmaAldrich, abcr, Acros Organics, Fisher Scientific), and, if necessary, subjected to further purification by standard routines immediately before use to achieve analytical purity. ^{1}H and ^{13}C NMR spectra were recorded at room temperature on Bruker Avance-300, Bruker Avance-400, and Bruker Avance-500 spectrometers. The spectrometer frequency is denoted in parentheses for each spectral data set. Chemical shifts were referred to the signals of the deuterosolvents (7.26 ppm and 77.0 ppm for $CDCl_3$, 2.49 ppm and 39.5 ppm for $(CD_3)_2SO$), 4.75 ppm for D_2O, respectively). Lorentz-Gauss apodization was used for precise measurement of the proton coupling constants values. The ratio of *syn*/*anti*-isomers was determined (where possible) based on the integral intensities of signals of the same type of protons.

TLC. The reaction progress and purity of the obtained compounds were controlled by TLC on Merck Silicagel 60G F_{254} plates.

Preparative chromatography. Carl Roth Silica gel 60, 0.04–0.063 mm was used for column chromatography.

HPLC-UV-MS. Samples were dissolved in acetonitrile or DMSO and diluted in 10-50 times by mixture of acetonitrile-water (40-60%). Data was obtained with using liquid chromatograph Dionex Ultimate 3000 (ThermoFisher Scientific, USA) with mass spectrometer AB Sciex QTRAP 3200 (AB Sciex, Canada), equipped with an electrospray ionization source (ESI). The separation was carried out using chromatographic column Acclaim C18 (150 × 2.1 mm, 3 µm, ThermoFisher Scientific, USA). Chromatograms were obtained in isocratic elution mode. As a mobile phase was used water and acetonitrile in relation in 60:40 volume % (for compounds **3a**, **4c**, **4o** – 40:60 and for **4d** – 10:90). UV detection was carried out in the wavelength range 190-400 nm. Injected sample volume was 0.5 µl for HPLC-MS and 20 µl for HPLC-UV. ESI-MS conditions on AB Sciex QTRAP 3200 were as follows: ESI in the registration mode of positive charge ions; ion spray voltage was 5500 V; ion source temperature was 300 °C; ion source gas 1 – air, 30 psi; ion source gas 2 – air, 40 psi; curtain gas – nitrogen, 15 psi; declustering potential +20 V; entrance potential +10 V; scanning speed 1000 Da/sec. Mass spectral data were obtained in the mass range m/z 100–800 Da.

HRMS-ESI. High-resolution mass spectra with electrospray ionization were recorded on a Bruker MicroOTOF II instrument.

Melting points. Melting points were determined by the capillary method on Electrothermal IA9000 instrument.

Compounds **1**[34 35], **2b**[34], **4c**[36], **4m**[34], **4r**[36], **4s**[37], **4t**[37], 1,5-diphenyl-1H-pyrazole-3-carboxylic acid[38], 5,7-dimethyl-1,3-diazaadamantan-6-one[34], 5,7-dimethyl-1,3-diazaadamantane[34], acryloyl chloride[39] and cinnamoyl chloride[40] were prepared as described earlier.

General schemes for the preparation of compounds **1**, **2**, **3**, and **4**:

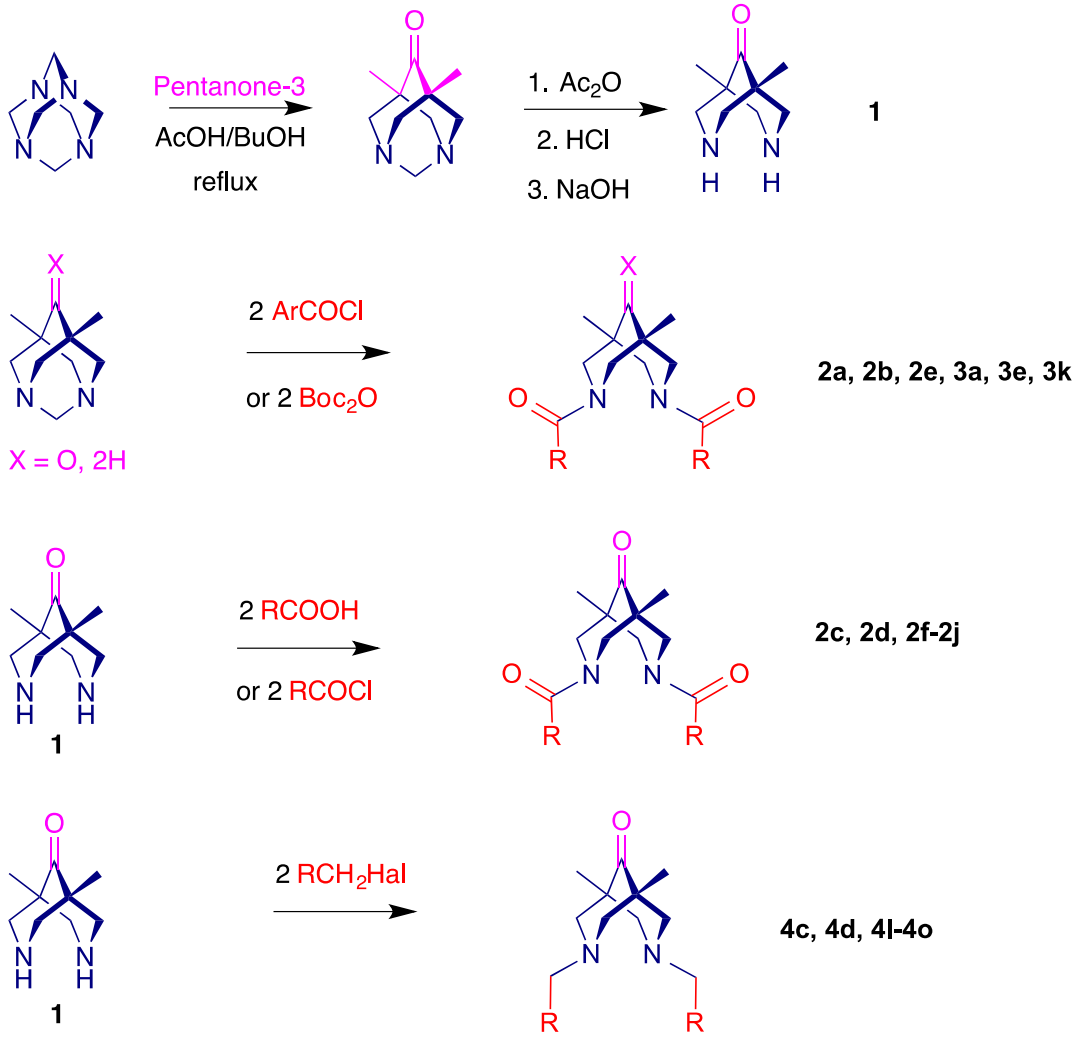

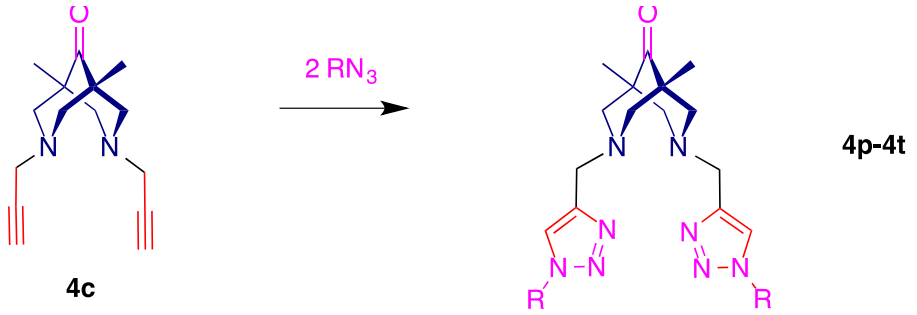

Figure S10. General schemes for the preparation of compounds 1, 2, 3, and 4.

Bridge-splitting reactions

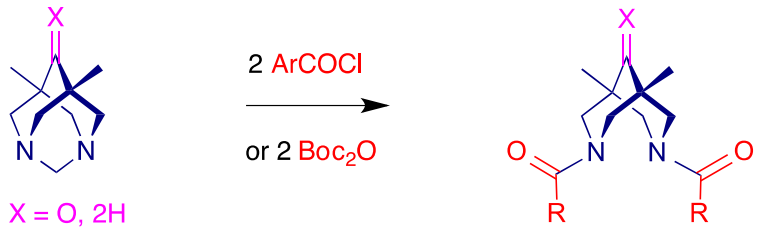

Scheme S1. General procedure for bridge-splitting reaction.

General procedure for bridge-splitting reaction. The solution of acid chloride (20 mmol) or Boc_2O (20 mmol) in benzene (10 ml) was added dropwise to the biphasic mixture of 5,7-dimethyl-1,3-diazaadamantan-6-one (10 mmol) or 5,7-dimethyl-1,3-diazaadamantane (10 mmol), sodium hydrogen carbonate (20 mmol) in benzene (10 ml) and water (5 ml) under vigorous stirring and ice-cooling conditions. The reaction mixture was stirred at room temperature. The reaction mixture was filtered, the powder was washed with water (30 ml), dissolved in minimal volume of DCM and washed with water (2*10 ml). The organic phase was separated, dried over sodium sulfate, and evaporated to dryness.

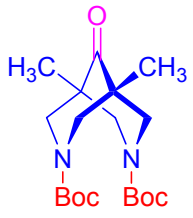

(Di-tert-butyl 1,5-dimethyl-9-oxo-3,7-diazabicyclo[3.3.1]nonane-3,7-dicarboxylate) (2a)

Reaction time 18 h. Purified with column chromatography on silica, eluent DCM:MeOH 50:1. R_f (DCM:MeOH 50:1) 0.11-0.27. White powder. Yield 80%. M.p. 186-188°C. Purity 95% (HPLC).

^{1}H NMR (400 MHz, $CDCl_3$, δ/ppm) 0.97 (s, 6 H), 1.45 (s, 18 H), 2.87 - 3.10 (m, 4 H), 4.12 - 4.53 (m, 4 H). ^{13}C NMR (101 MHz, $CDCl_3$, δ/ppm) 16.49; 27.96; 45.57; 55.54; 56.33; 80.01; 153.97; 213.32. HRMS-ESI. Calc for [$C_{19}H_{32}N_2O_5$+Na^+]: 391.2209. Found: 391.2202

^{1}H NMR spectra of compound **2a** ($CDCl_3$, 400 MHz):

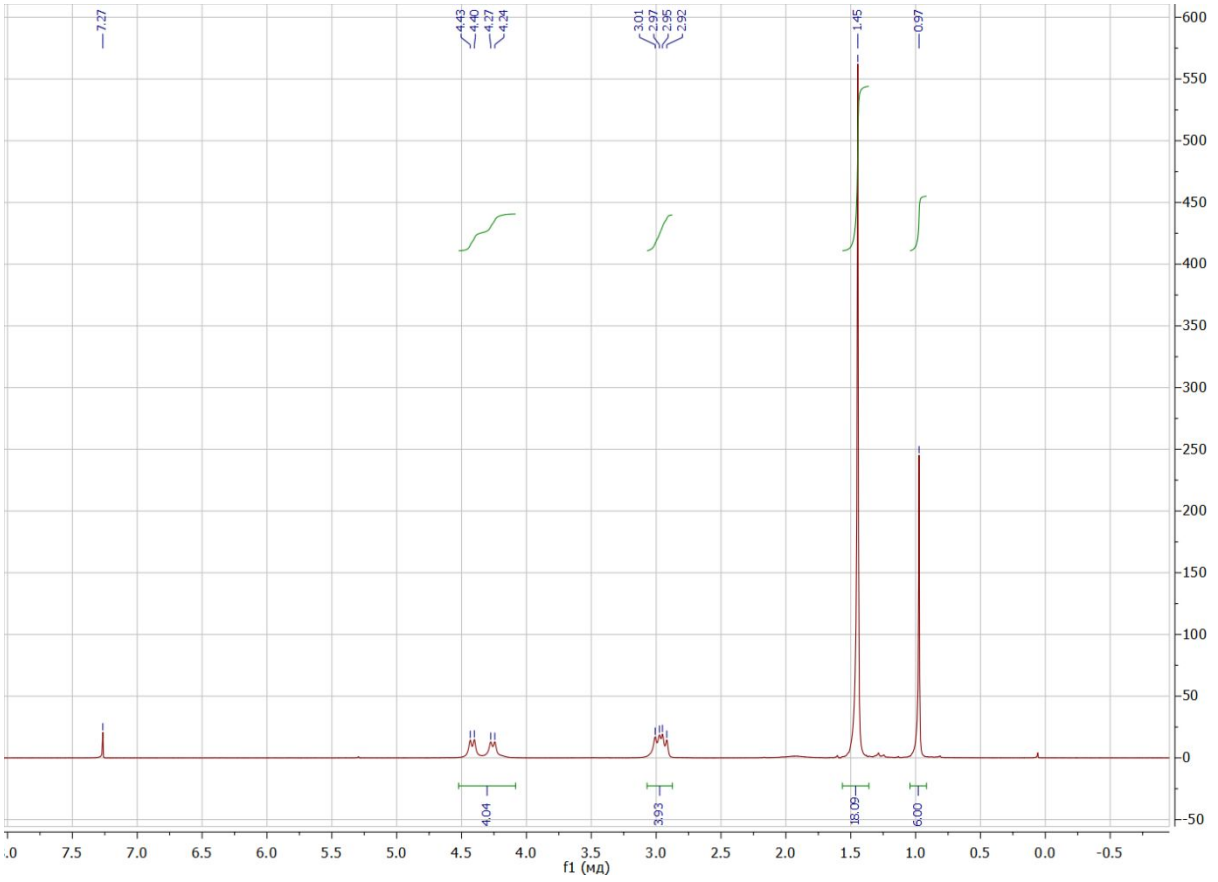

^{13}C NMR spectra of compound **2a** ($CDCl_3$, 101 MHz):

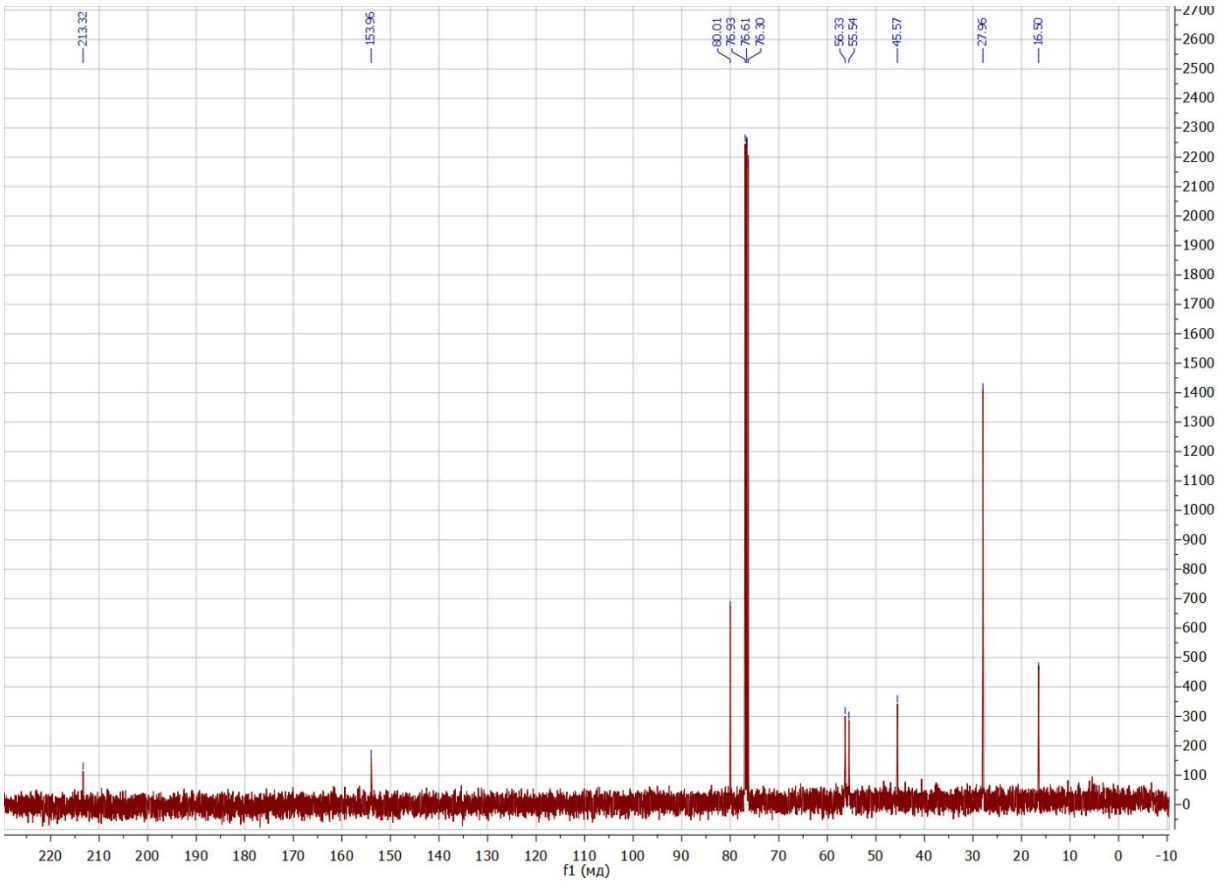

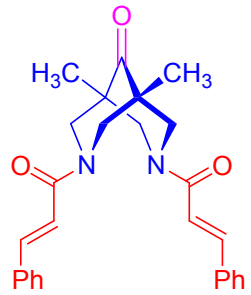

((2E,2'E)-1,1'-(-1,5-Dimethyl-9-oxo-3,7-diazabicyclo[3.3.1]nonane-3,7-diyl)bis(3-phenylprop-2-en-1-one)) (2e)

Reaction time 2 h. Recrystallized from ethanol. Colorless needles. Yield 85%. M.p. 245-247°C. Purity 98% (HPLC).

^{1}H NMR (400 MHz, $CDCl_3$, δ/ppm) 1.10 (s, 6 H), 2.89 (d, *J*=13.57 Hz, 2 H), 3.33 (d, *J*=12.96 Hz, 2 H), 4.39 (d, *J*=12.90 Hz, 2 H), 5.09 (d, *J*=13.51 Hz, 2 H), 6.92 (d, *J*=15.47 Hz, 2 H), 7.08 - 7.42 (m, 7 H), 7.42 - 7.62 (m, 5 H). ^{13}C NMR (100 MHz, $CDCl_3$, δ/ppm) 16.57; 45.26; 53.99; 57.18; 117.31; 127.85; 128.62; 129.55; 135.07; 143.05; 168.47; 211.77. HRMS-ESI. Calc for [$C_{27}H_{28}N_2O_3$+H^+]: 429.2178. Found: 429.2197

^{1}H NMR spectra of compound **2e** ($CDCl_3$, 400 MHz):

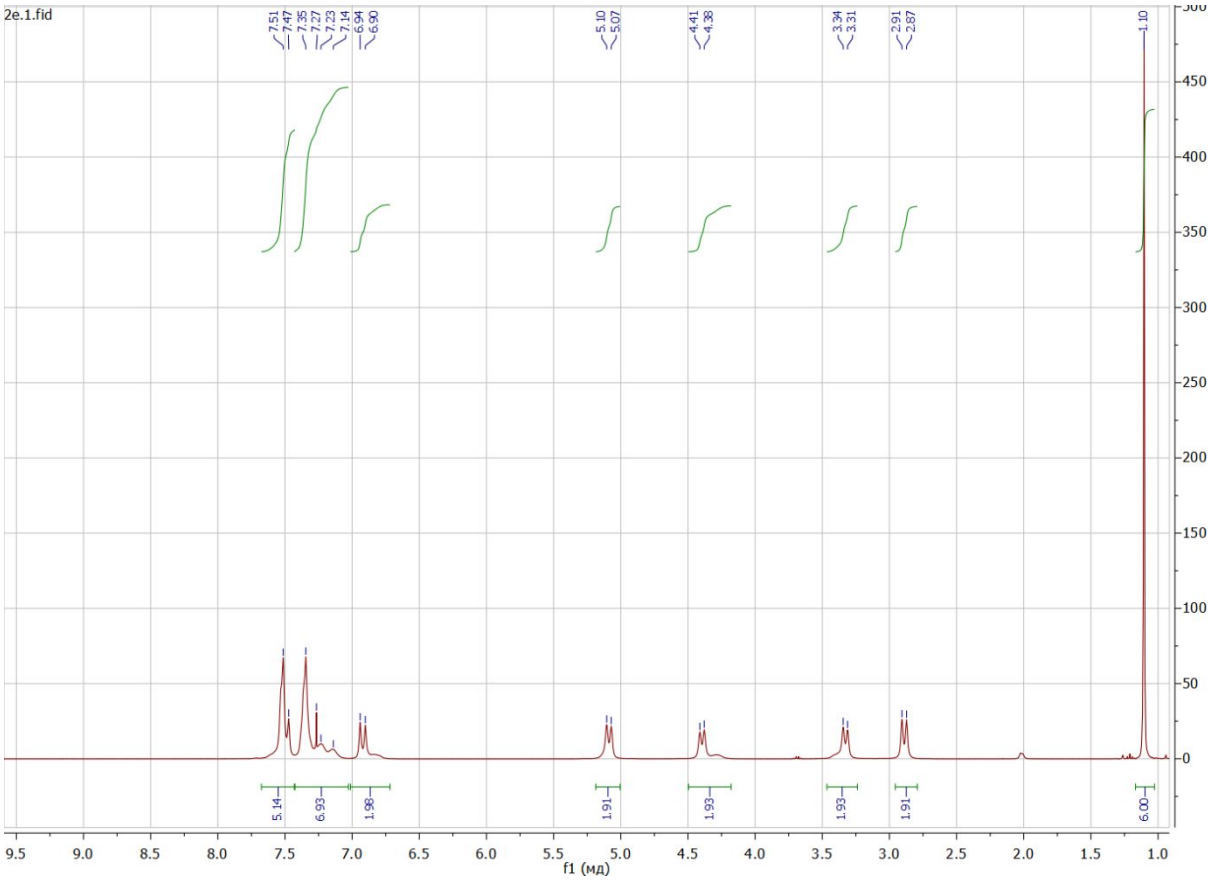

^{13}C NMR spectra of compound **2e** ($CDCl_3$, 100 MHz):

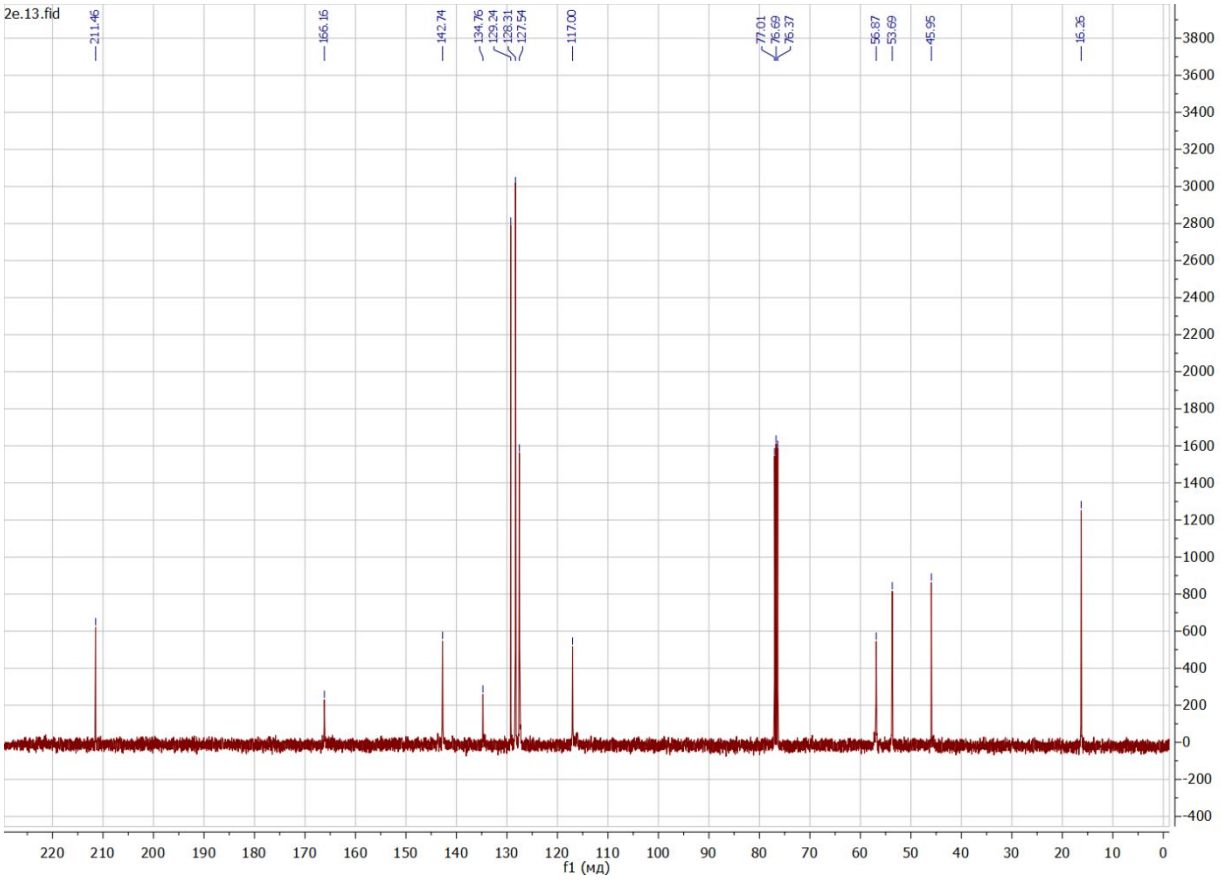

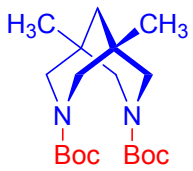

(Di-tert-butyl 1,5-dimethyl-3,7-diazabicyclo[3.3.1]nonane-3,7-dicarboxylate) (3a)

Reaction time 18 h. Purified with column chromatography on silica, eluent DCM:MeOH 50:1. R_f (DCM:MeOH 50:1) 0.13-0.18. White powder. Yield 87%. M.p. 118-120°C. Purity 99% (HPLC).

^{1}H NMR (400 MHz, $CDCl_3$, δ/ppm) 0.83 (s, 6 H), 1.23 (s, 2 H), 1.38 (s, 18 H), 2.39 - 2.58 (m, 4 H), 3.70 - 4.01 (m, 4 H). ^{13}C NMR (101 MHz, $CDCl_3$, δ/ppm) 24.57; 27.98; 29.99; 45.57; 52.48; 53.65; 78.83; 154.26. HRMS-ESI. Calc for [$C_{19}H_{34}N_2O_4$+H^+]: 355.2597. Found: 355.2601

^{1}H NMR spectra of compound **3a** ($CDCl_3$, 400 MHz):

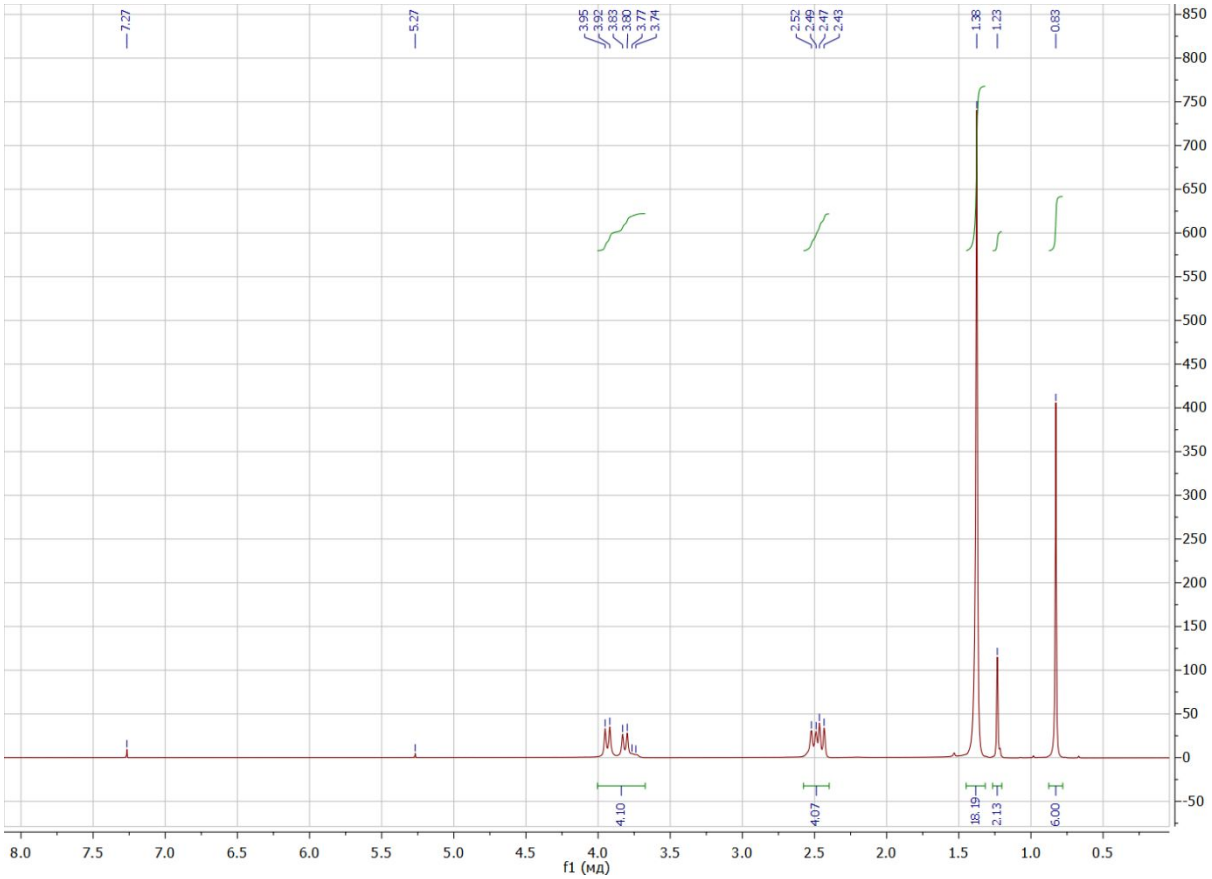

^{13}C NMR spectra of compound **3a** ($CDCl_3$, 101 MHz)

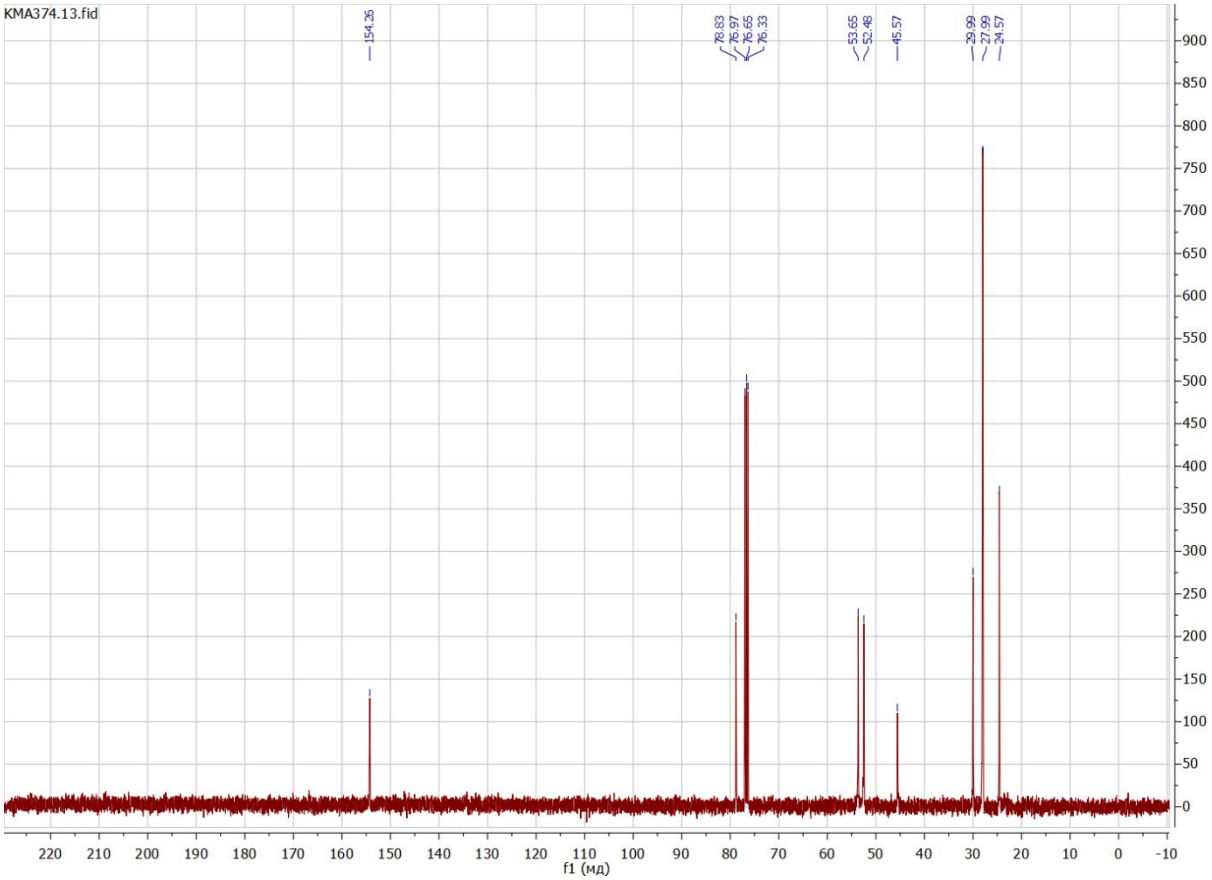

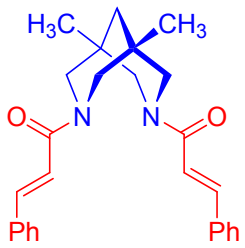

(2E,2'E)-1,1'-(-1,5-Dimethyl-3,7-diazabicyclo[3.3.1]nonane-3,7-diyl)bis(3-phenylprop-2-en-1-one) (3e)

Reaction time 2 h. Purified with column chromatography on silica, eluent DCM:MeOH 50:1. White powder. Yield 58%. M.p. 168-170°C. Purity 99% (HPLC).

^{1}H NMR (400 MHz, $CDCl_3$, δ/ppm) 1.00 (s, 6 H), 1.50 (s, 2 H), 2.53 (d, *J*=13.20 Hz, 3 H), 2.93 (d, *J*=12.78 Hz, 3 H), 3.99 (d, *J*=13.08 Hz, 3 H), 4.67 (d, *J*=13.39 Hz, 3 H), 6.86 (d, *J*=15.47 Hz, 3 H), 7.06 - 7.26 (m, 3 H), 7.29 - 7.63 (m, 10 H). ^{13}C NMR (75 MHz, $CDCl_3$, δ/ppm) 24.21; 30.64; 46.61; 51.23; 53.13; 55.02; 118.25; 127.42; 128.20; 128.83; 135.12; 141.30; 166.10. HRMS-ESI. Calc for [$C_{27}H_{30}N_2O_2$+H^+]: 415.2386. Found: 415.2360

^{1}H NMR spectra of compound **3e** ($CDCl_3$, 400 MHz):

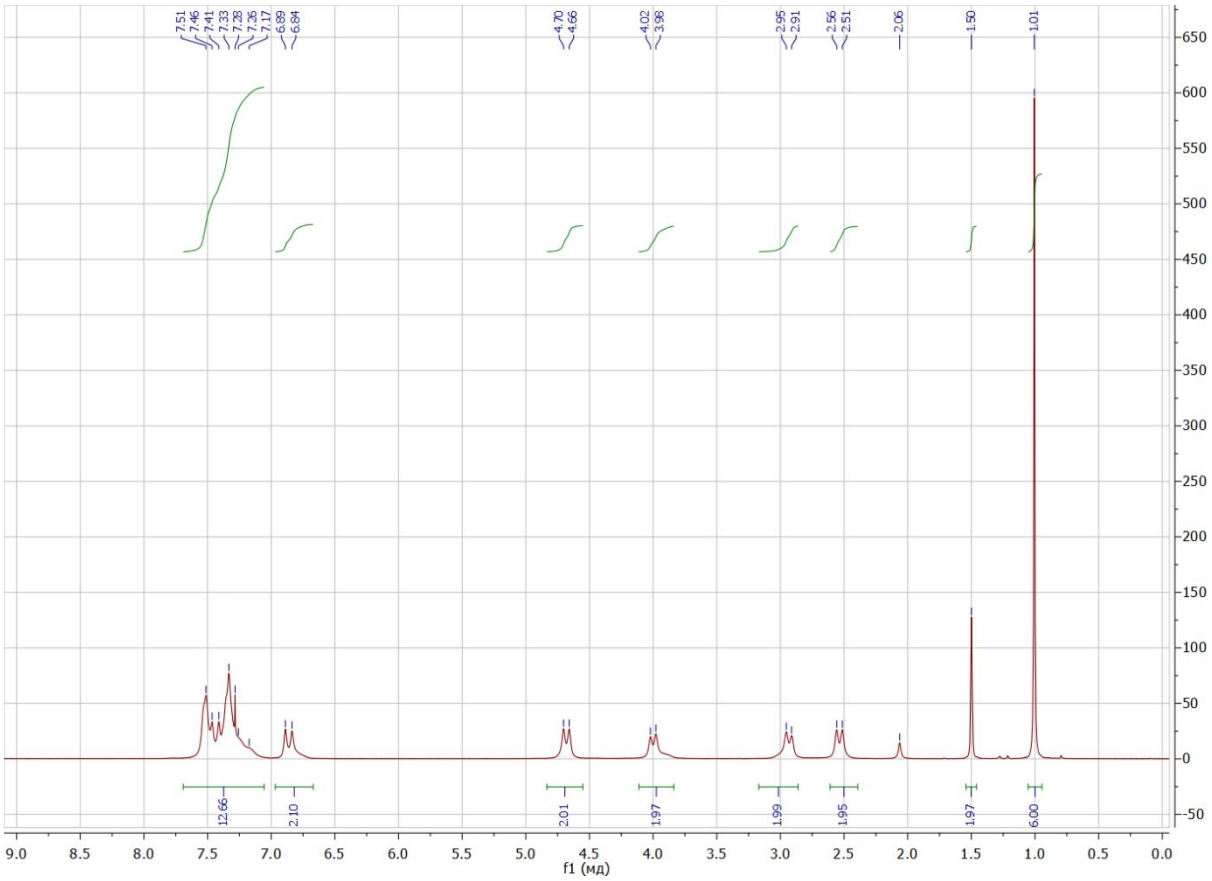

^{13}C NMR spectra of compound **3e** ($CDCl_3$, 75 MHz):

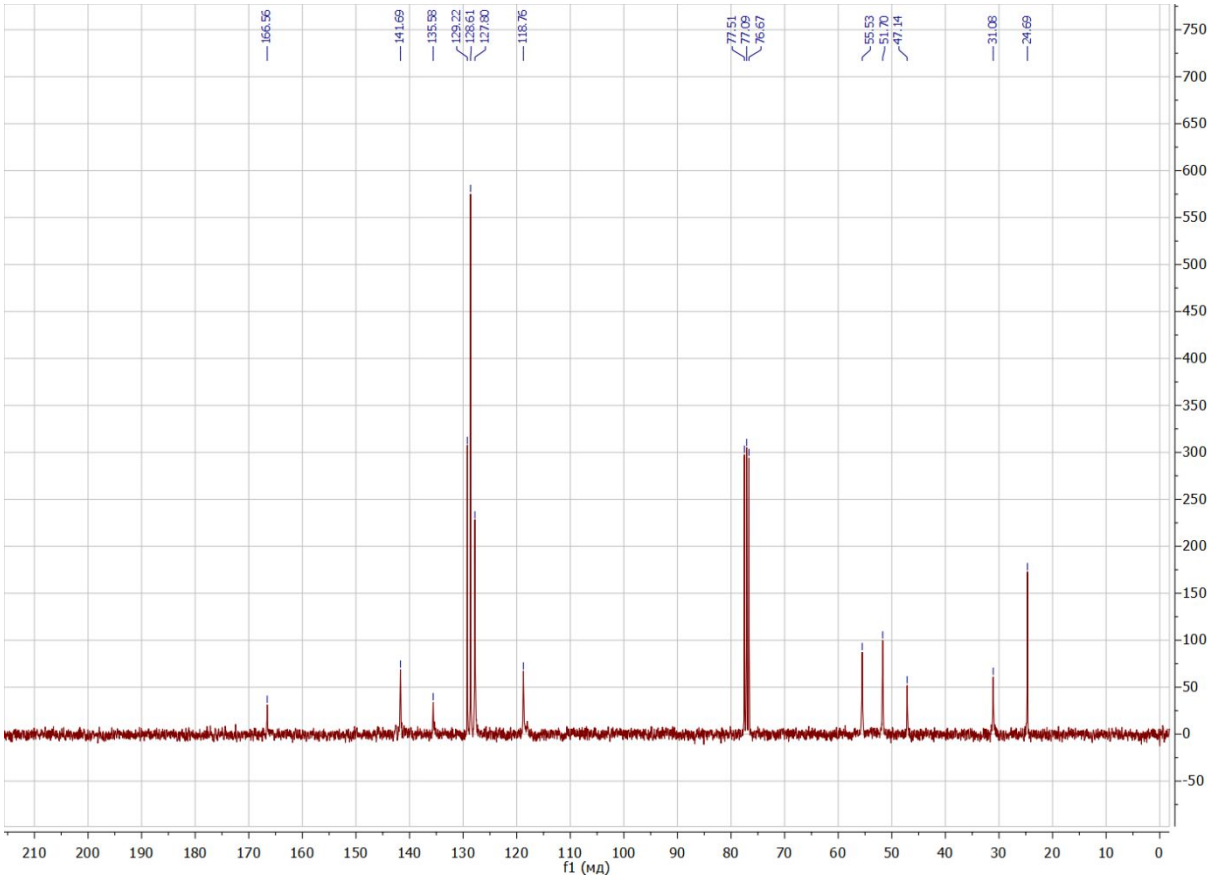

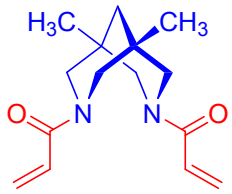

(1,1'-(-1,5-Dimethyl-3,7-diazabicyclo[3.3.1]nonane-3,7-diyl)bis(prop-2-en-1-one)) (3k)

Reaction time 2 h. Purified with column chromatography on silica, eluent DCM:MeOH 50:1. White powder. Yield 46 %. M.p. 155-157°C. Purity 99% (HPLC).

^{1}H NMR (400 MHz, $CDCl_3$, δ/ppm) 0.95 (s, 6 H), 1.45 (s, 2 H), 2.45 (d, *J*=13.57 Hz, 2 H), 2.85 (d, *J*=13.08 Hz, 2 H), 3.86 (d, *J*=13.08 Hz, 2 H), 4.59 (d, *J*=13.51 Hz, 2 H), 5.59 (dd, *J*=10.70, 1.77 Hz, 2 H), 6.07 (d, *J*=16.93 Hz, 2 H), 6.53 (dd, *J*=16.90, 10.73 Hz, 2 H). ^{13}C NMR (75 MHz, $CDCl_3$, δ/ppm) 24.59; 30.86; 47.10; 51.26; 55.36; 126.98; 128.56; 166.34. HRMS-ESI. Calc for [$C_{15}H_{22}N_2O_2$+H^+]: 263.1760. Found: 263.1767

^{1}H NMR spectra of compound **3k** ($CDCl_3$, 400 MHz):

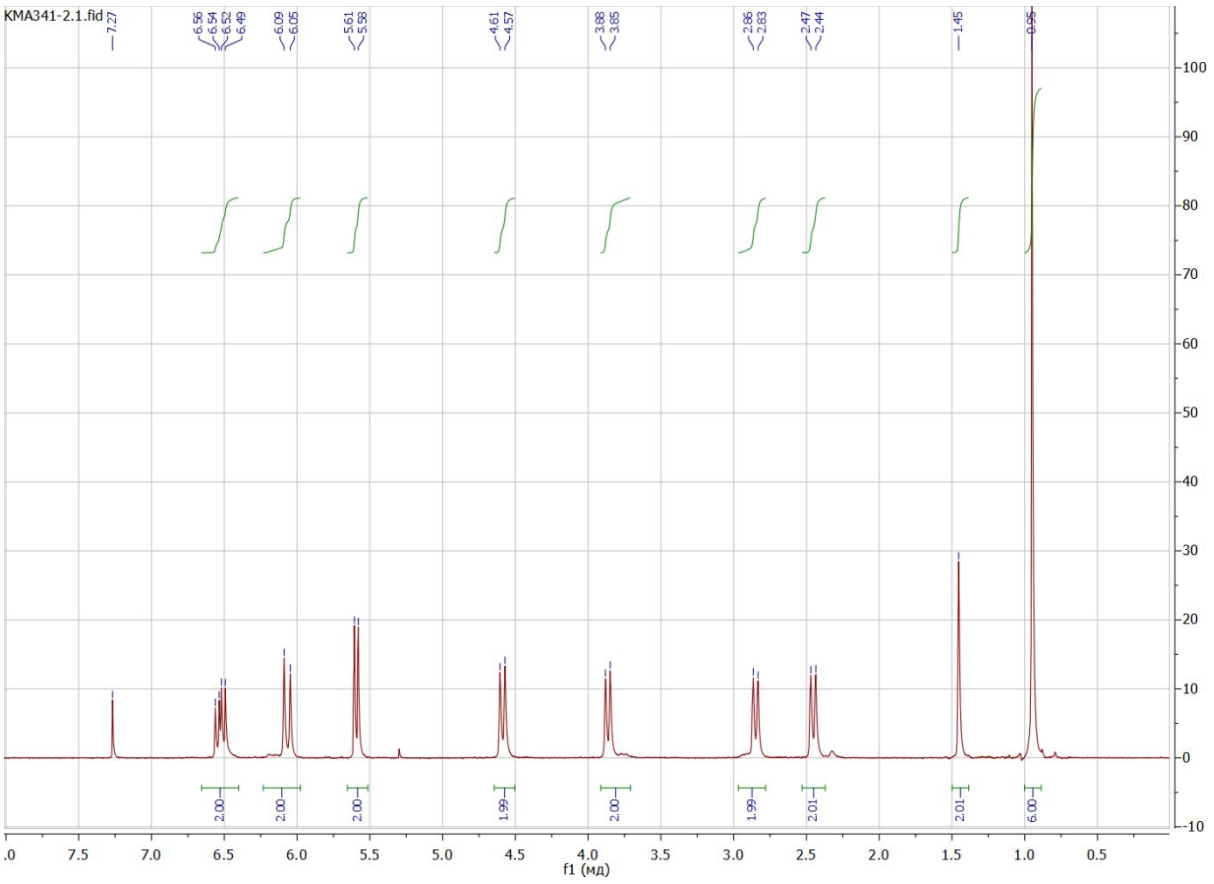

^{13}C NMR spectra of compound **3k** ($CDCl_3$, 75 MHz):

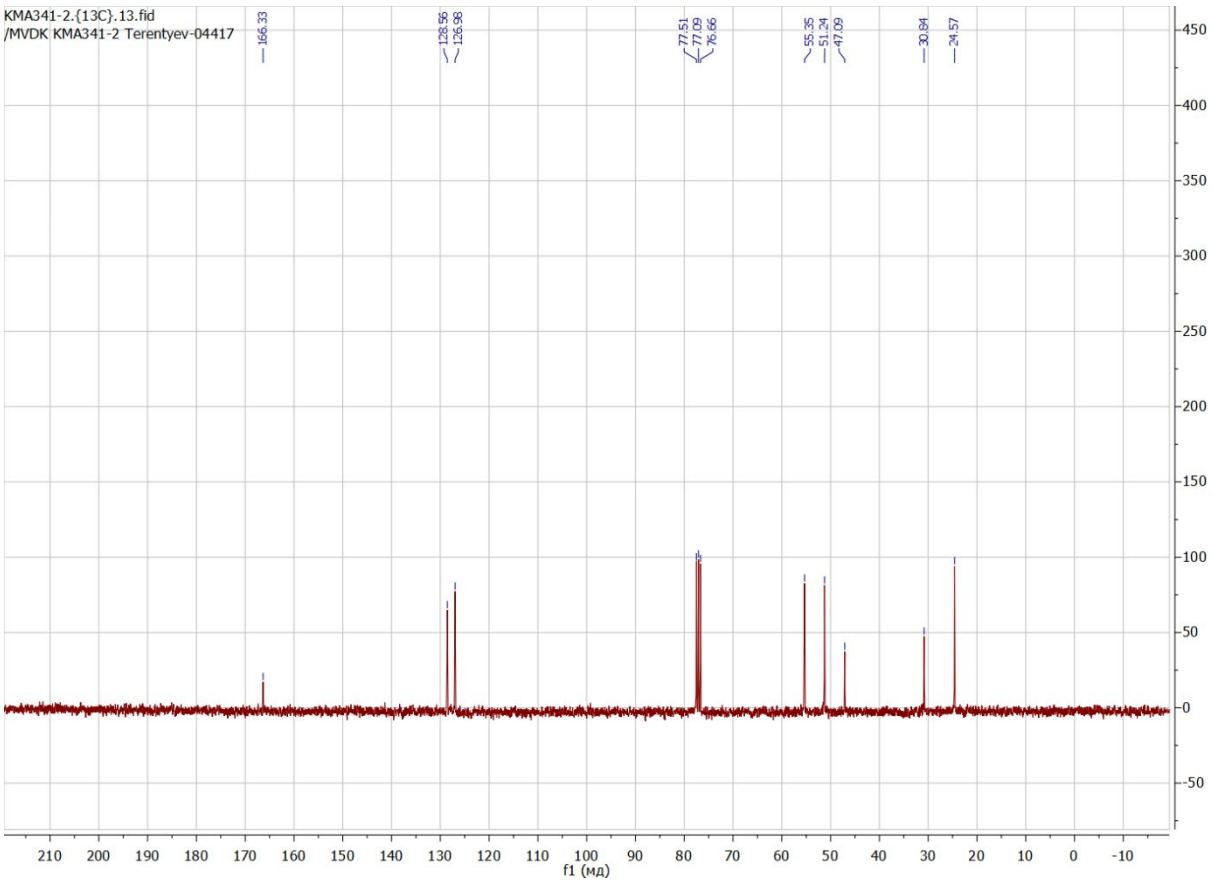

Preparation of amides

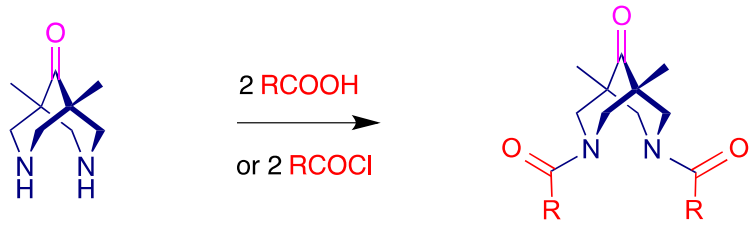

Scheme S2. General procedure for preparation of amides.

Coupling reaction

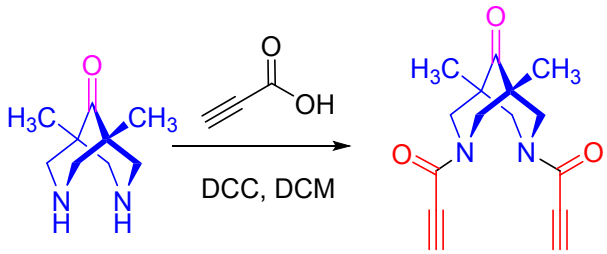

Scheme S3. Preparation of 1,1'-(-1,5-dimethyl-9-oxo-3,7-diazabicyclo[3.3.1]nonane-3,7-diyl)bis(prop-2-yn-1-one).

(1,1'-(-1,5-Dimethyl-9-oxo-3,7-diazabicyclo[3.3.1]nonane-3,7-diyl)bis(prop-2-yn-1-one)) (2c). N,N'-Dicyclohexylcarbodiimide (1.24 g, 6.0 mmol) was added by portions to the solution of propiolic acid (0.37 ml, 6.0 mmol) in dry DCM (6 ml) at -20°C. The solution of 1,5-dimethyl-3,7-diazabicyclo[3.3.1]nonan-9-one (0.50 g, 3.0 mmol) in dry DCM (3 ml) was added dropwise to the reaction mixture. The latter was stirred for 30 min at -20°C and for 11 h at room temperature. The suspension was filtered through Celite and the filtrate was evaporated to dryness. The residue was purified with column chromatography on silica, eluent DCM:MeOH 50:1.

White powder. Yield 0.543 g (66%). M.p. 188-192°C (dec). Purity 95% (HPLC).

^{1}H NMR (300 MHz, $CDCl_3$, δ/ppm) 1.10 - 1.13 (m, 6 H), 2.82 - 2.91 (m, 2 H), 3.22 - 3.40 (m, 4 H), 4.67 - 4.78 (m, 2 H), 4.87 - 5.01 (m, 2 H).^{13}C NMR (75 MHz, $CDCl_3$, δ/ppm) 16.53 (*anti*-), 16.68 (*syn*-), 45.60 (*syn*-), 45.85 (*syn*-), 46.20 (*anti*-), 52.60 (*anti*-), 52.87 (*syn*-), 58.13, 74.57 (*anti*-), 74.96 (*syn*-), 77.28, 81.02 (*anti*-), 81.19 (*syn*-), 151.81 (*syn*-), 151.92 (*anti*-), 210.57 (*anti*-), 210.64 (*syn*-). HRMS-ESI. Calc for [$C_{15}H_{16}N_2O_3$+H^+]: 273.1239. Found: 273.1246

^{1}H NMR spectra of compound **2c** ($CDCl_3$, 300 MHz):

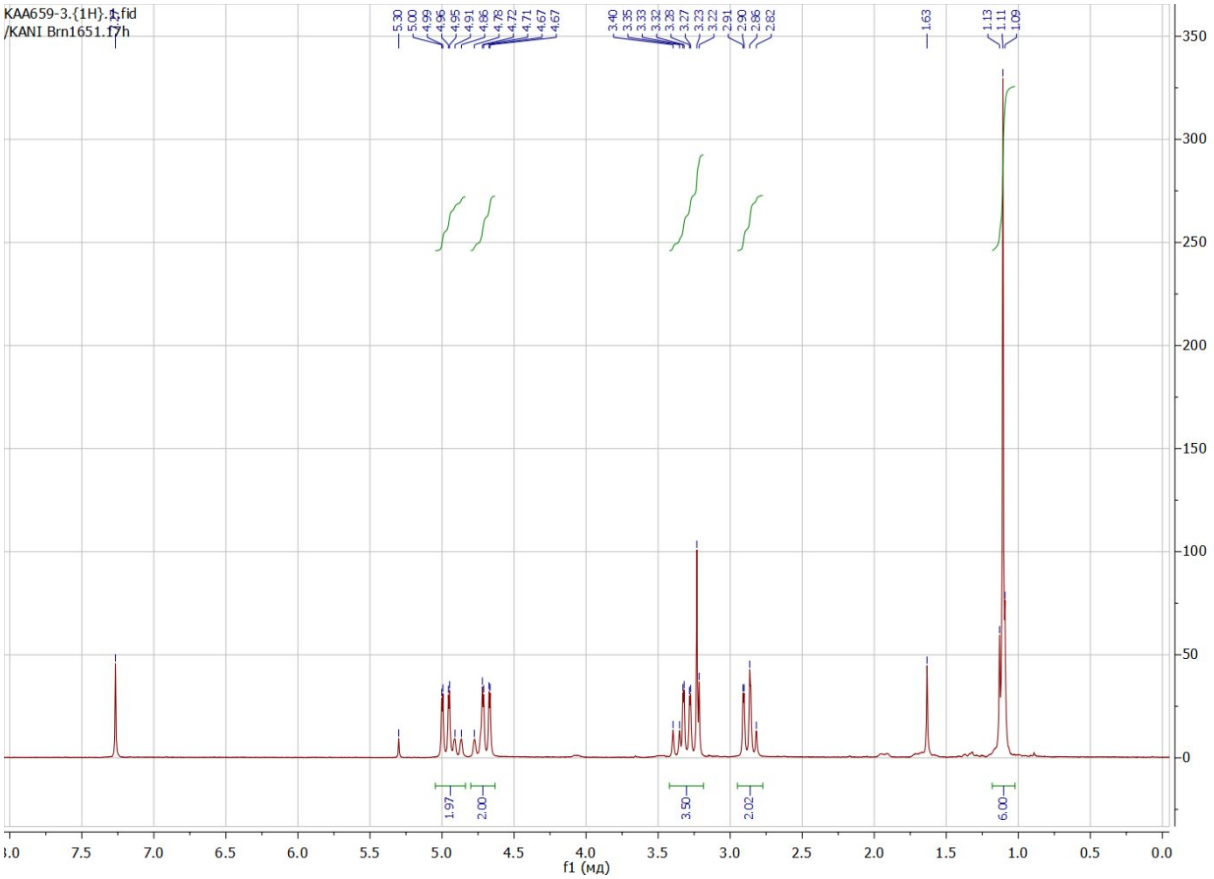

^{13}C NMR spectra of compound **2c** ($CDCl_3$, 75 MHz):

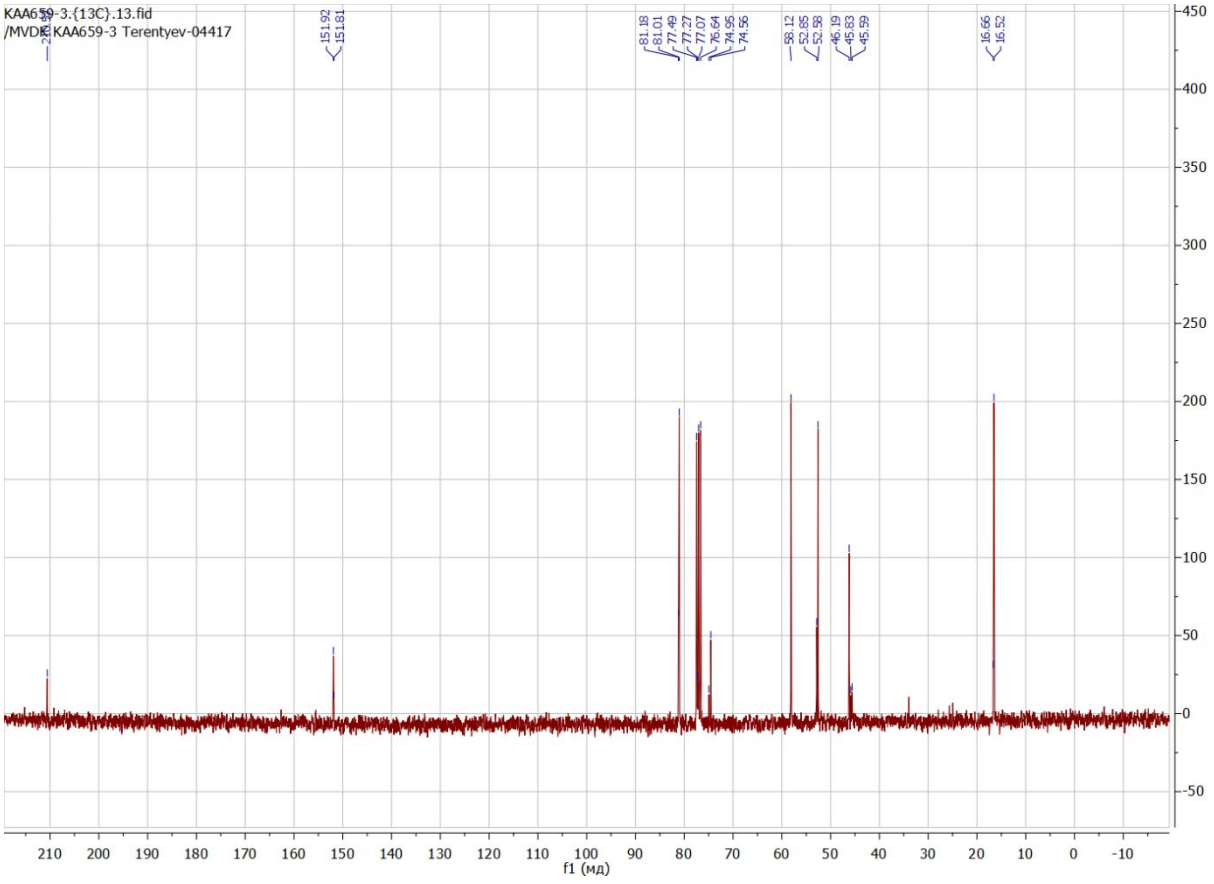

Acylation reactions

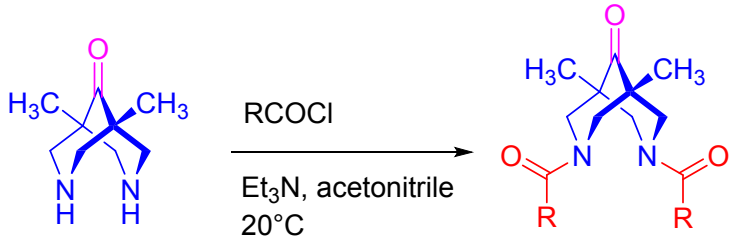

Scheme S4. General procedure for the synthesis of compounds **2d**, **2f - 2j**.

General procedure for the synthesis of compounds 2d, 2f - 2j:

The corresponding acyl chloride (6 mmol) was added to a solution of 1,5-dimethyl-3,7-diazabicyclo[3.3.1]nonan-9-one (3 mmol) and triethylamine (6 mmol) in dry acetonitrile (40 ml) under vigorous stirring. The mixture was stirred at room temperature and then poured into water (150 ml). The precipitate was filtered off, washed with acetonitrile, and dried in vacuo over P_2O_5.

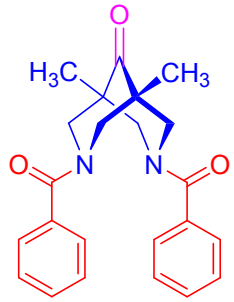

(1,5-Dimethyl-9-oxo-3,7-diazabicyclo[3.3.1]nonane-3,7-diyl)bis(phenylmethanone)) (2d). 1,5-Dimethyl-3,7-diazabicyclo[3.3.1]nonan-9-one (**1**) (0.3 g, 1.8 mmol), benzoyl chloride (0.5 g, 3.6 mmol) and Et_3N (0.5 ml, 3.6 mmol) were dissolved in acetonitrile (32 ml). The reaction mixture was stirred for 4 hours at room temperature. Then water (180 ml) was added, the reaction mixture was filtered and washed with water. The filtrate was extracted with dichloromethane. Organic phase was dried over sodium sulfate. Solvent was evaporated, residues were combined. The product was dried in vacuo over P_2O_5.

White solid. Yield 0.604 g (89%). M.p. 255-256°C. Purity 95% (HPLC).

^{1}H NMR (400 MHz, $CDCl_3$, δ/ppm) 0.99 (6H, s); 3.01 (2H, d, *J* = 13.65 Hz); 3.33 (2H, d, *J* = 13.10 Hz); 4.11 (2H, d, *J*=12.93 Hz); 4.96 (2H, d, *J*=13.71 Hz); 7.47-7.42 (6H, m); 7.60-7.53 (4H, m). ^{13}C NMR (101 MHz, $CDCl_3$, δ/ppm) 16.30; 48.80; 48.84; 53.52; 59.18; 127.10;

128.25; 129.60; 132.99; 134.36; 170.70; 211.88. HRMS-ESI. Calc for [$C_{23}H_{24}N_2O_3$+H^+]: 376.1865. Found: 376.1876.

^{1}H NMR spectra of compound **2d** ($CDCl_3$, 400 MHz):

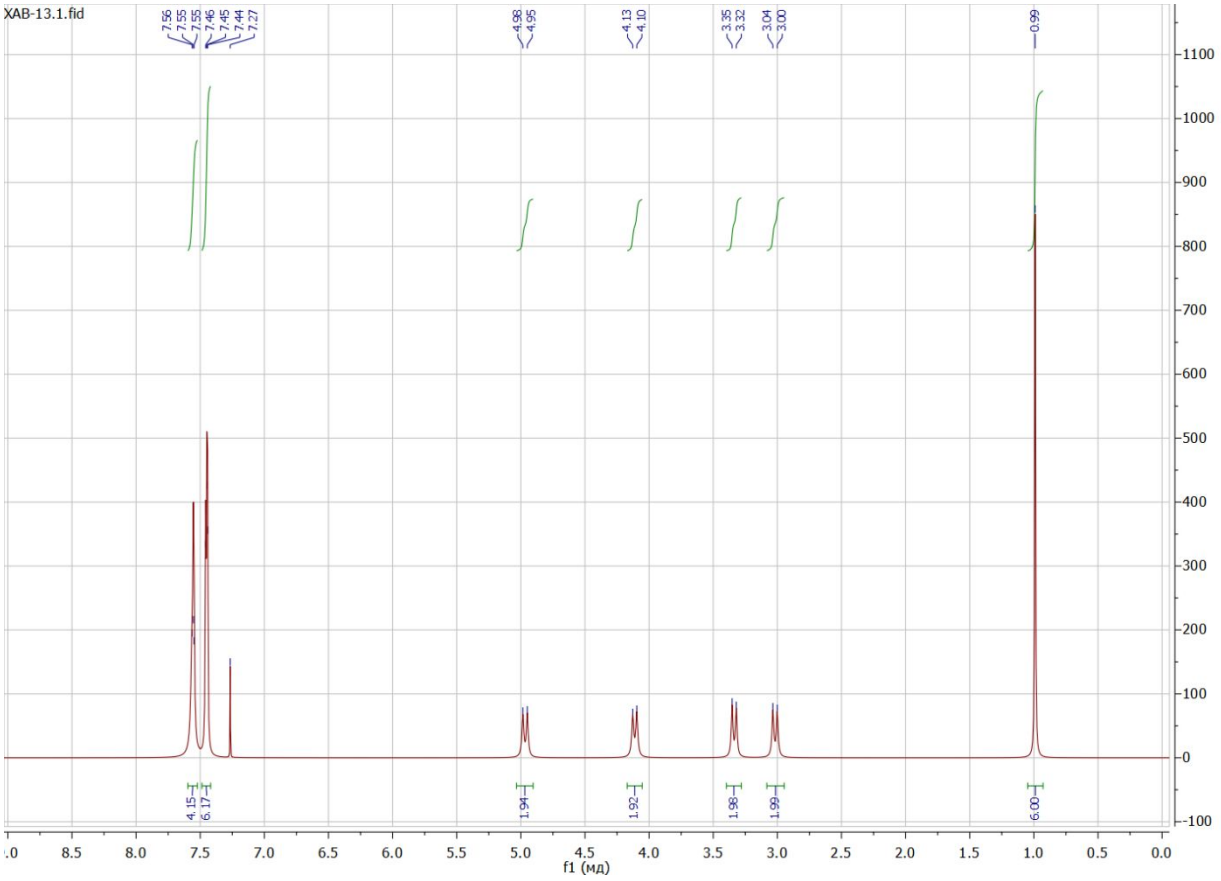

^{13}C NMR spectra of compound **2d** ($CDCl_3$, 101 MHz):

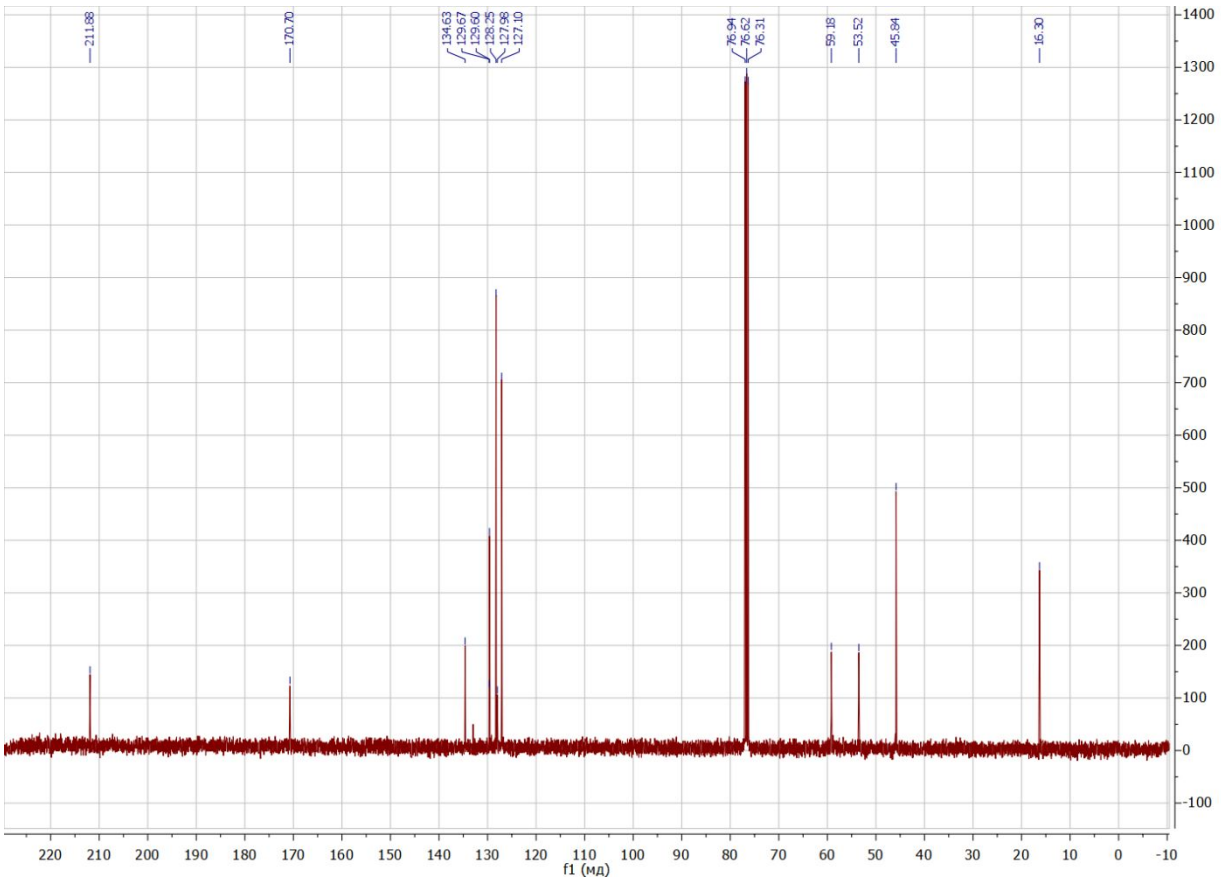

Synthesis of 1*H*-pyrazole-3-carboxylic acids

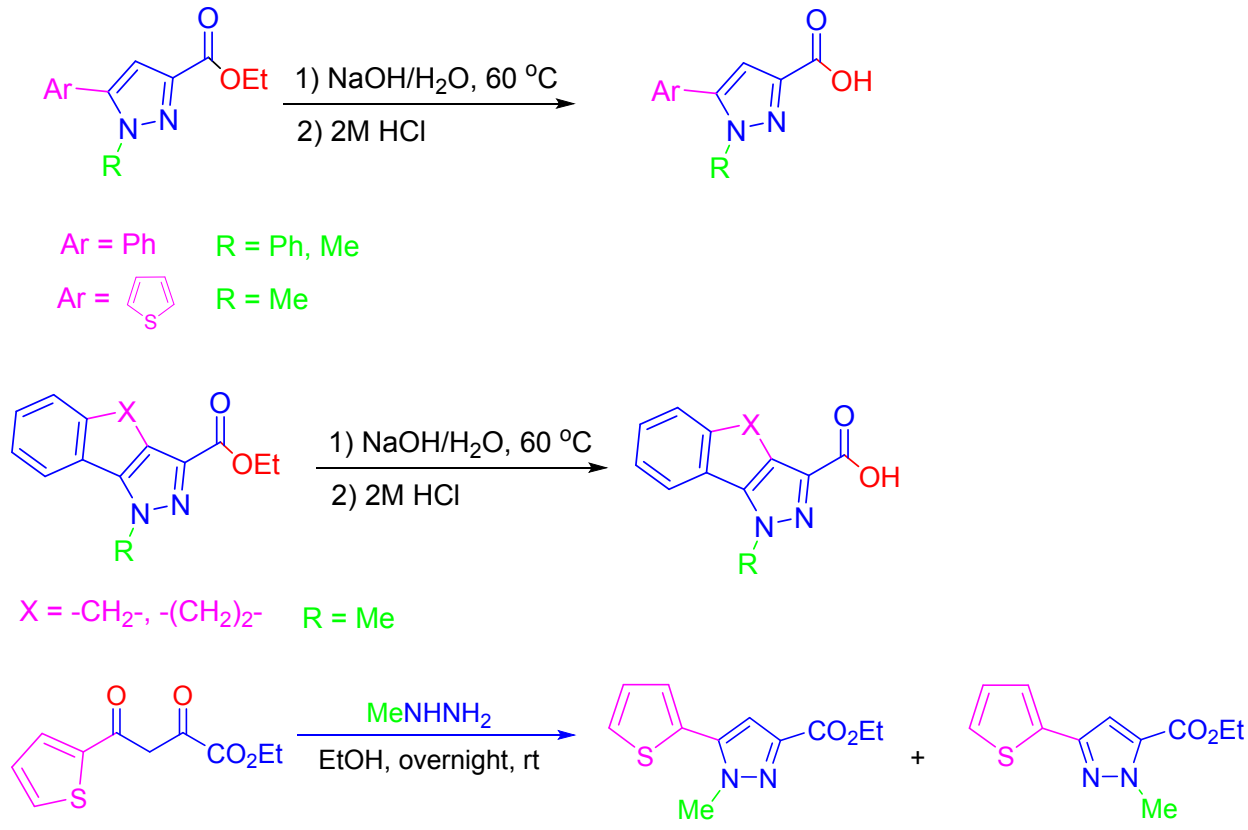

Figure S10. General schemes for the preparation of 1H-pyrazole-3-carboxylic acids.

Ethyl 1-methyl-5-(thiophen-2-yl)-1*H*-pyrazole-3-carboxylate and ethyl 1-methyl-3-(thiophen-2-yl)-1*H*-pyrazole-5-carboxylate

To the 50 ml solution of 12.9 g (57 mmol) of ethyl 2,4-dioxo-4-(thiophen-2-yl)butanoate prepared according to[41] in absolute ethanol 3 ml (2.63 g, 57 mmol) of methylhydrazine was added with stirring. The reaction mixture was left overnight at rt. Then the solvent was evaporated under reduced pressure and the residue was dried in vacuo over P_2O_5. Isomers were isolated as individual products using column chromatography (silica gel; petroleum ether:ethyl acetate 4:1).

Ethyl 1-methyl-5-(thiophen-2-yl)-1*H*-pyrazole-3-carboxylate(SI-1)

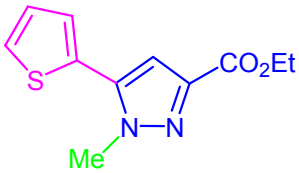

Brown oil. Yield 11 g (82%). R_f (petroleum ether-ethylacetate 3:1) = 0.18

^{1}H NMR (300 MHz, $CDCl_3$, δ/ppm) 1.42 (t, *J* = 7.12 Hz, 3H), 4.06 (s, 3H), 4.43 (q, *J* = 7.13 Hz, 2H), 6.93 (s, 1H), 7.15 (t, *J* = 4.79 Hz, 1H), 7.21 (d, *J* = 3.38 Hz, 1H), 7.46 (d, *J* = 5.01 Hz, 1H). ^{13}C NMR (101 MHz, $CDCl_3$, δ/ppm) 14.5; 38.7; 61.1; 109.5; 127.3; 127.7; 127.89; 127.9; 130.1; 138.3; 142.7; 162.2. HRMS-ESI. Calc for [$C_{11}H_{12}N_2O_2S$ +H^+]: 237.0692. Found: 237.0696

^{1}H NMR spectra of **ethyl 1-methyl-5-(thiophen-2-yl)-1*H*-pyrazole-3-carboxylate (SI-1)** ($CDCl_3$, 300 MHz):

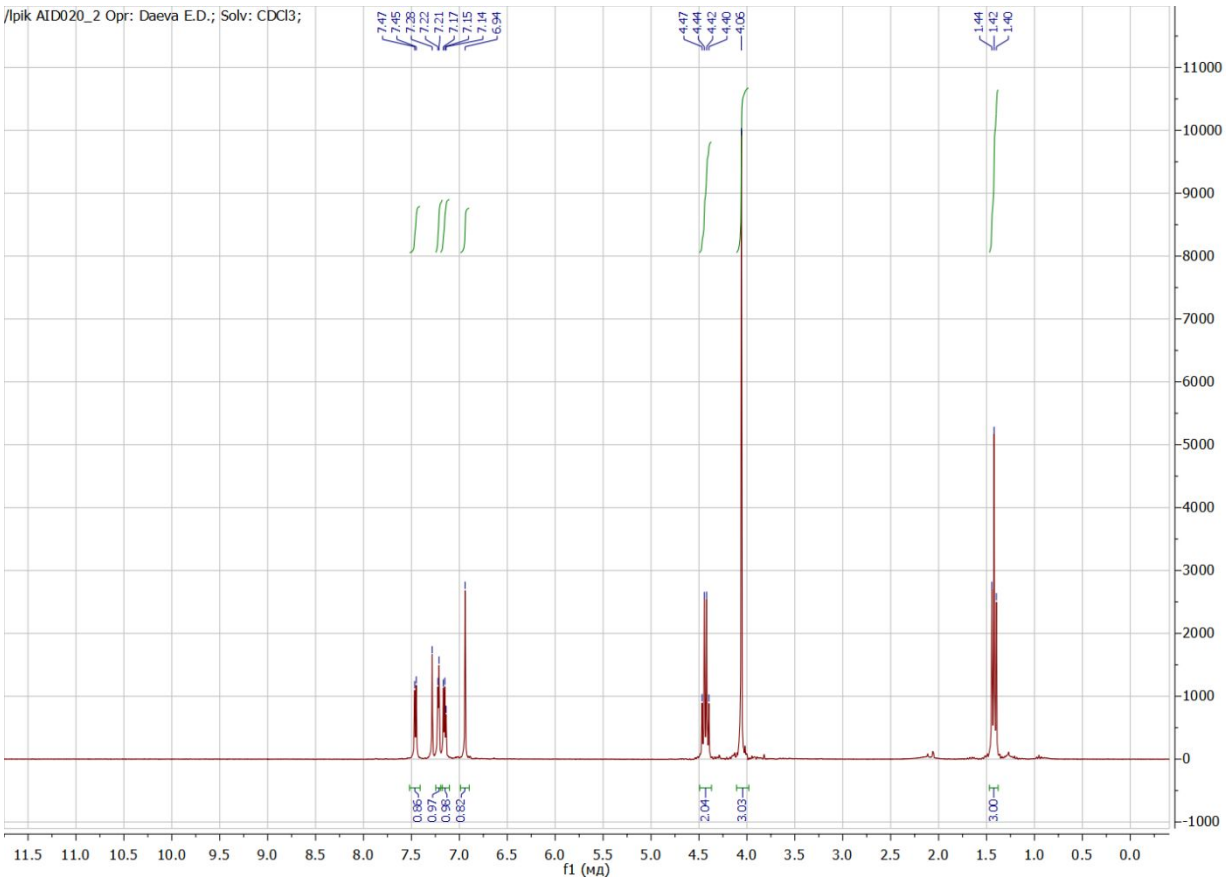
/lpik AID020_2 Opr: Daeva E.D.; Solv: CDCl3;
7.47
7.45
7.28
7.22
7.21
7.17
7.15
7.14
6.94
4.47
4.44
4.42
4.40
4.06
1.44
1.42
1.40
0.86
0.97
0.98
0.82
2.04
3.03
3.00
f1 (мд)

^{13}C NMR spectra of **ethyl 1-methyl-5-(thiophen-2-yl)-1*H*-pyrazole-3-carboxylate(SI-1)** ($CDCl_3$, 101 MHz):

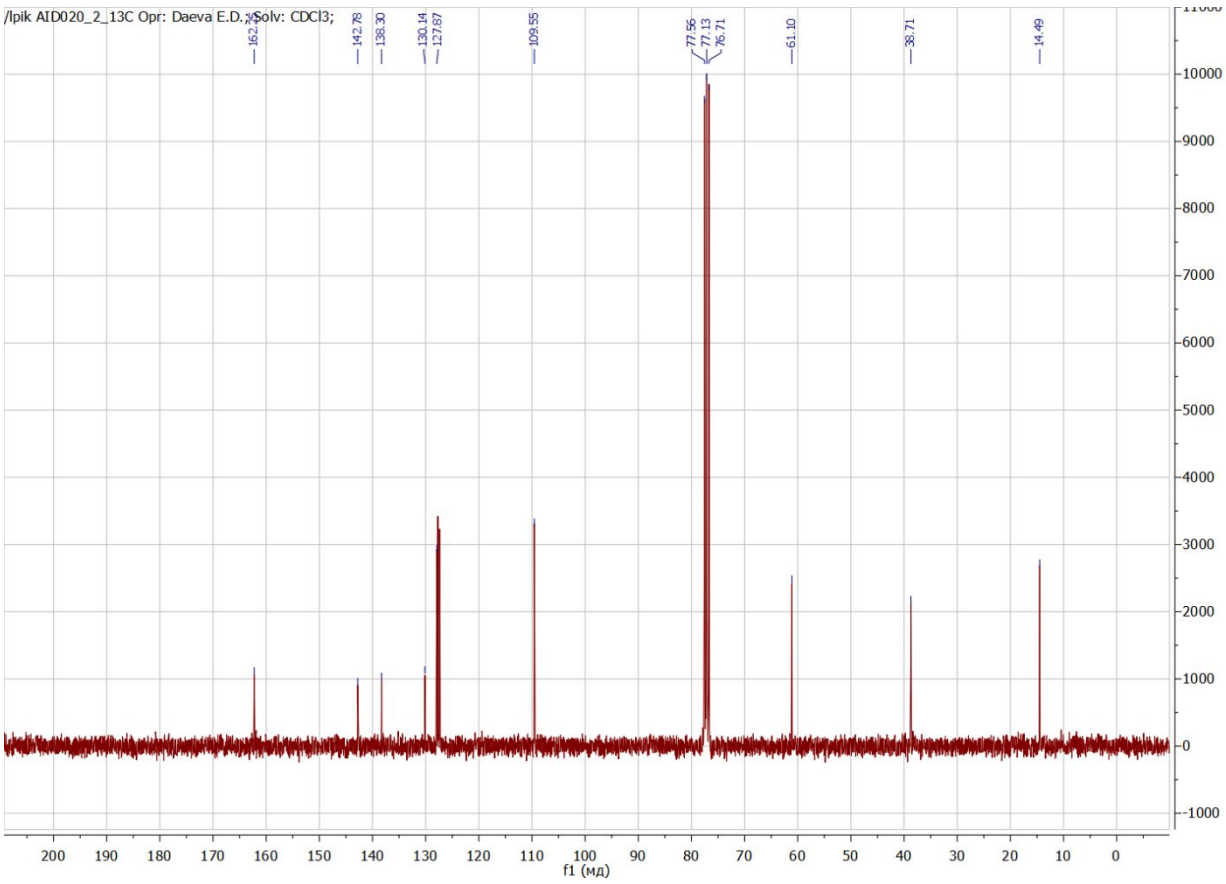

Ethyl 1-methyl-3-(thiophen-2-yl)-1*H*-pyrazole-5-carboxylate(SI-2)

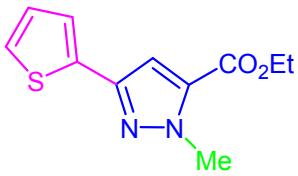

White solid. Yield 1.8 g (13%). R_f (petroleum ether-ethylacetate 3:1) = 0.53

^{1}H NMR (300 MHz, $CDCl_3$, δ/ppm) 1.42 (t, *J* = 7.1 Hz, 3H), 4.22 (s, 3H), 4.39 (q, *J* = 7.2 Hz, 2H), 7.03 (s, 1H), 7.07 (t, *J* = 4.1 Hz, 1H), 7.27 (d, *J* = 4.7 Hz, 1H), 7.34 (d, *J* = 3.4 Hz, 1H) ^{13}C NMR (101 MHz, $CDCl_3$, δ/ppm) 14.3, 39.6, 61.2, 107.8, 123.9, 127.7, 124.9, 127.6, 133.8, 135.7, 145.3, 159.8. HRMS-ESI. Calc for [$C_{11}H_{12}N_2O_2S$ +H^+]: 237.0692. Found: 237.0684

^{1}H NMR spectra of **ethyl 1-methyl-3-(thiophen-2-yl)-1*H*-pyrazole-5-carboxylate(SI-2)** ($CDCl_3$, 300 MHz):

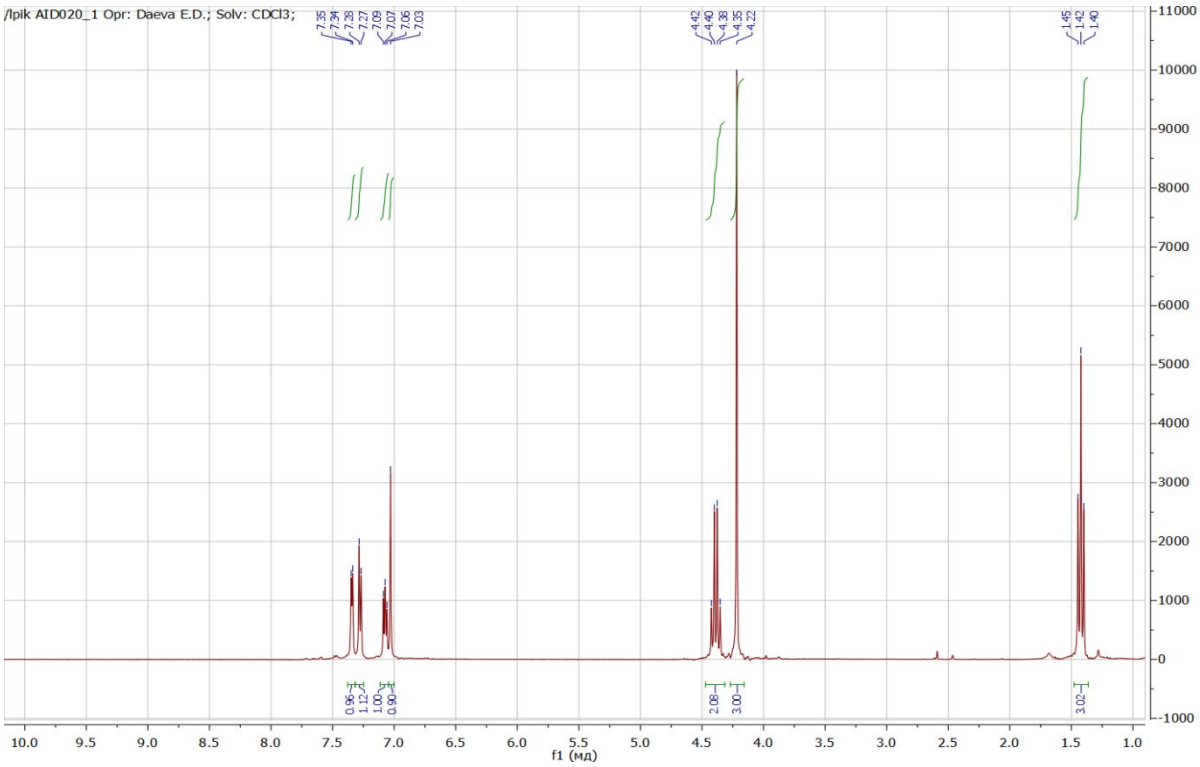

^{13}C NMR spectra of **ethyl 1-methyl-3-(thiophen-2-yl)-1*H*-pyrazole-5-carboxylate** ($CDCl_3$, 101 MHz):

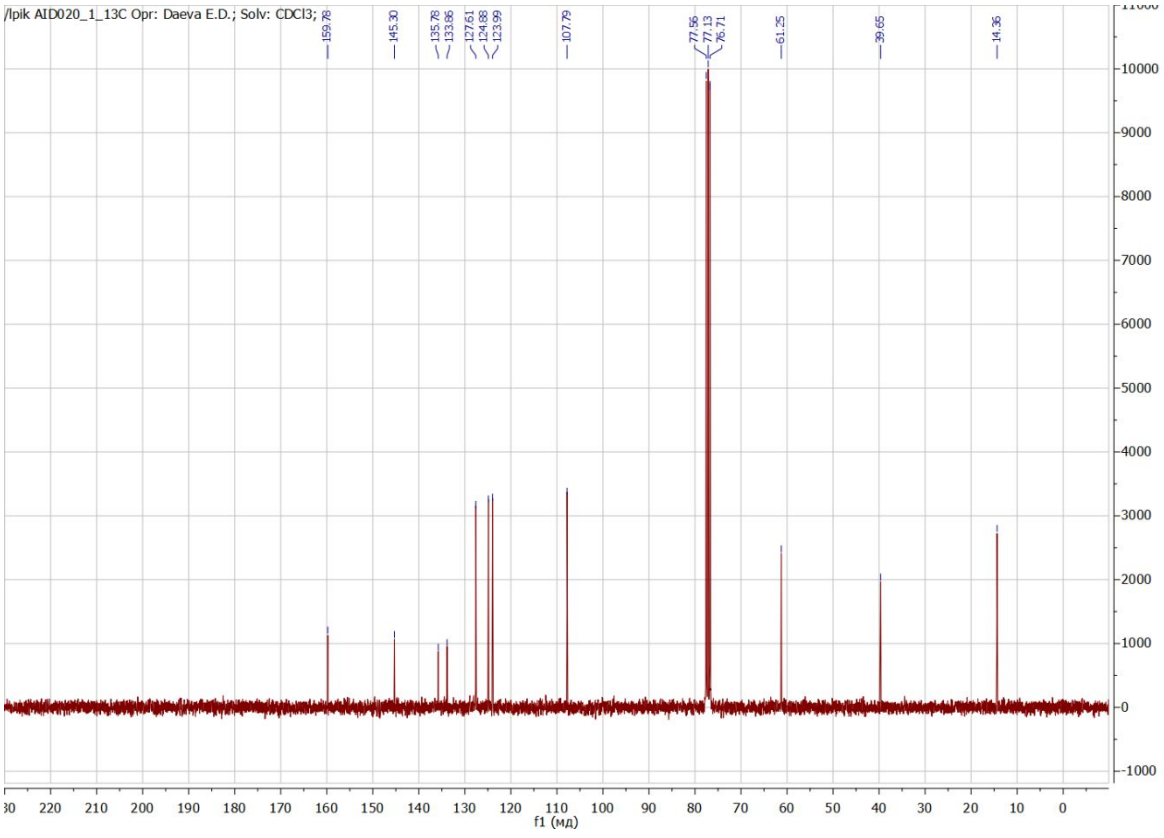

General procedure for 1*H*-pyrazole-3-carboxylic acids preparation

9 mmol of corresponding pyrazolecarboxylate was suspended in 50 ml aqueous solution of 14 mmol NaOH. The hydrolysis was carried out for 2 hours with stirring at 60 ° C until a homogeneous solution was formed. Then the solution was acidified with 2M HCl to pH 1. The precipitate formed was filtered off and washed on the filter with a small amount of water. The filtrate was extracted with ethyl acetate. The organic layer was separated and dried over anhydrous Na_2SO_4 and then concentrated under reduced pressure. The product was dried in vacuo over P_2O_5.

1-Methyl-5-(thiophen-2-yl)-1*H*-pyrazole-3-carboxylic acid (SI-3)

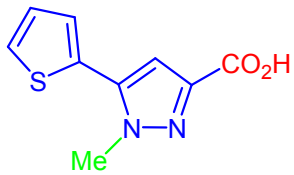

White solid. Yield 1.50 g (80%).

^{1}H NMR (300 MHz, DMSO-d_6, δ/ppm) 4.02 (s, 3H), 6.91 (s, 1H), 7.23 (t, J = 4.5 Hz, 1H), 7.49 (d, J = 3.5 Hz, 1H), 7.76 (d, J = 5.1 Hz, 1H), 12.79 (s, 1H) ^{13}C NMR (75 MHz, DMSO-d_6, δ/ppm) 38.6, 108.5, 127.9, 128.2, 129.5, 137.6, 142.4, 162.8 HRMS-ESI. Calc for [$C_9H_8N_2O_2S+H^+$]: 209.0379. Found: 209.0381

^{1}H NMR spectra of **1-methyl-5-(thiophen-2-yl)-1*H*-pyrazole-3-carboxylic acid (SI-3)**

(DMSO-d_6, 300 MHz):

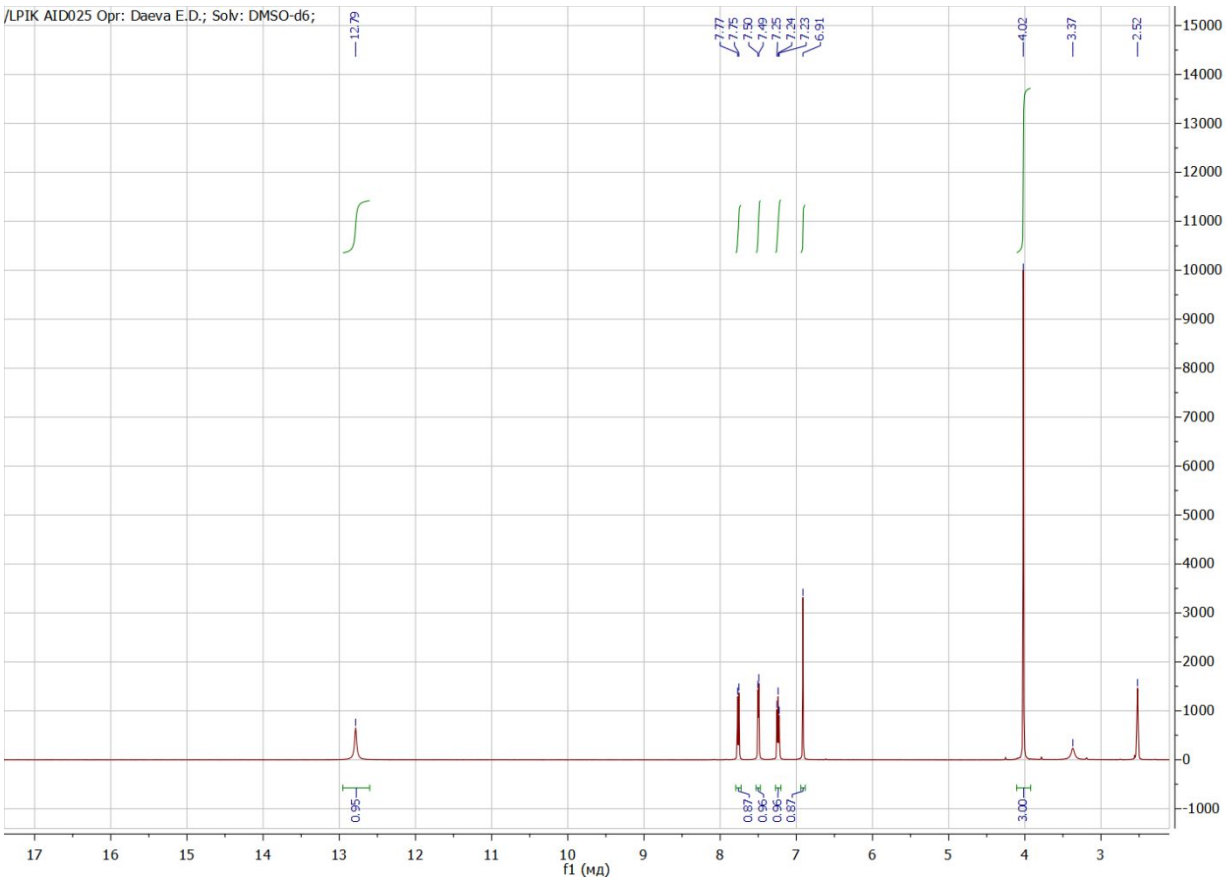
/LPIK AID025 Opr: Daeva E.D.; Solv: DMSO-d6;
12.79
7.77
7.75
7.50
7.49
7.25
7.24
7.23
6.91
4.02
3.37
2.52
0.95
0.87
0.96
0.96
0.87
3.00
f1 (мд)

^{13}C NMR spectra of **1-methyl-5-(thiophen-2-yl)-1*H*-pyrazole-3-carboxylic acid(SI-3)**

(DMSO-d_6, 75 MHz):

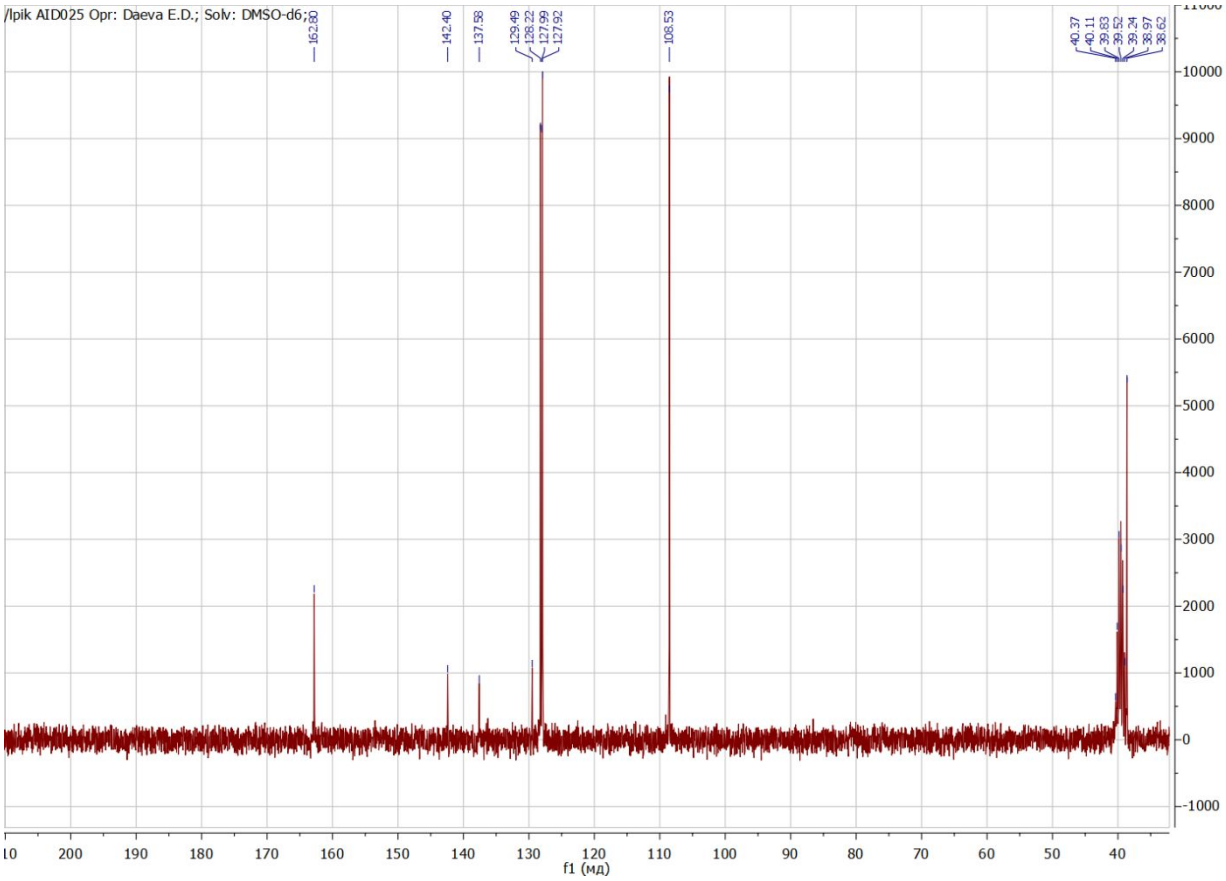

1-methyl-4,5-dihydro-1*H*-benzo[g]indazole-3-carboxylic acid (SI-4)

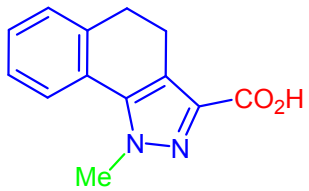

White solid. Yield 1.85 g (90%).

^{1}H NMR (300 MHz, DMSO-d_6, δ/ppm) 2.88 (s, 4H), 4.18 (s, 3H), 7.27 – 7.39 (m, 3H), 7.74 (d, J = 7.2 Hz, 1H), 12.65 (br. s, 1H). ^{13}C NMR (75 MHz, DMSO-d_6, δ/ppm) 19.9, 28.3, 39.4, 121.5, 126.8, 127.6, 128.5, 128.8, 129.4, 136.0, 145.7, 161.2. HRMS-ESI. Calc for [$C_{13}H_{12}N_2O_2$+H^+]: 229.0972. Found: 229.0973

^{1}H NMR spectra of **1-methyl-4,5-dihydro-1*H*-benzo[g]indazole-3-carboxylic acid (SI-4)** (DMSO-d_6, 300 MHz):

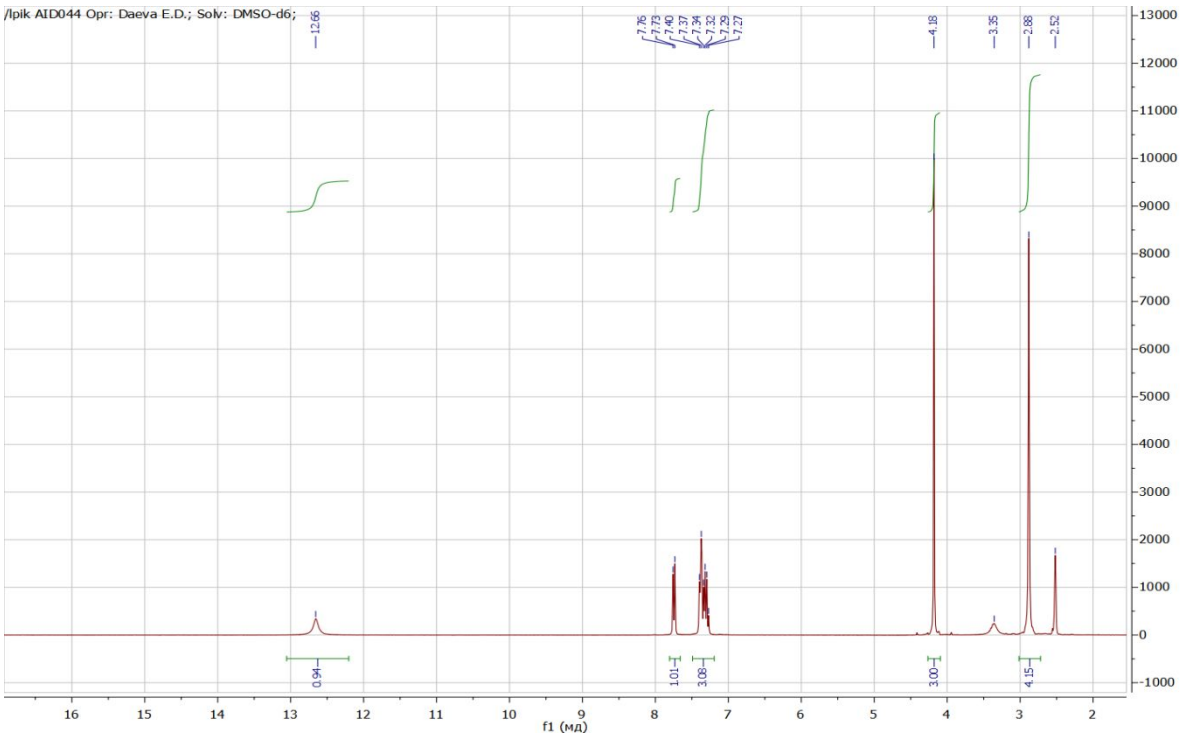

^{13}C NMR spectra of **1-methyl-4,5-dihydro-1*H*-benzo[g]indazole-3-carboxylic acid(SI-4)** (DMSO-d_6, 75 MHz):

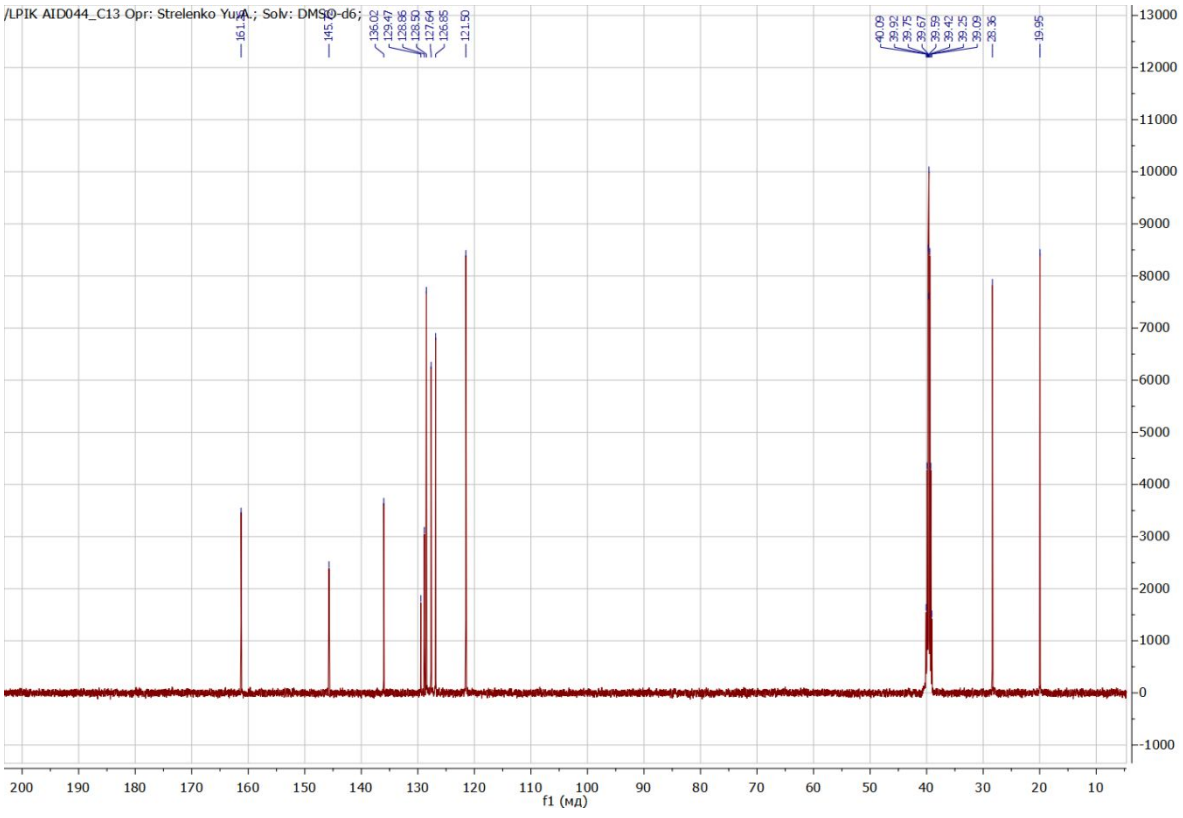

1-Methyl-5-phenyl-1*H*-pyrazole-3-carboxylic acid, 1,5-diphenyl-1*H*-pyrazole-3-carboxylic acid and 1-methyl-1,4-dihydroindeno[1,2-c]pyrazole-3-carboxylic acid were prepared according to[38,42,43].

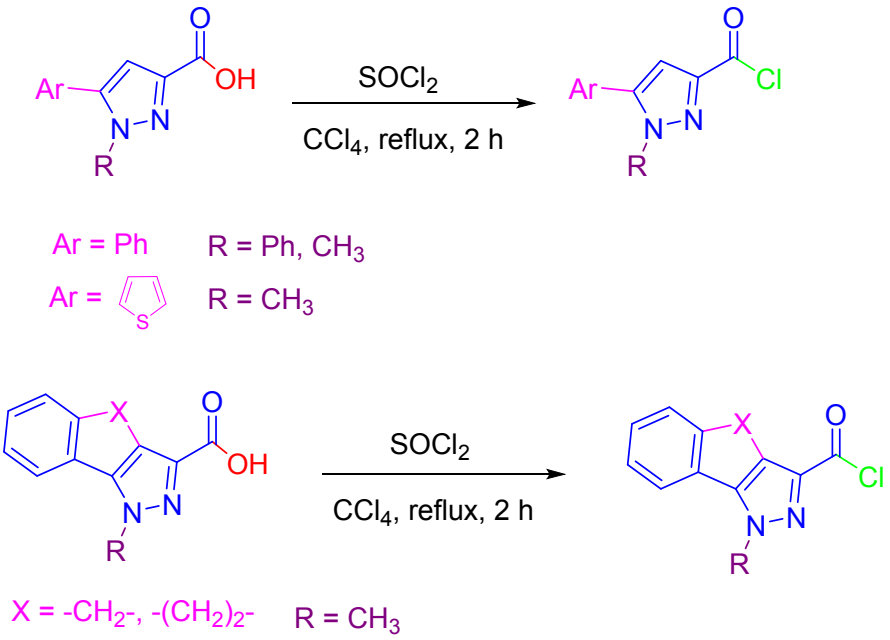

Figure S11. General schemes for the preparation pyrazole chloroanhydrides.

General procedure for pyrazole chloroanhydrides preparation:

Thionyl chloride (1 ml, 13.7 mmol) was added dropwise with stirring to the solution of 1,5-disubstituted 1H-pyrazole-3-carboxylic acid (4 mmol) in CCl_4 (50 ml). The mixture was refluxed until gas evolution stopped and the solution completely homogenized in 2 hours. The solvent evaporated to dryness and the product was dried in vacuo over P_2O_5. The product was used without further characterization.

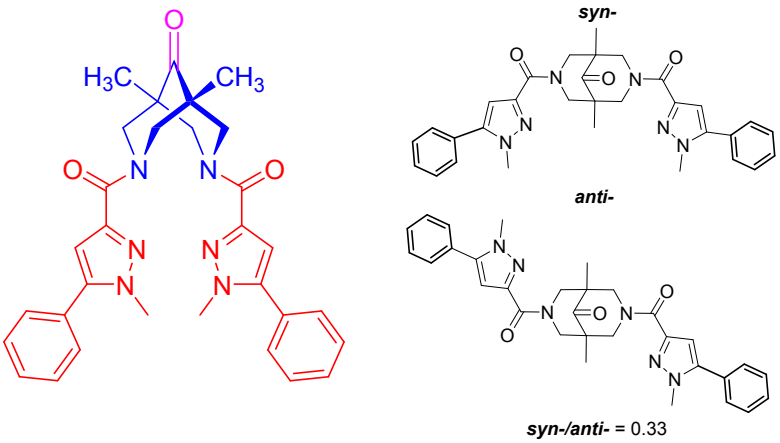

(1,5-dimethyl-9-oxo-3,7-diazabicyclo[3.3.1]nonane-3,7-diyl)bis((1-methyl-5-phenyl-1H-pyrazol-3-yl)methanone)) (2f)

Reaction time 2 h. Colorless solid. Yield 0.215 g (61%). *Syn*-/*anti*- = 0.33. M.p. 229-230°C. Purity 96% (HPLC).

^{1}H NMR (500 MHz, $CDCl_3$, δ /ppm) 1.07 (s, CCH_3 (*syn*-, *anti*-)); 1.15 (br s, CCH_3 (*syn*-)); 2.96 (d, $^2J_{HH}$ = 13.6, H(ax) (*anti*-)), 2.98, 3.42 (both br d, H(ax) (*syn*-)); 3.45 (d, $^2J_{HH}$ = 13.3, H(ax) (*anti*-)); 3.67 (br s, NCH_3 (*syn*-)); 3.88 (s, NCH_3 (*anti*-)); 5.05 (d, $^2J_{HH}$ = 13.3, $H^{2,4,6,,8}$(eq) (*anti*-)); 5.22, 5.52 (both br d, $^2J_{HH}$ = 12.0, H(eq) (*syn*-)); 6.54 (br s, $H^{4'}$ (*syn*-)); 6.84 (s, $H^{4'}$ (*anti*-)); 7.14 (br), 7.29 (br), 7.35 – 7.46 (set of m) (Ph (*syn*-, *anti*-)). ^{13}C NMR (125 MHz, $CDCl_3$, δ/ppm): 16.65 (C*C*H_3 (*anti*-)); 16.7, 16.8 (both br, C*C*H_3 (*syn*-)); 37.86 (NCH_3 (*syn*-, *anti*-)); 46.3, 46.5 (both br, $C^{1,5}$ (*syn*-)); 46.68 ($C^{1,5}$ (*anti*-)); 54.03, 58.60 (CH_2N (*anti*-)); 54.7, 57.7 (both br, CH_2N (*syn*-)); 109.08 ($CH^{4'}$ (*anti*-)); 109.6 (br, $CH^{4'}$ (*syn*-)); 128.17, 128.39,128.59, 128.62, 128.88 (*o*-CH, *m*-CH, *p*-CH (*syn*-, *anti*-)); 129.5 (br, *i*-C (*syn*-)); 129.88 (*i*-C (*anti*-)); 143.7,146.0 (both br, $C^{3',5'}$ (*syn*-)); 144.34, 145.53 ($C^{3',5'}$ (*anti*-)); 162.2 (br, C(O)N (*syn*-)); 163.59 (C(O)N (*anti*-)); 212.91 (C^9=O (*anti*-)). HRMS-ESI. Calc for [$C_{31}H_{32}N_6O_3$+H^+]: 537.2609. Found: 537.2608

^{1}H NMR spectra of compound **2f** ($CDCl_3$, 500 MHz):

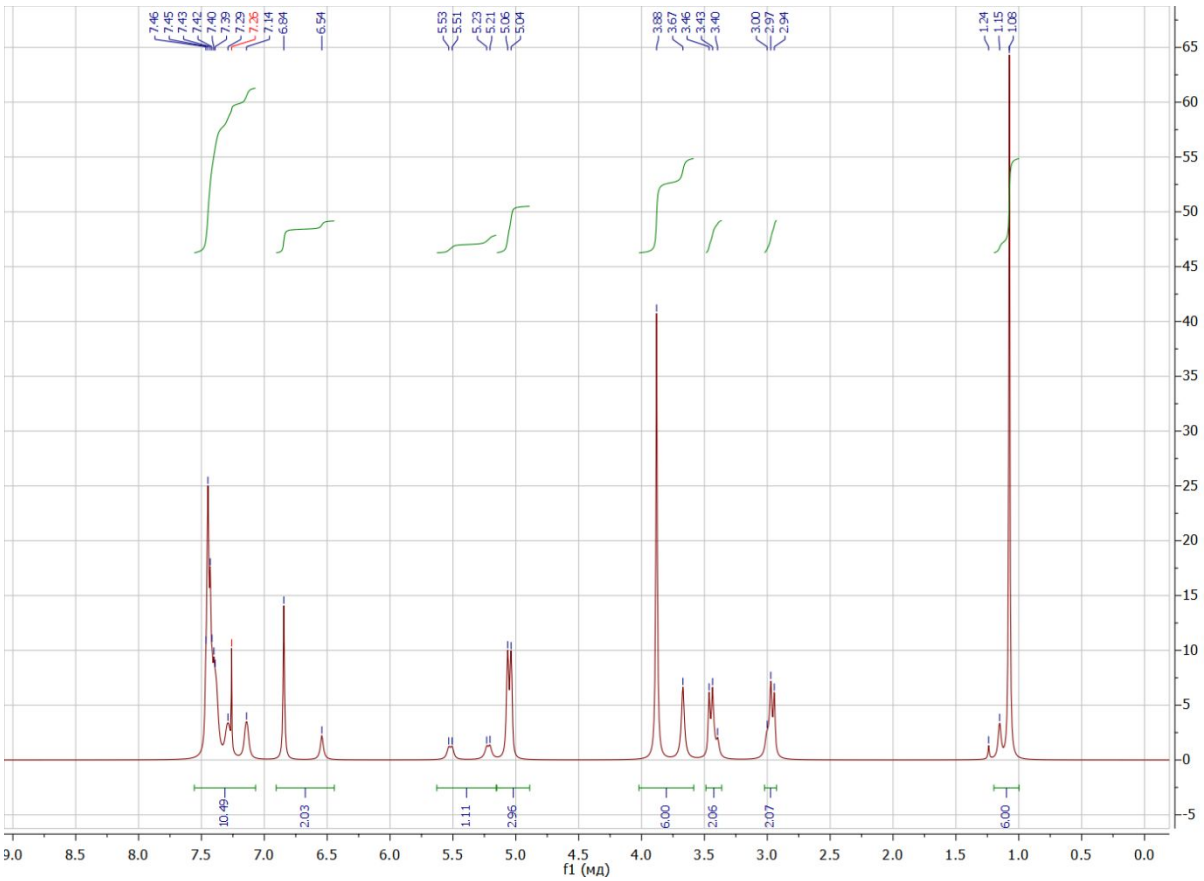

^{13}C NMR spectra of compound **2f** ($CDCl_3$, 125 MHz):

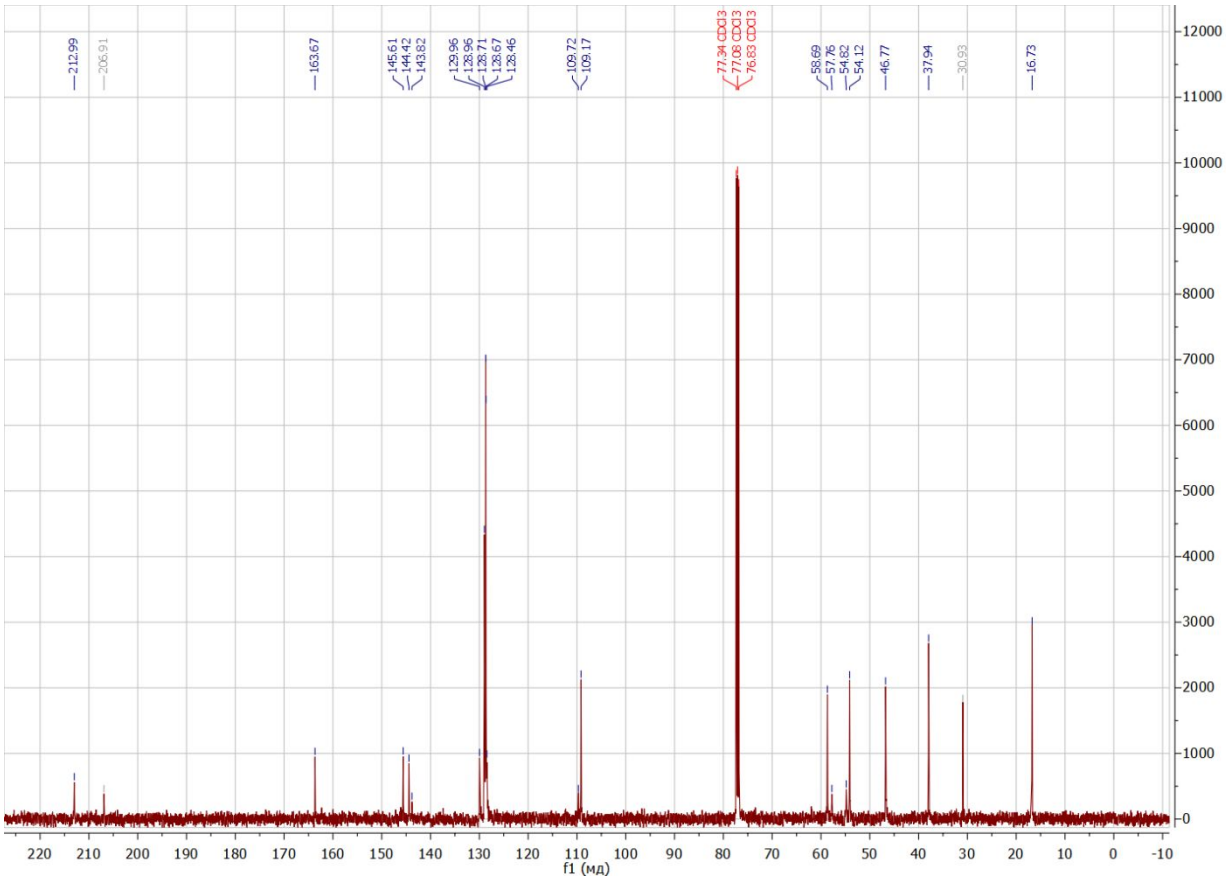

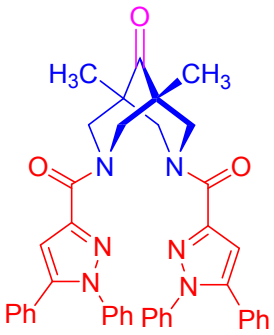

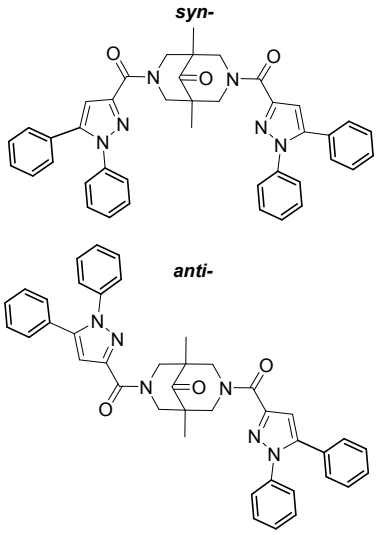

(1,5-Dimethyl-9-oxo-3,7-diazabicyclo[3.3.1]nonane-3,7-diyl)bis((1,5-diphenyl-1H-pyrazol-3-yl)methanone)) (2h)

Reaction time 2 h. Colorless solid. Yield 0.527 g (89%). M.p. 293-294°C. Purity 95% (HPLC).

Syn-/anti-forms are observed. ^{1}H NMR (400 MHz, $CDCl_3$, δ/ppm) 1.10 – 1.20 (m, 6H, CCH_3 (*syn-, anti-*)), 3.03 (t, *J* = 14.3 Hz, 2H, CH_2 (H_{ax}) (*syn-, anti-*)), 3.54 (t, *J* = 13.3 Hz, 2H, CH_2 (H_{ax}) (*syn-, anti-*)), 5.11 (t, *J* = 11.8 Hz, 2H, CH2 (H_{eq}) (*anti-*)), 5.34, 5.85 (both d, *J* = 13.6 Hz, 1H, CH2 (H_{eq}) (*syn-*)), 6.79 (s, 2H), 6.95 – 7.14 (m, 4H), 7.21 – 7.39 (m, 17H).^{13}C NMR (101 MHz, $CDCl_3$, δ/ppm) 16.72, 16.91, 16.92, 46.71, 46.91, 54.03, 54.87, 57.65, 58.80, 110.72, 111.56, 124.52, 125.37, 127.74, 127.92, 128.43, 128.46, 128.51, 128.66, 128.94, 129.01, 129.81, 139.50, 139.72, 143.37, 144.03, 147.34, 147.92, 161.86, 163.67, 212.78.

HRMS-ESI. Calc for [$C_{41}H_{36}N_6O_3$+H^+]: 661.2922. Found: 661.2949

^{1}H NMR spectra of compound **2h** ($CDCl_3$, 400 MHz):

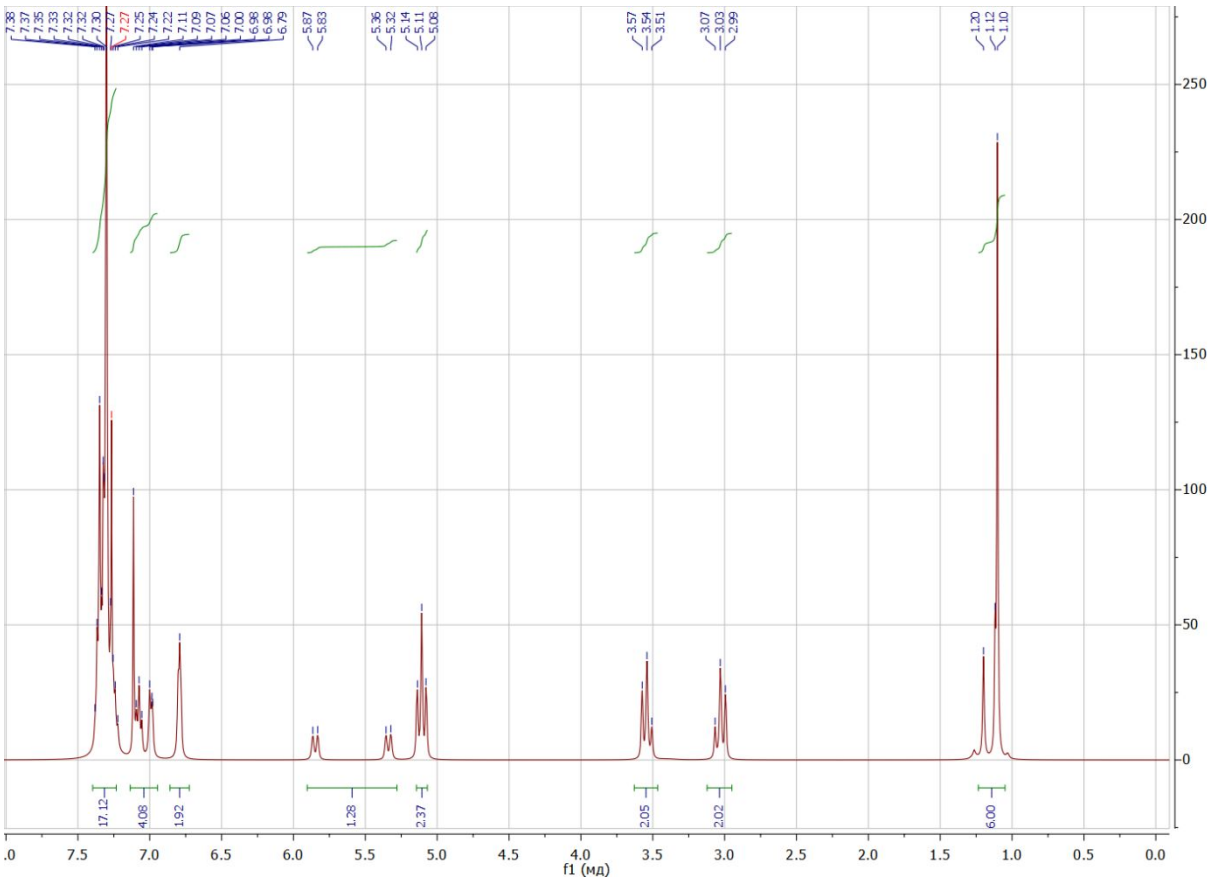
7.38
7.37
7.35
7.33
7.32
7.32
7.30
7.27
7.27
7.25
7.24
7.22
7.11
7.09
7.07
7.06
7.00
6.98
6.98
6.79
5.87
5.83
5.36
5.32
5.14
5.11
5.08
3.57
3.54
3.51
3.07
3.03
2.99
1.20
1.12
1.10
17.12
4.08
1.92
1.28
2.37
2.05
2.02
6.00
f1 (мд)

^{13}C NMR spectra of compound **2h** ($CDCl_3$, 101 MHz):

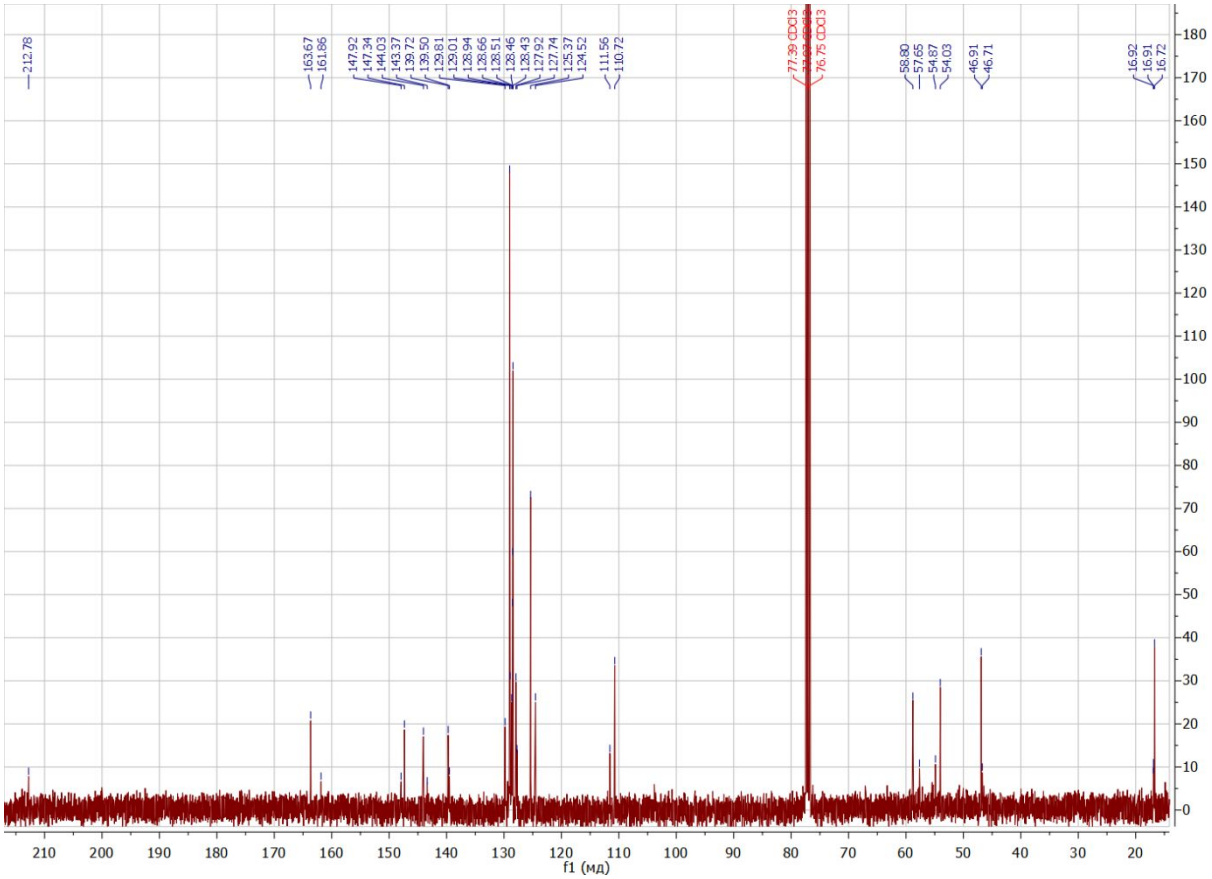

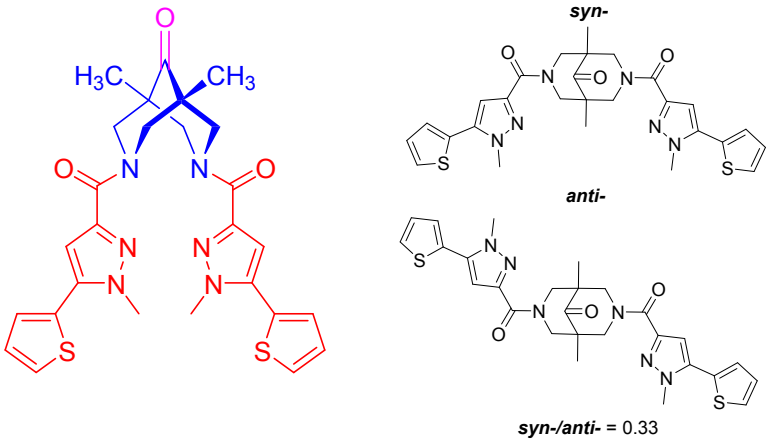

(1,5-Dimethyl-9-oxo-3,7-diazabicyclo[3.3.1]nonane-3,7-diyl)bis((1-methyl-5-(thiophen-2-yl)-1H-pyrazol-3-yl)methanone)) (2g)

Reaction time 24 h. White solid. Yield 87%. *Syn-*/*anti-* = 0.33. M.p. 256-257°C. Purity 97% (HPLC).

^{1}H NMR (500 MHz, $CDCl_3$, δ /ppm) 1.06 (s, CCH_3 (*syn-*, *anti-*)); 1.14 (s, CCH_3 (*syn-*)); 2.94 (d, $^{2}J_{HH}$ = 13.9 Hz, H(ax) (*anti-*)), 2.99, 3.37 (both d, $^{2}J_{HH}$ = 13.3 Hz, $H_{(ax)}$ (*syn-*)); 3.43 (d, $^{2}J_{HH}$ =

13.5 Hz, $H_{(ax)}$ (*anti*-)); 3.77 (s, NCH_3 (*syn*-)); 3.96 (s, NCH_3 (*anti*-)); 5.02, 5.05 (overlapping doublets, $^2J_{HH}$ = 12.6 Hz, $^2J_{HH}$ = 12.8 Hz, $H_{(eq)}$ (*anti*-)); 5.19, 5.48 (both d, $^2J_{HH}$ = 13.3 Hz, $H_{(eq)}$ (*syn*-)); 6.62 (s, $H^{4'}$ (*syn*-)); 6.91 (s, $H^{4'}$ (*anti*-)); 6.93, 6.99 (both br, $H^{3'',4''}$ (*syn*-)); 7.10 (br t, $^3J_{HH}$ = 4.2 Hz, $H^{4''}$ (*anti*-)); 7.21 (br d, $^3J_{HH}$ = 2.8 Hz, $H^{3''}$ (*anti*-)); 7.31 (br, $H^{5''}$(*syn*-)); 7.40 (br d, $^3J_{HH}$ = 4.8 Hz, $H^{5''}$ (*anti*-)). ^{13}C NMR (125 MHz, $CDCl_3$, δ /ppm) 16.61 ($C\underline{\mathbf{C}}H_3$ (*syn*-, *anti*-)); 16.83 ($C\underline{\mathbf{C}}H_3$ (*syn*-)); 38.19 (NCH_3 (*syn*-, *anti*-)); 46.23, 46.53 ($C^{1,5}$ (*syn*-)); 46.69 ($C^{1,5}$ (*anti*-)); 54.01, 58.54 (CH_2N (*anti*-)); 54.71, 57.58 (CH_2N (*syn*-)); 109.83 ($CH^{4'}$ (*anti*-)); 110.15 ($CH^{4'}$ (*syn*-)); 126.76, 126.91,126.97, 127.53, 127.56 ($CH^{3'',4'',5''}$ (*syn*-, *anti*-)); 130.17 ($C^{2''}$ (*syn*-)); 130.35 ($C^{2''}$ (*anti*-)); 136.99 ($C^{5'}$ (*syn*-)); 137.55 ($C^{5'}$ (*anti*-)); 145.52 ($C^{3'}$ (*anti*-)); 145.91 ($C^{3'}$ (*syn*-)); 161.96 (C(O)N (*syn*-)); 163.19 (C(O)N (*anti*-)); 212.81 (C^9=O (*anti*-)); 213.05 (C^9=O (*syn*-)). HRMS-ESI. Calc for [$C_{27}H_{28}N_6O_3S_2$+H^+]: 549.1737. Found: 549.1731

^{1}H NMR spectra of compound **2g** ($CDCl_3$, 500 MHz):

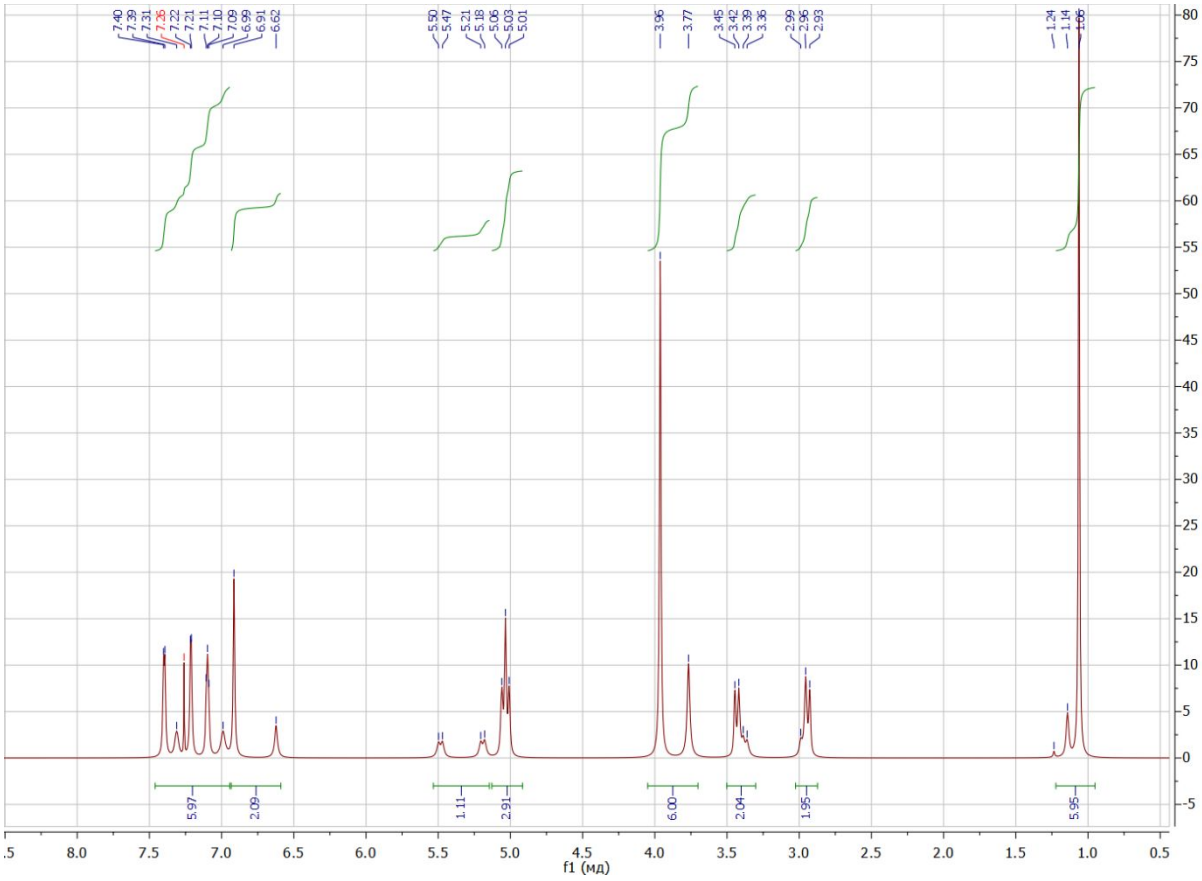

^{13}C NMR spectra of compound **2g** ($CDCl_3$, 125 MHz):

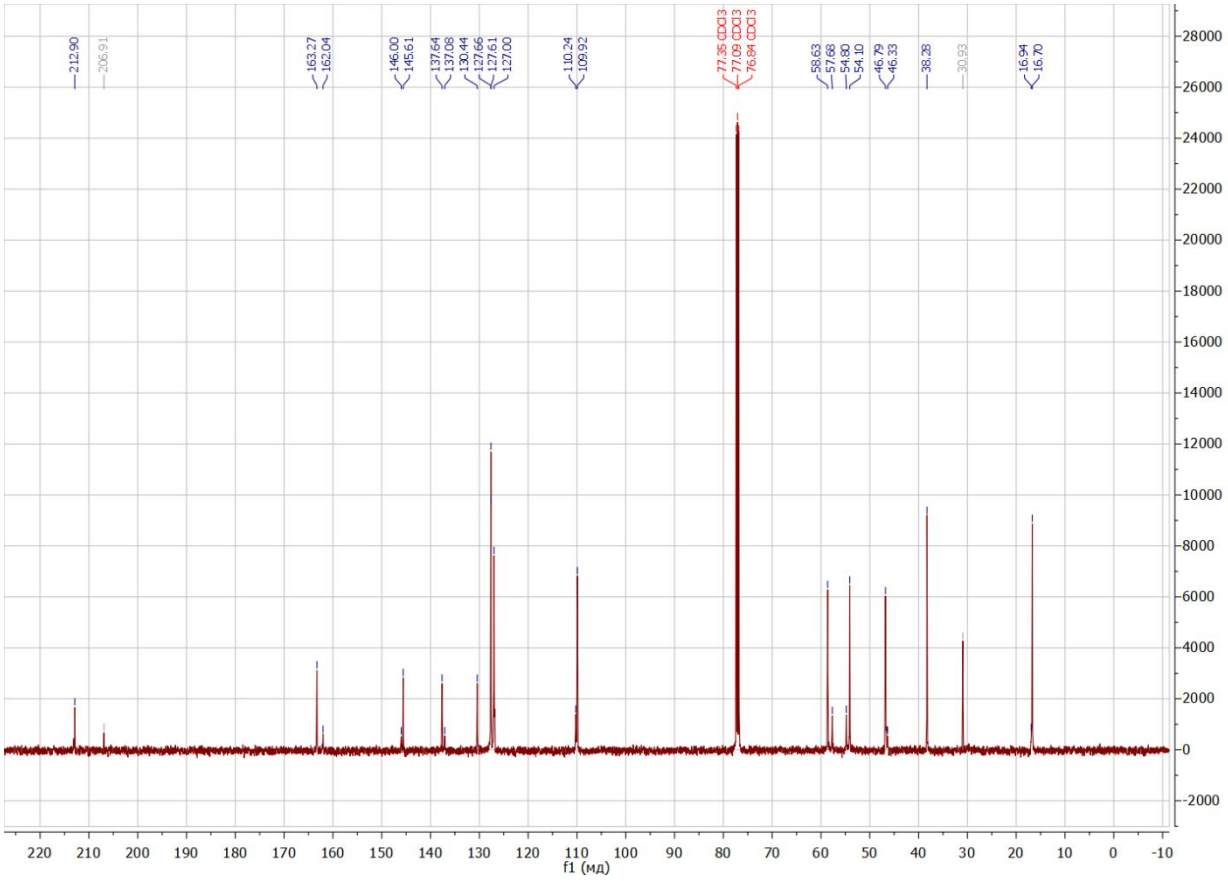

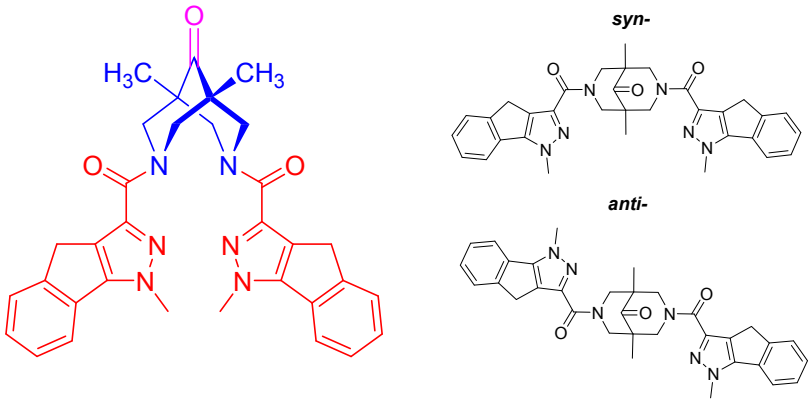

syn-/anti- = 1.43

(1,5-Dimethyl-9-oxo-3,7-diazabicyclo[3.3.1]nonane-3,7-diyl)bis((1-methyl-1,4-dihydroindeno[1,2-c]pyrazol-3-yl)methanone)) (2i)

Reaction time 24h. White solid. Yield 88%. *Syn-*/*anti-* = 1.43. M.p. 297-298°C. Purity 95% (HPLC).

^{1}H NMR (500 MHz, $CDCl_3$, δ /ppm) 1.08 (s, CCH_3 (*anti-*)); 1.09, 1.15 (both s, CCH_3 (*syn-*)); 2.96 (d, $^2J_{HH}$ = 13.7 Hz, $H_{(ax)}$ (*anti-*)); 2.97 (d, $^2J_{HH}$ = 13.4 Hz, $H_{(ax)}$ (*syn-*)), 3.18, 3.45 (both d, $^2J_{HH}$ = 21.7 Hz, CH_2 (*syn-*)); 3.32 (d, $^2J_{HH}$ = 13.5 Hz, $H_{(ax)}$ (*syn-*)); 3.46 (d, $^2J_{HH}$ = 13.5 Hz, $H_{(ax)}$

(*anti*-)); 3.71, 3.79 (*AB*-system, $^{2}J_{HH}$ = 21.5 Hz, CH_2 (*anti*-)); 3.79 (s, NCH_3 (*syn*-)); 4.15 (s, NCH_3 (*anti*-)); 5.00 (d, $^{2}J_{HH}$ = 13.7 Hz, $H_{(eq)}$ (*anti*-)); 5.24 (d, $^{2}J_{HH}$ = 13.3 Hz, $H_{(eq)}$ (*syn*-)); 5.32 (d, $^{2}J_{HH}$ = 13.5 Hz, $H_{(eq)}$ (*anti*-)); 5.94 (d, $^{2}J_{HH}$ = 13.5 Hz, $H_{(eq)}$ (*syn*-)); 6.95 – 7.11 (set of m, $H_{(Ar)}$ (*syn*-)); 7.25 (t, $^{3}J_{HH}$ = 7.4 Hz, $H_{(Ar)}$ (*anti*-)); 7.34 (t, $^{3}J_{HH}$ = 7.5 Hz, $H_{(Ar)}$ (*anti*-)); 7.42 (d, $^{3}J_{HH}$ = 7.4 Hz, $H_{(Ar)}$ (*anti*-)); 7.53 (d, $^{3}J_{HH}$ = 7.5 Hz, $H_{(Ar)}$ (*anti*-)). ^{13}C NMR (125 MHz, $CDCl_3$, δ /ppm) 16.63, 16.91 ($C\underline{C}H_3$ (*syn*-)); 16.74 ($C\underline{C}H_3$ (*anti*-)); 29.69 (CH_2 (*syn*-)); 30.18 (CH_2 (*anti*-)); 37.69 (NCH_3 (*syn*-)); 38.15 (NCH_3 (*anti*-)); 46.33, 46.78 ($C^{1,5}$ (*syn*-)); 46.92 ($C^{1,5}$ (*anti*-)); 54.04, 58.61 (CH_2N (*anti*-)); 54.60, 57.04 (CH_2N (*syn*-)); 117.46, 125.96, 126.05, 126.18 (CH(Ar) (*syn*-)); 118.21, 126.24, 126.33, 126.52 (CH(Ar) (*anti*-)); 129.78, 131.56 (C(Ar) (*anti*-)); 130.67, 131.18 (C(Ar) (*syn*-)); 139.80 ($C^{3'}$ (*anti*-)); 139.98 ($C^{3'}$ (*syn*-)); 148.46, 149.00 ($C^{4',5'}$ (*syn*-)); 149.45, 149.54 ($C^{4',5'}$ (*anti*-)); 161.79 (C(O)N (*syn*-)); 162.75 (C(O)N (*anti*-)); 213.18 (C^{9}=O (*anti*-)); 213.30 (C^{9}=O (*syn*-)). HRMS-ESI. Calc for [$C_{33}H_{32}N_6O_3$+H^+]: 561.2609. Found: 561.2591

^{1}H NMR spectra of compound **2i** ($CDCl_3$, 500 MHz):

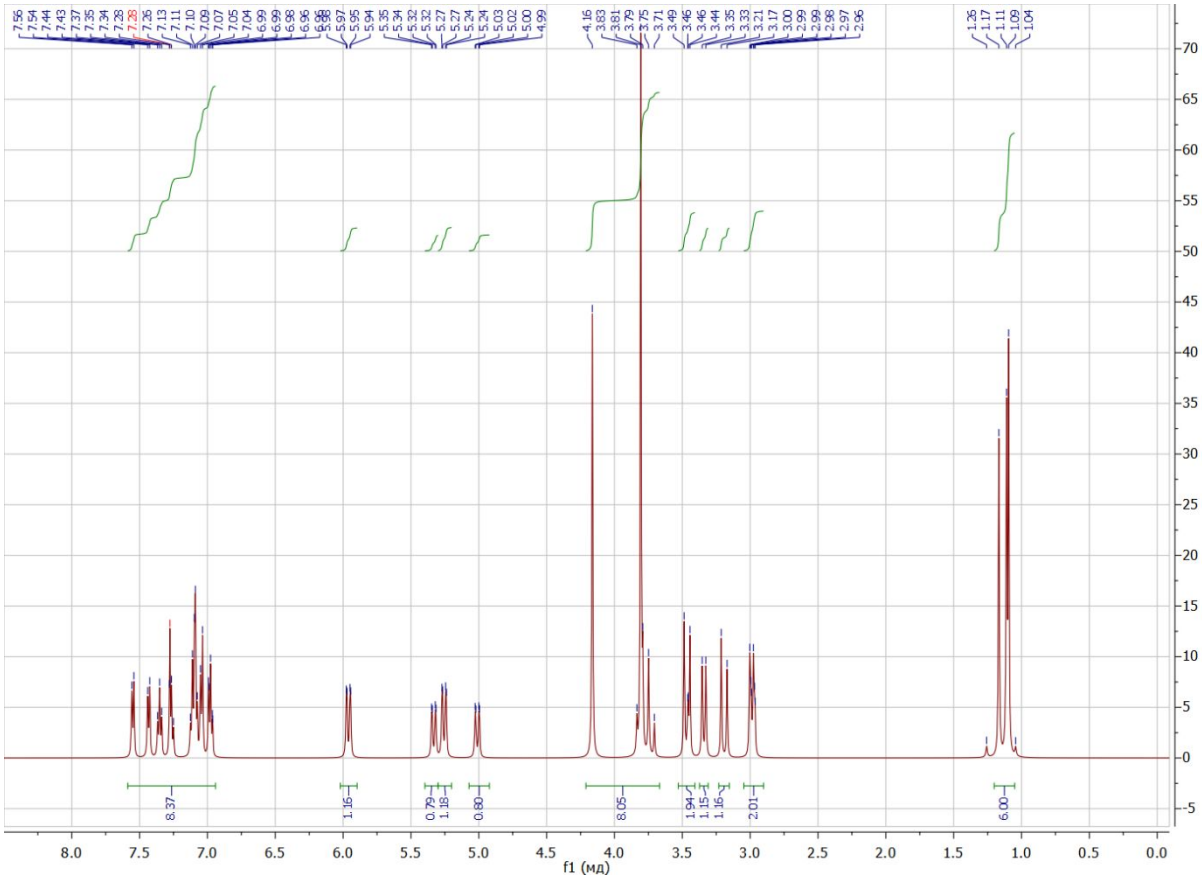

^{13}C NMR spectra of compound **2i** ($CDCl_3$, 125 MHz):

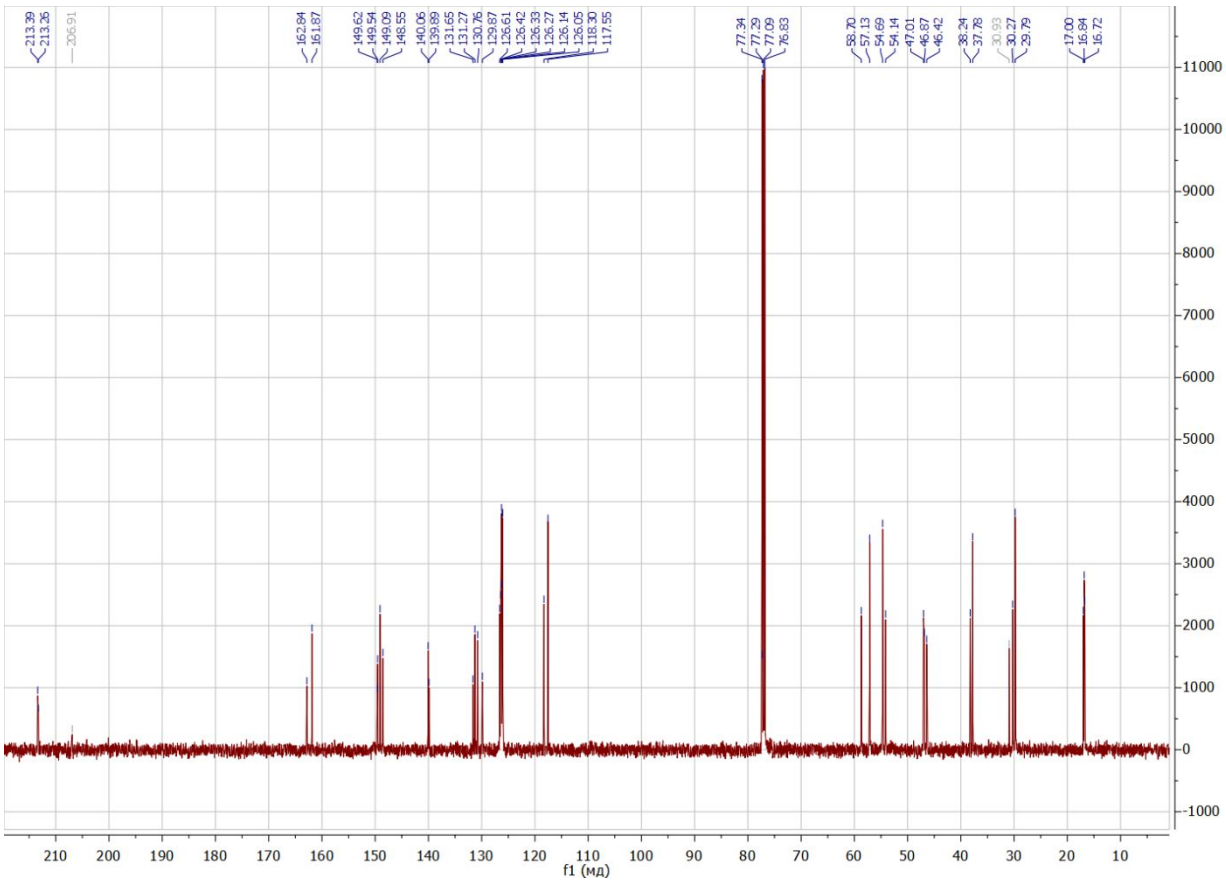

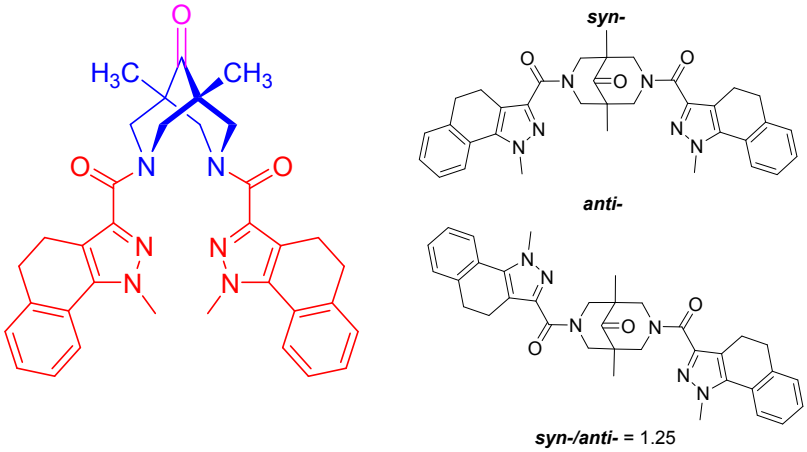

(1,5-Dimethyl-9-oxo-3,7-diazabicyclo[3.3.1]nonane-3,7-diyl)bis((1-methyl-4,5-dihydro-1H-benzo[g]indazol-3-yl)methanone)) (2j)

Reaction time 24h. Yield 91%. *Syn-*/*anti-* = 1.25. M.p. 302-303°C. Purity 95% (HPLC).

^{1}H NMR (500 MHz, $CDCl_3$, δ/ppm) 1.07, 1.15 (both s, CCH_3 (*syn-*)); 1.09 (s, CCH_3 (*anti-*)); 2.38 – 2.92 (set of m, CH_2CH_2 (*syn-*, *anti-*)); 2.98 (d, $^2J_{HH}$ = 13.4 Hz, $H_{(ax)}$ (*syn-*)), 2.99 (d,

$^{2}J_{HH}$ = 13.5 Hz, $H_{(ax)}$ (*anti*-)); 3.35 (d, $^{2}J_{HH}$ = 13.4 Hz, $H_{(ax)}$ (*syn*-)), 3.42 (d, $^{2}J_{HH}$ = 13.5 Hz, $H_{(ax)}$ (*anti*-)); 3.86 (s, NCH_3 (*syn*-)); 4.17 (s, NCH_3 (*anti*-)); 5.07, 5.38 (both d, $^{2}J_{HH}$ = 13.5 Hz, $H_{(eq)}$ (*anti*-)); 5.18, 5.64 (both d, $^{2}J_{HH}$ = 13.4 Hz, $H_{(eq)}$ (*syn*-)); 7.10 – 7.30 (set of m, $H_{(Ar)}$ (*syn*-, *anti*-)); 7.55 (d, $^{3}J_{HH}$ = 7.6, $H_{(Ar)}$ (*anti*-)). ^{13}C NMR (125 MHz, $CDCl_3$, δ /ppm) 16.74 ($C\underline{\mathbf{C}}H_3$ (*syn*-)); 16.94 ($C\underline{\mathbf{C}}H_3$ (*syn*-, *anti*-)); 19.47, 29.95 (CH_2CH_2 (*syn*-)); 19.86, 30.55 (CH_2CH_2 (*anti*-)); 39.52 (NCH_3 (*syn*-)); 39.95 (NCH_3 (*anti*-)); 46.41, 46.60 ($C^{1,5}$ (*syn*-)); 46.66 ($C^{1,5}$ (*anti*-)); 54.23, 58.39 (CH_2N (*anti*-)); 54.47, 57.43 (CH_2N (*syn*-)); 121.39, 122.01, 122.09, 122.85, 126.36, 126.44, 126.59, 126.87, 127.58, 127.59, 128.84, 128.95 (C(Ar), CH(Ar) (*syn*-, *anti*-)); 137.69, 137.91, 138.21, 138.72, 140.61, 140.79 ($C^{3',4',5'}$ (*syn*-, *anti*-)); 162.57 (C(O)N (*syn*-)); 162.82 (C(O)N (*anti*-)); 213.54, 213.56 (C^{9}=O (*syn*-, *anti*-)). HRMS-ESI. Calc for [$C_{35}H_{36}N_6O_3$+H^+]: 589.2922. Found: 589.2911

^{1}H NMR spectra of compound **2j** ($CDCl_3$, 500 MHz):

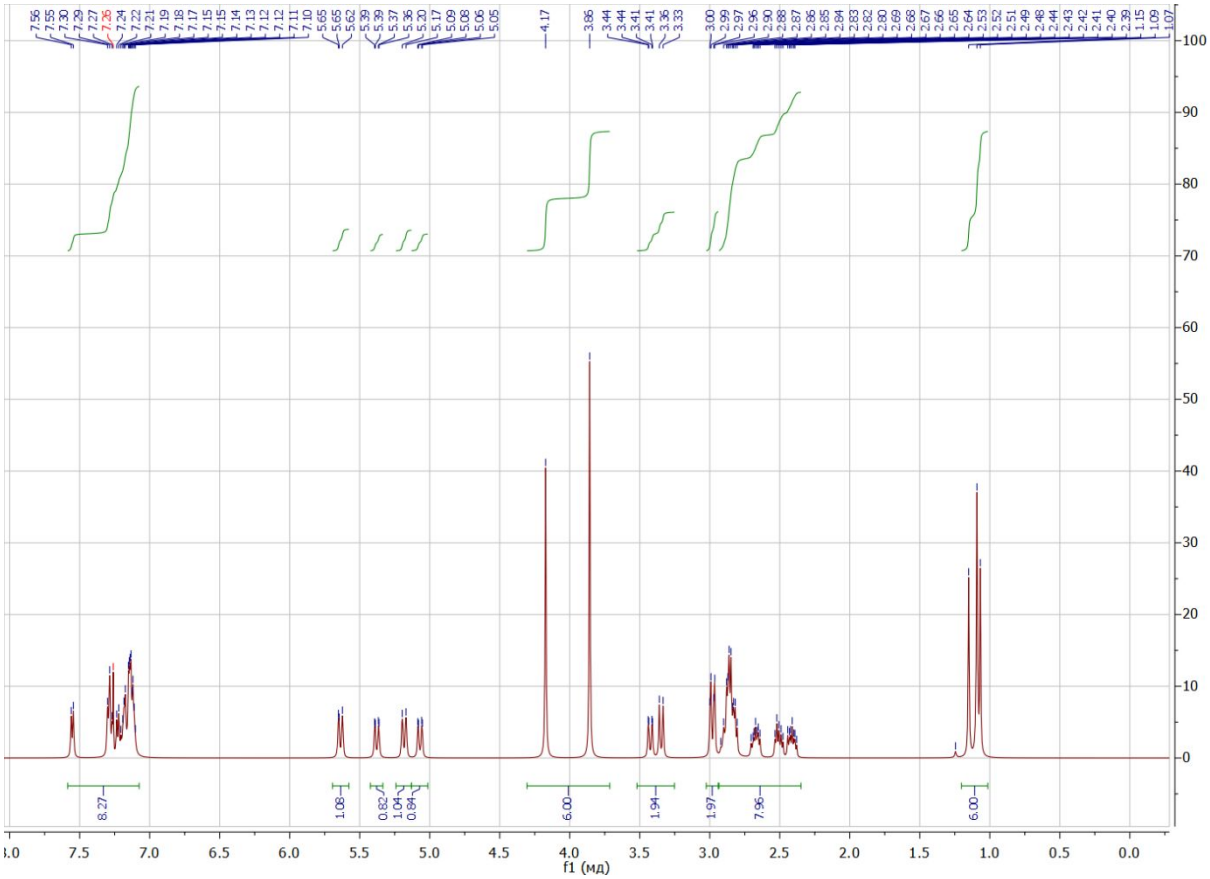

^{13}C NMR spectra of compound **2j** ($CDCl_3$, 125 MHz):

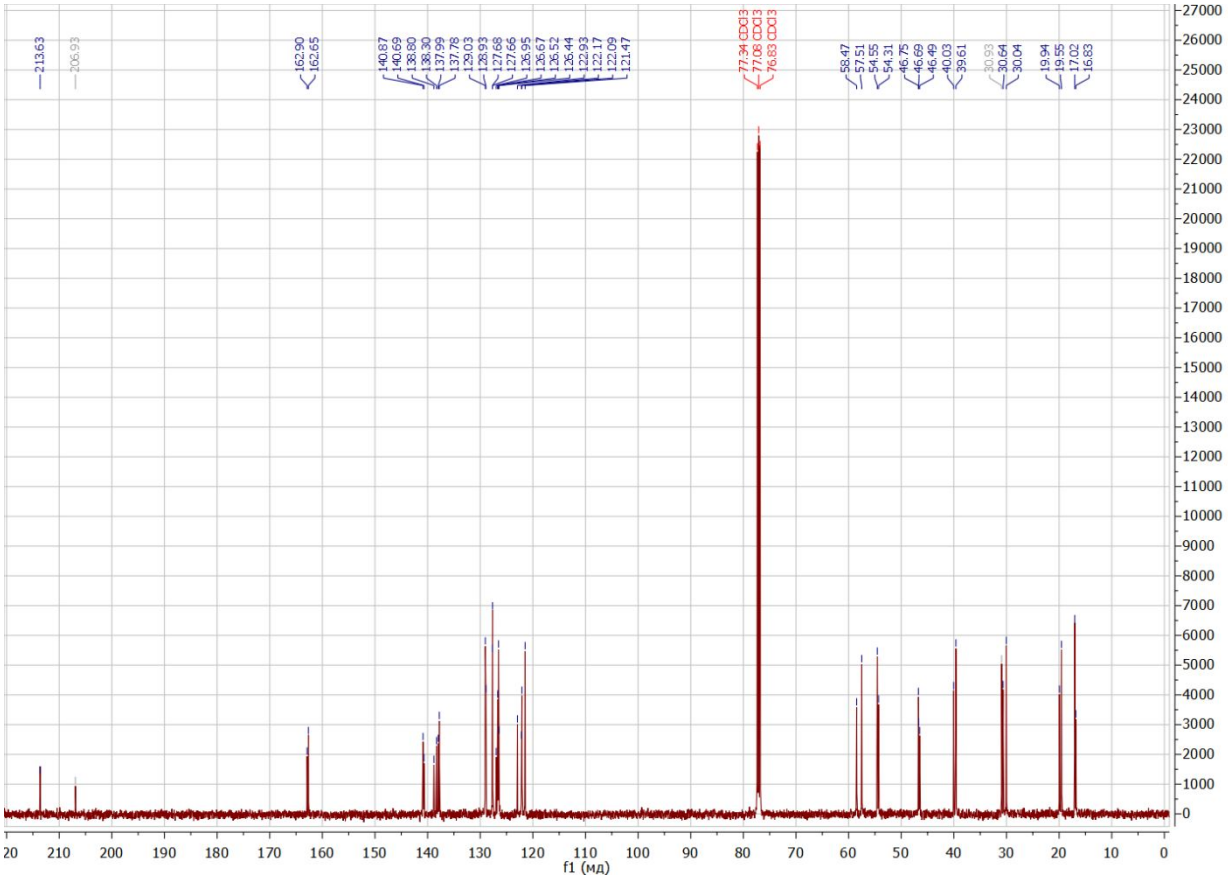

Alkylation reactions

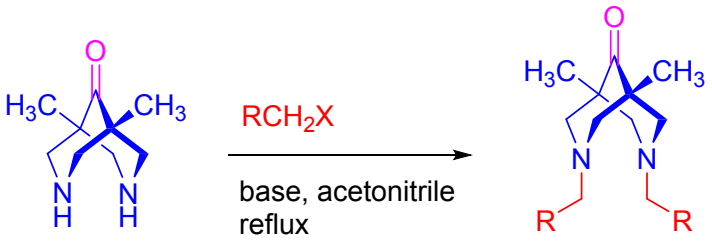

Scheme S5. General procedure for alkylation.

General procedure for alkylation. Alkylating agent (6 mmol) and DIPEA (6 mmol) or triethylamine (6 mmol) were added to the solution of amine (3 mmol) in dry acetonitrile (11 ml). The reaction mixture was refluxed for 18 h, cooled to room temperature and evaporated to dryness. The residue was diluted in DCM (25 ml) and water (15 ml). The organic phase was separated, dried over sodium sulfate, and evaporated to dryness to give the product.

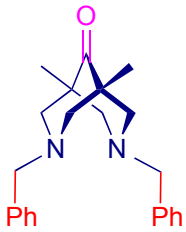

(3,7-Dibenzyl-1,5-dimethyl-3,7-diazabicyclo[3.3.1]nonan-9-one) (4d). Dry K_2CO_3 (1.07 g, 7.76 mmol) was added to the solution of 1,5-dimethyl-3,7-diazabicyclo[3.3.1]nonan-9-one (0.326 g, 1.94 mmol) in dry DMF (10 ml). The solution of benzyl bromide (0.461 ml, 3.88 mmol) in dry DMF (7 ml) was added. The suspension was refluxed for 10 hours. The orange suspension was filtered, the powder was washed 2*5 ml DCM. The filtrate was evaporated, and the residue was dissolved in DCM (25 ml) and water (4 ml). The organic layer was separated, washed with brine, and dried over sodium sulfate. All volatiles were removed to give the beige powder. Yield 0.508 g (75%).

Purity 99% (HPLC).

^{1}H NMR (300 MHz, $CDCl_3$, δ/ppm) 0.96 (s, 6 H), 2.39 (d, *J*=10.27 Hz, 4 H), 2.96 - 3.17 (m, 4 H), 3.54 (s, 4 H), 7.33 (br. s., 10 H). ^{13}C NMR (75 MHz, $CDCl_3$, δ/ppm) 20.04; 46.77; 61.37; 65.53; 127.12; 128.32; 128.76; 138.45; 215.79 HRMS-ESI. Calc for [$C_{23}H_{28}N_2O$+H^+]: 349.2274. Found: 349.2282

^{1}H NMR spectra of compound **4d** ($CDCl_3$, 300 MHz):

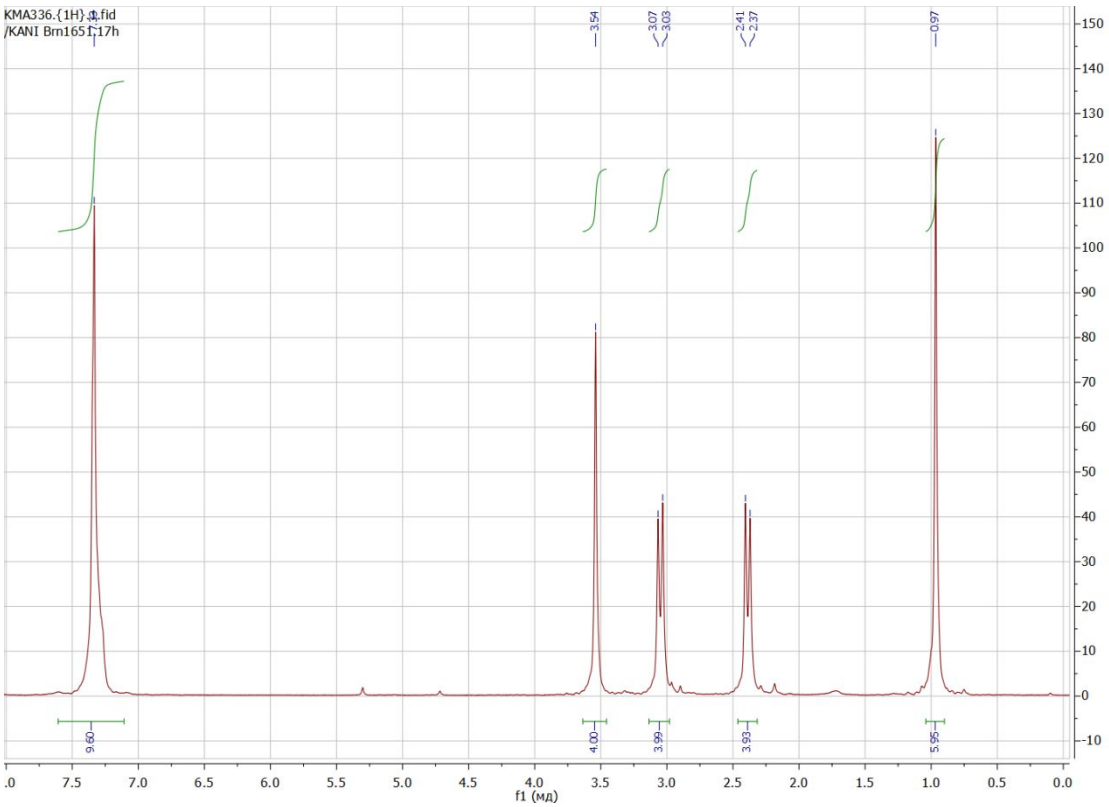

^{13}C NMR spectra of compound **4d** ($CDCl_3$, 75 MHz):

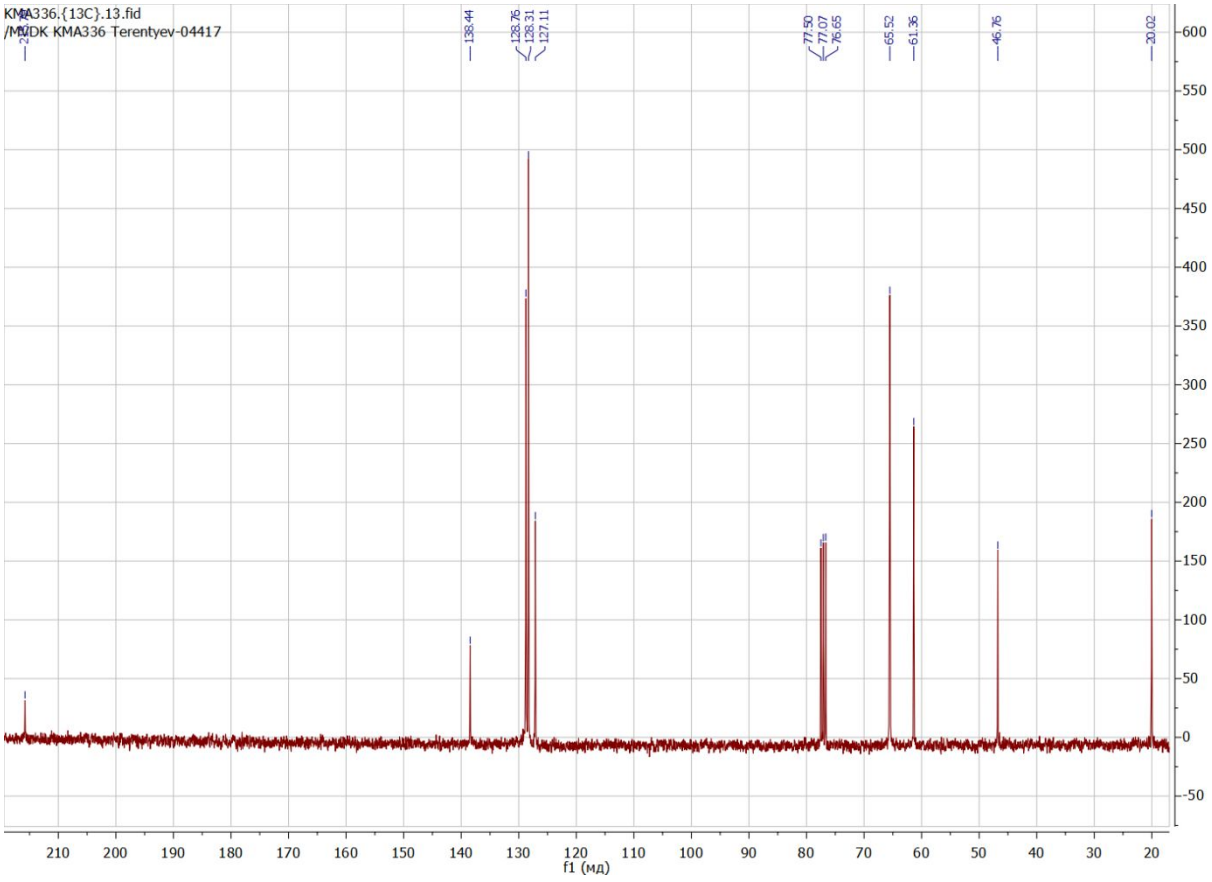

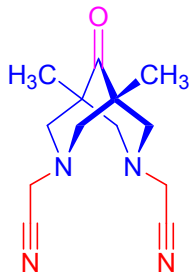

(2,2'-(-1,5-Dimethyl-9-oxo-3,7-diazabicyclo[3.3.1]nonane-3,7-diyl)diacetonitrile) (4l)

Beige powder. Yield 88%. RCH_2X – chloroacetonitrile, base – DIPEA, reflux time 18 h.

M.p. 137-139°C. Purity 95% (HPLC).

^1H NMR (400 MHz, $CDCl_3$, δ /ppm) 1.04 (s, 6 H), 2.63 (d, *J*=11.00 Hz, 4 H), 3.11 (d, *J*=11.00 Hz, 4 H), 3.58 (s, 4 H). ^{13}C NMR (100 MHz, $CDCl_3$, δ /ppm) 19.35, 44.94, 48.12, 64.07, 114.06, 211.75. HRMS-ESI. Calc for $[C_{13}H_{18}N_4O+H^+]$: 247.1553. Found: 247.1568

^{1}H NMR spectra of compound **4l** ($CDCl_3$, 400 MHz):

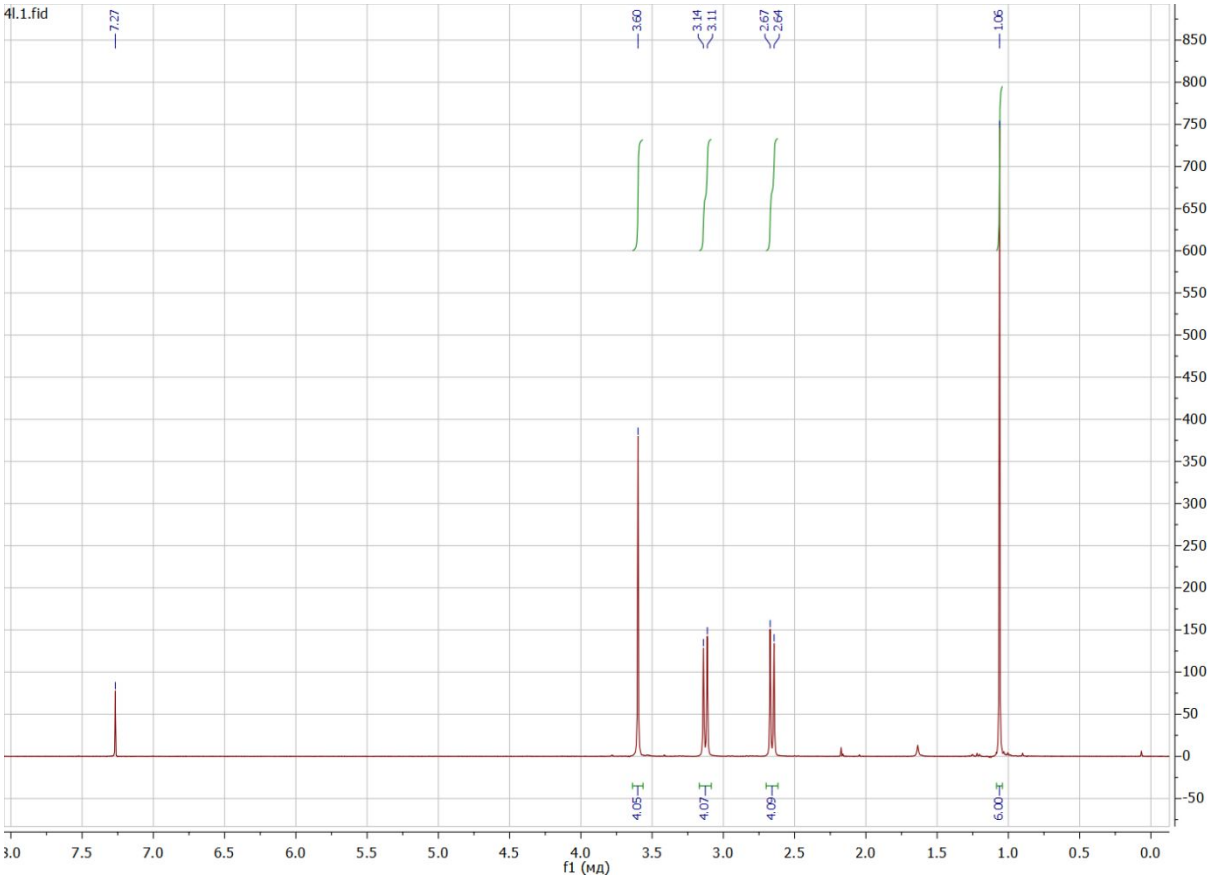

^{13}C NMR spectra of compound **4l** ($CDCl_3$, 100 MHz):

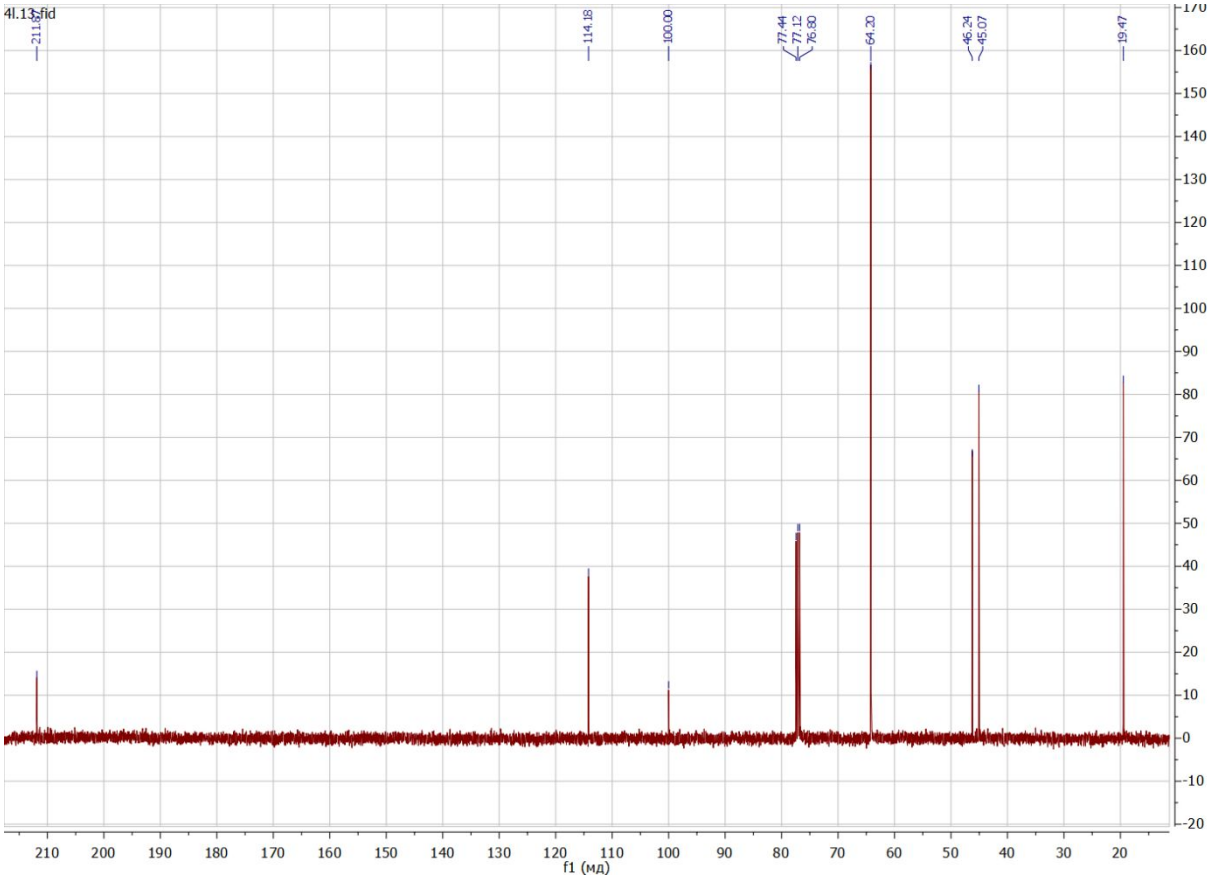

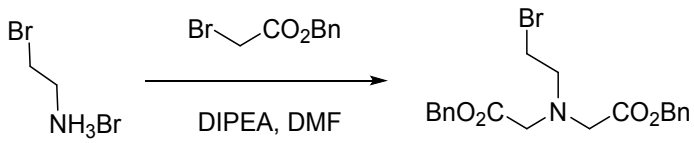

SI-5

Scheme S6. Preparation of dibenzyl 2,2'-((2-bromoethyl)azanediyl)diacetate.

Dibenzyl 2,2'-((2-bromoethyl)azanediyl)diacetate (SI-5). The benzyl bromoacetate (1.37 g, 6 mmol) and DIPEA (2.09 ml, 12 mmol) were added to the solution of 2-bromoethylamine hydrobromide (0.62 g, 3 mmol) in DMF (6 ml). The suspension was stirred for 2 h. The volatiles were removed, and the residue was quenched with ethyl acetate (25 ml) and water (5*18 ml). The organic layer was separated, dried over sodium sulfate, and evaporated to dryness. The product was purified with column chromatography on silica, eluent – petroleum ether: ethyl acetate 9:1.

Light yellow oil. Yield 0.88 g (70%)

^{1}H NMR (400 MHz, $CDCl_3$, δ/ppm) 3.21 (d, *J*=7.46 Hz, 2 H), 3.41 (d, *J*=7.58 Hz, 2 H), 3.69 (s, 4 H), 5.15 (s, 4 H), 7.29 - 7.44 (m, 10 H). ^{13}C NMR (101 MHz, $CDCl_3$, δ/ppm) 29.81, 55.38, 55.49, 66.54, 128.34, 128.60, 135.39, 170.72.

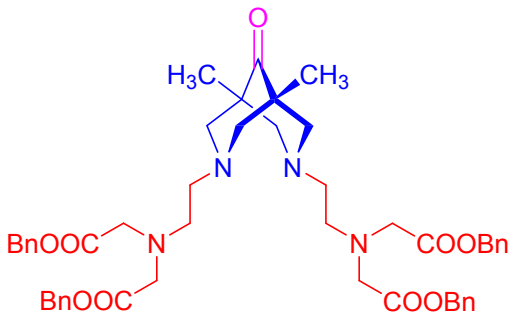

(Tetrabenzyl 2,2',2'',2'''-(((-1,5-dimethyl-9-oxo-3,7-diazabicyclo[3.3.1]nonane-3,7-diyl)bis(ethane-2,1-diyl))bis(azanetriyl))tetraacetate) (SI-6)

White sticky foam. Yield 55%. Purified with gradient column chromatography on silica eluting from DCM:MeOH 40:1 to DCM:MeOH 20:1 and to DCM:MeOH:25% NH3·H2O 1:1:0.01. RCH2X – SI-1, base – DIPEA, reflux time 18 h.

^{1}H NMR (300 MHz, $CDCl_3$, δ /ppm) 1.05 (s, 6 H), 3.01 (br. s., 12 H), 3.62 (s, 8 H), 3.92 (d, *J*=11.37 Hz, 4 H), 5.09 (s, 8 H), 7.11 - 7.58 (m, 21 H), 11.21 - 11.71 (m, 1 H). ^{13}C NMR (100 MHz, $CDCl_3$, δ /ppm) 16.15, 45.95, 50.72, 53.48, 56.00, 63.90, 66.67, 128.20, 128.57, 135.24, 171.21, 208.28.

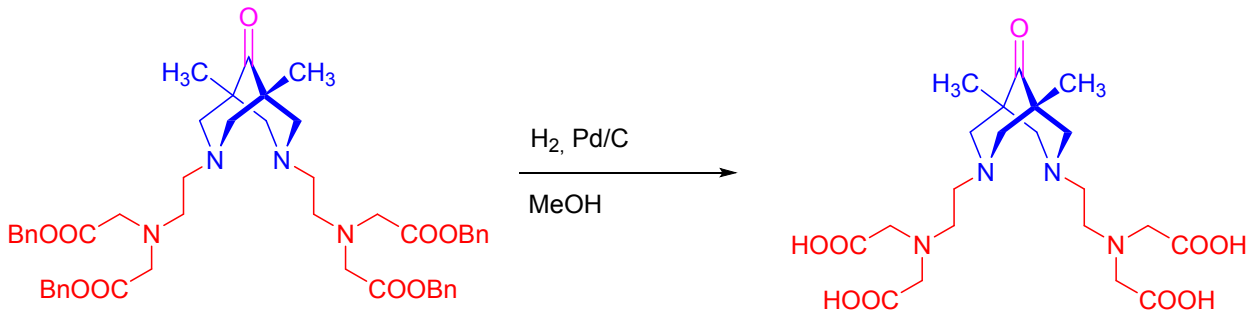

Scheme S6. Preparation of 2,2',2'',2'''-(((1,5-Dimethyl-9-oxo-3,7-diazabicyclo[3.3.1]nonane-3,7-diyl)bis(ethane-2,1-diyl))bis(azanetriyl))tetraacetic acid.

(2,2',2'',2'''-(((1,5-Dimethyl-9-oxo-3,7-diazabicyclo[3.3.1]nonane-3,7-diyl)bis(ethane-2,1-diyl))bis(azanetriyl))tetraacetic acid) (**4n**) Palladium (10% on carbon) (0.5 mmol) was suspended in methanol (5 ml) and the solution of **SI-2** (1 mmol) was added all at once. The flask was filled with hydrogen and the reaction mixture was vigorously stirred for 48 h at room temperature. The catalyst was filtered off the Celite and filtrate was evaporated to dryness.

White powder. Contains two molecules of methanol per target product. Yield 0.318 g (99%).

Purity 98% (HPLC).

^{1}H NMR (300 MHz, D_2O, δ /ppm, mixture of *gem*-diol and ketone[34]) 0.84 - 1.09 (m, 6 H), 2.85 (d, *J*=11.55 Hz, 4 H), 3.00 - 3.27 (m, 6 H), 3.62 (br. s., 5 H), 4.03 (d, *J*=4.22 Hz, 7 H). ^{13}C NMR (75 MHz, D_2O, δ /ppm, mixture of *gem*-diol and ketone) 14.65, 15.39, 39.84, 45.81, 51.96, 52.13, 52.27, 52.54, 56.50, 56.57, 60.32, 64.05, 93.61, 170.15, 170.42, 211.74. HRMS-ESI: Calc for [$C_{21}H_{34}N_4O_9$+H^+]: 487.2404. Found: 487.2413

^{1}H NMR spectra of compound **4n** (D_2O, 300 MHz):

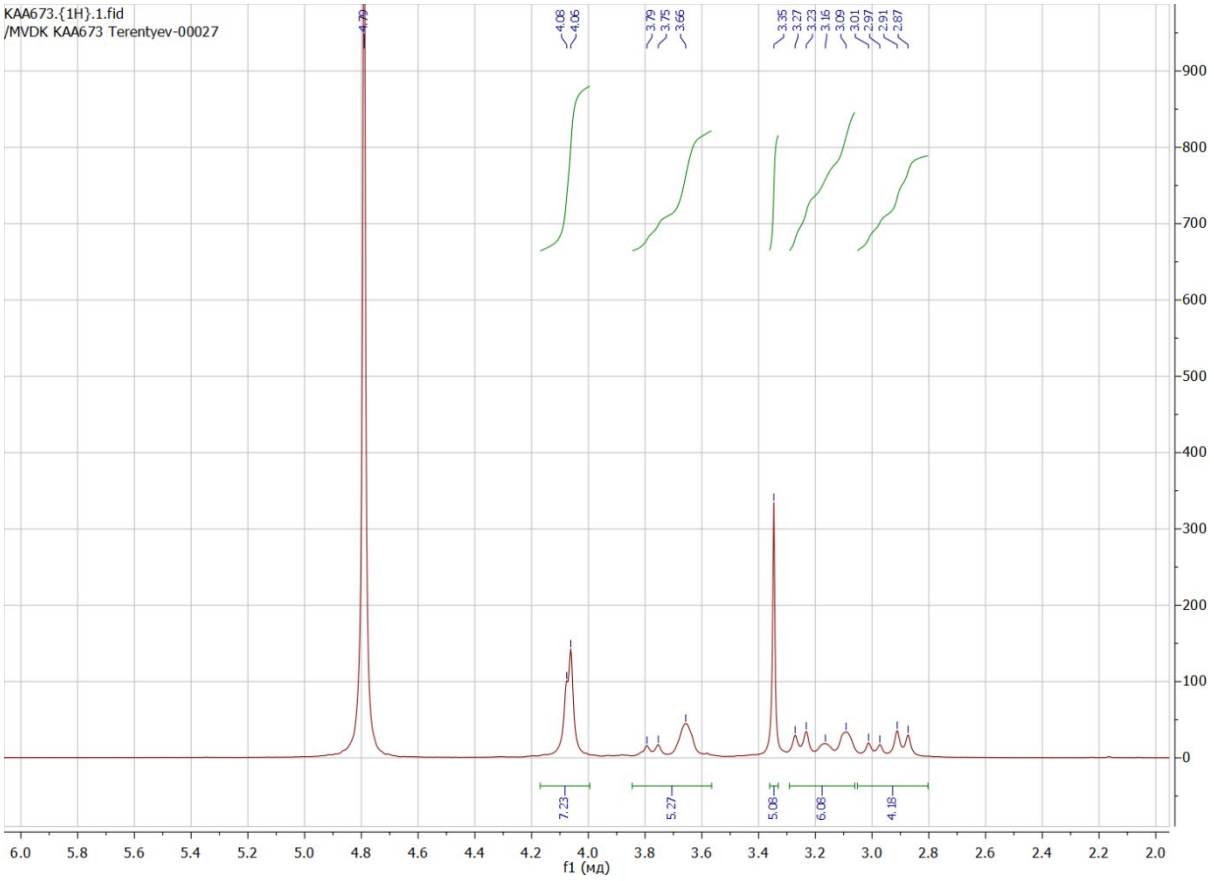

^{13}C NMR spectra of compound **4n** (D_2O, 75 MHz):

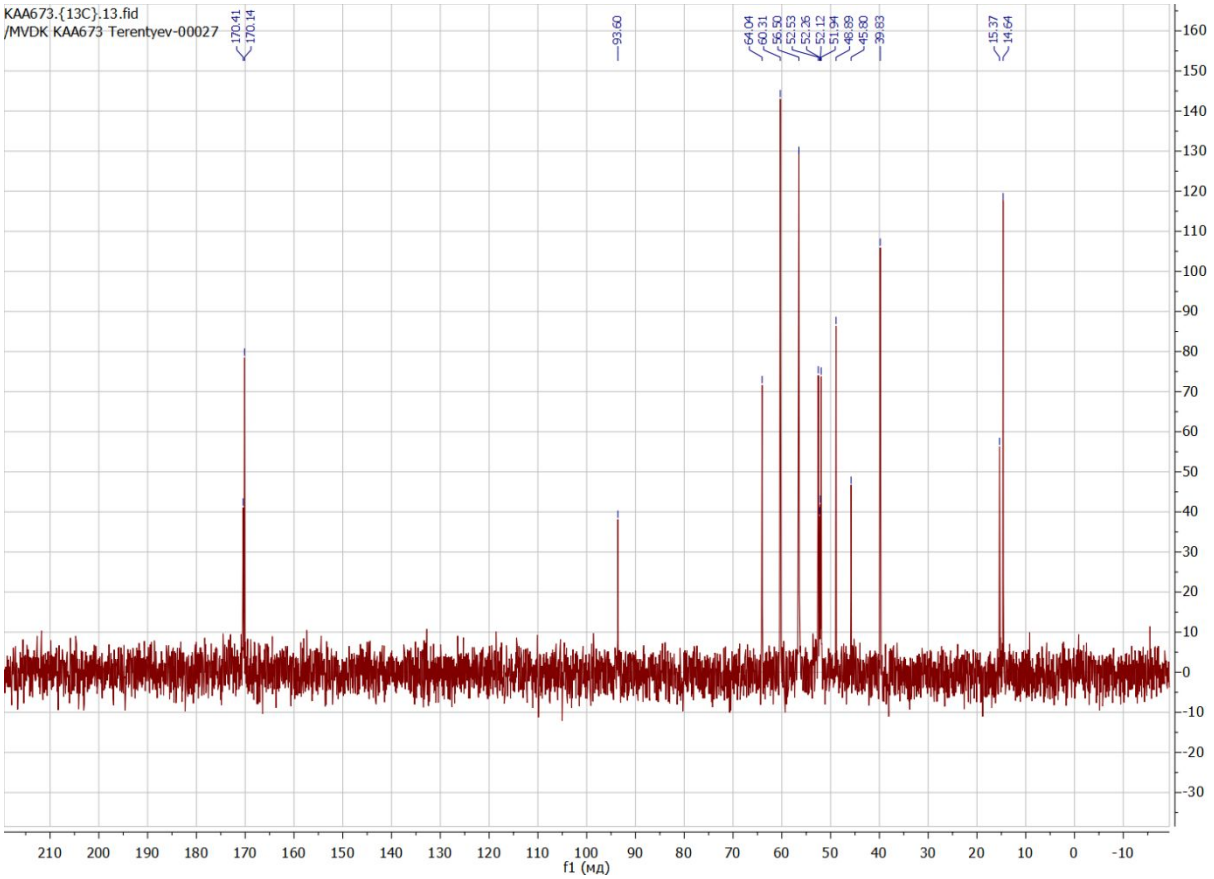

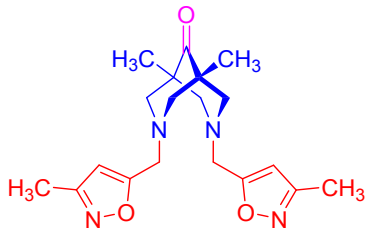

(1,5-Dimethyl-3,7-bis((3-methylisoxazol-5-yl)methyl)-3,7-diazabicyclo[3.3.1]nonan-9-one) (4o). 5-(Chloromethyl)-3-methylisoxazole (0.79 g, 6 mmol) and triethylamine (1 ml, 7 mmol) were added to a solution of 1,5-dimethyl-3,7-diazabicyclo[3.3.1]nonan-9-one (0.5 g, 3 mmol) in dry acetonitrile (20 ml). The mixture was refluxed for 3 h and then was poured into 100 ml of cold water with stirring. The white precipitate was filtered off and additionally washed with water. The product was dried in vacuo over P_2O_5.

White solid. Yield 0.874 g (81%). M.p. 115-116°C. Purity 99% (HPLC).

^{1}H NMR (400 MHz, $CDCl_3$, δ /ppm) 0.98 (s, 6 H), 2.31 (s, 6 H), 2.48 (d, *J* = 10.9 Hz, 4 H), 3.08 (d, *J* = 11.0 Hz, 4 H), 3.69 (s, 4 H), 5.99 (s, 2 H). ^{13}C NMR (101 MHz, $CDCl_3$, δ /ppm) 11.49, 19.83, 46.71, 51.96, 65.05, 103.81, 159.84, 169.12, 214.24. HRMS-ESI. Calc for [$C_{19}H_{26}N_4O_3$+H^+]: 359.2078. Found: 359.2085

^{1}H NMR spectra of compound **4o** ($CDCl_3$, 400 MHz):

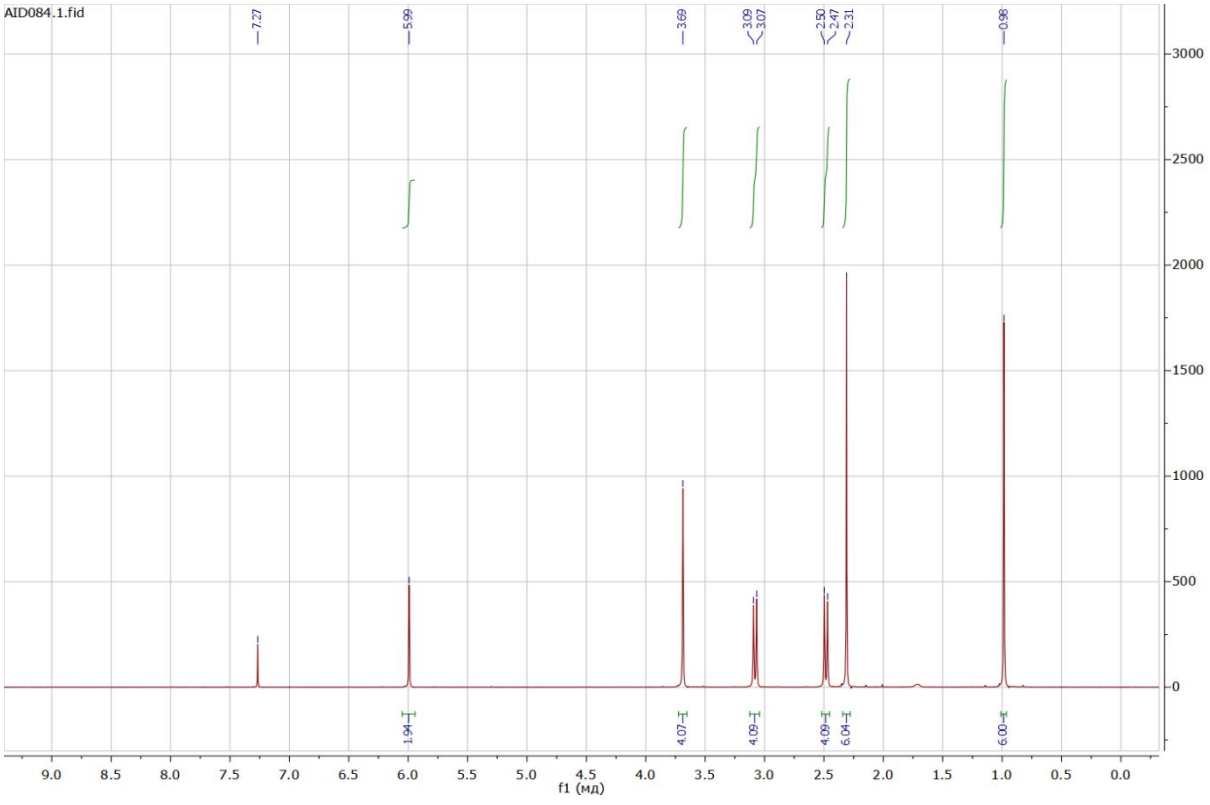

^{13}C NMR spectra of compound **4o** ($CDCl_3$, 101 MHz):

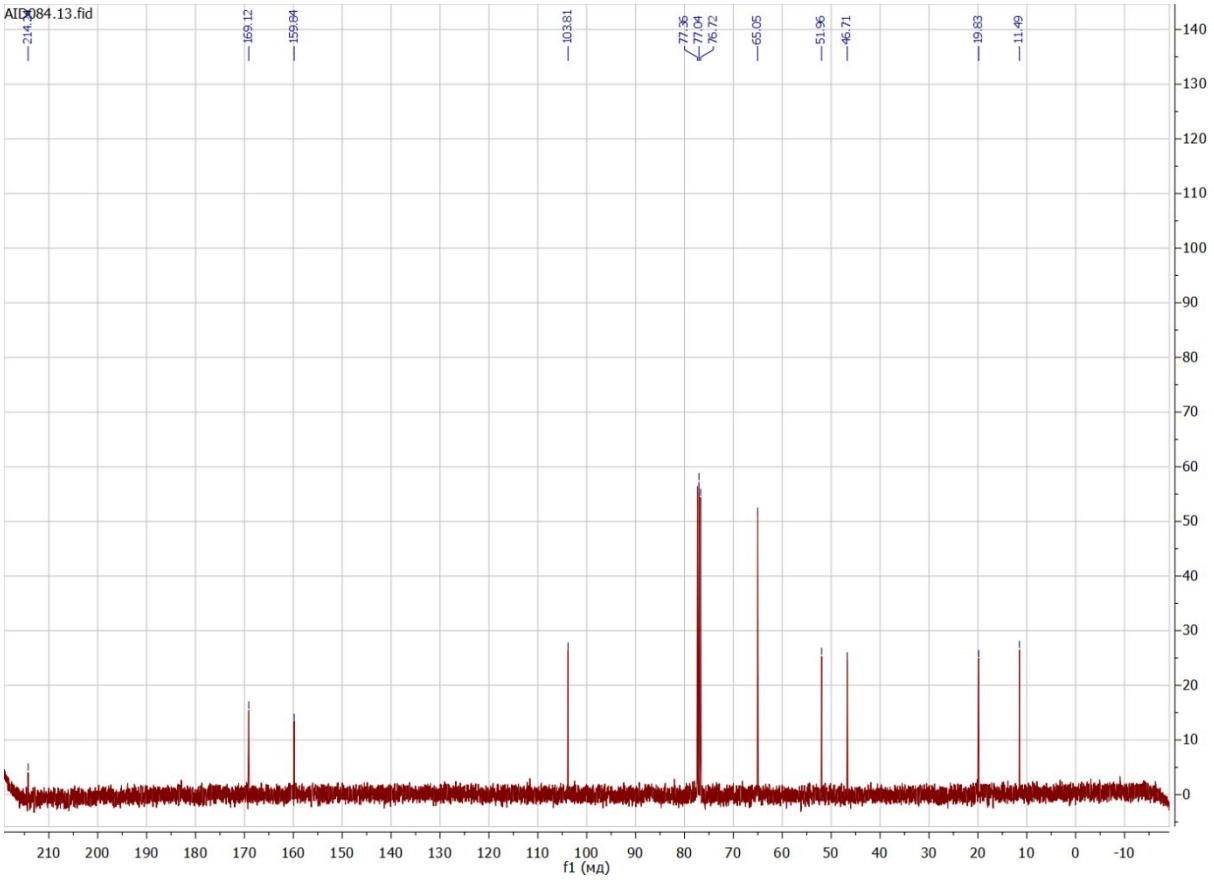

[3+2]-Cycloaddition reaction

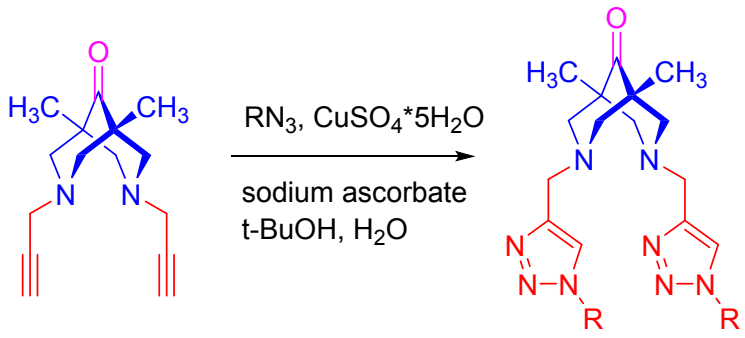

Scheme S7. General procedure for [3+2]-cycloaddition.

General procedure for [3+2]-cycloaddition. To a solution of 1,5-dimethyl-3,7-di(prop-2-yn-1-yl)-3,7-diazabicyclo[3.3.1]nonan-9-one (**4c**) (1 mmol) and respective azide (2 mmol) in 10 ml of tert-butanol the solutions of sodium ascorbate (0.2 mmol) in 2.5 ml of water and $CuSO_4 \cdot 5H_2O$ (0.1 mmol) in 2.5 ml of water were added sequentially. The reaction mixture was stirred for 36 h at room temperature under argon. The solution was evaporated to dryness and quenched with 30 ml of DCM and 10 ml of water. The organic

layer was separated and washed with water until discoloration of water layer. The organic phase was dried with sodium sulfate and evaporated to dryness.

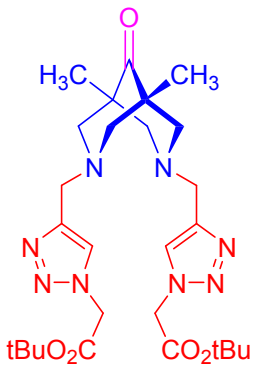

(Di-tert-butyl 2,2'-(((-1,5-dimethyl-9-oxo-3,7-diazabicyclo[3.3.1]nonane-3,7-diyl)bis(methylene))bis(1H-1,2,3-triazole-4,1-diyl))diacetate) (4p)

White foam. Yield 80%. M.p. 57-59°C. Purity 98% (HPLC).

^{1}H-NMR (400 MHz, $CDCl_3$, δ /ppm) 0.93 (s, 6 H) 1.48 (s, 18 H), 2.42 (d, 4 H, *J*=10.8 Hz), 3.05 (d, 4 H, *J*=10.8 Hz), 3.69 (s, 4 H), 5.08 (s, 4 H), 7.66 (s, 2 H). ^{13}C-NMR (100 MHz, $CDCl_3$, δ, ppm) 19.68, 27.91, 46.57, 51.43, 51.83, 65.10, 83.55, 124.24, 145.09, 165.37, 215.21. HRMS-ESI. Calc for [$C_{27}H_{42}N_8O_5$+H^+]: 559.3351. Found: 559.3356

^{1}H NMR spectra of compound **4p** ($CDCl_3$, 400 MHz):

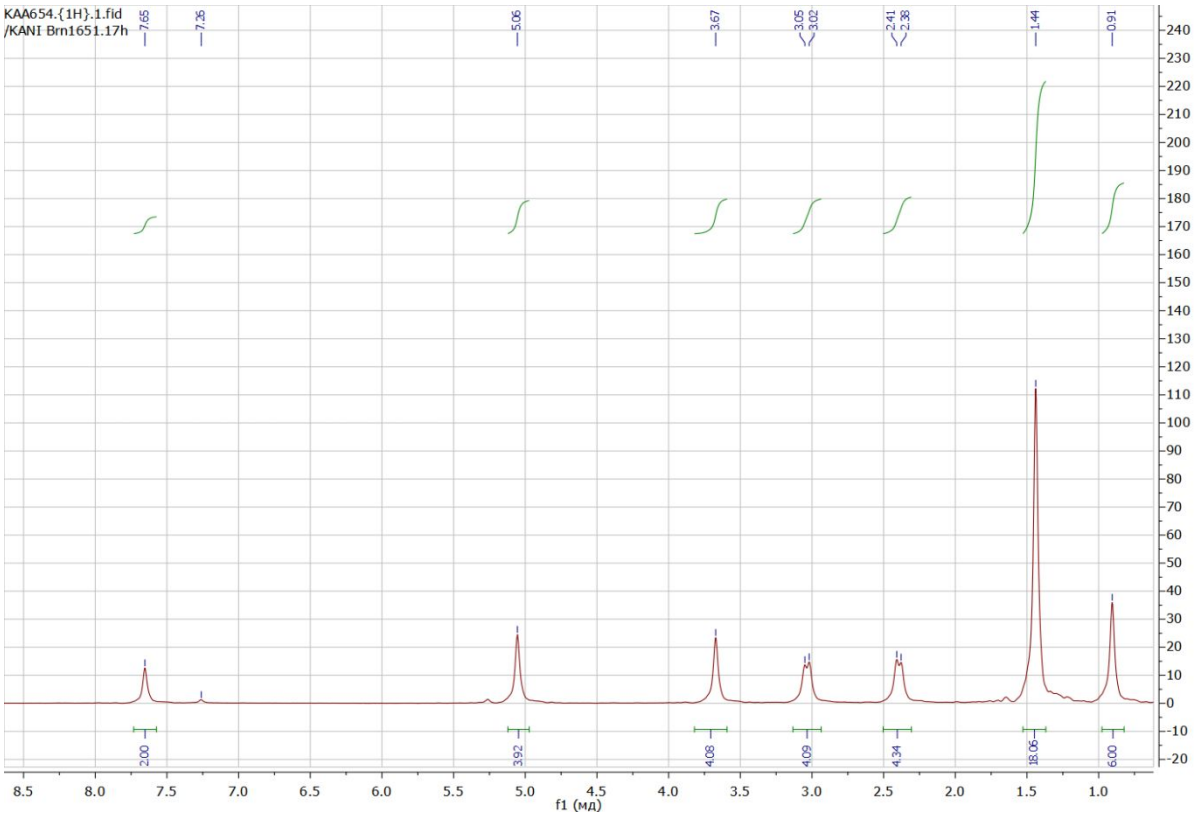

^{13}C NMR spectra of compound **4p** ($CDCl_3$, 100 MHz):

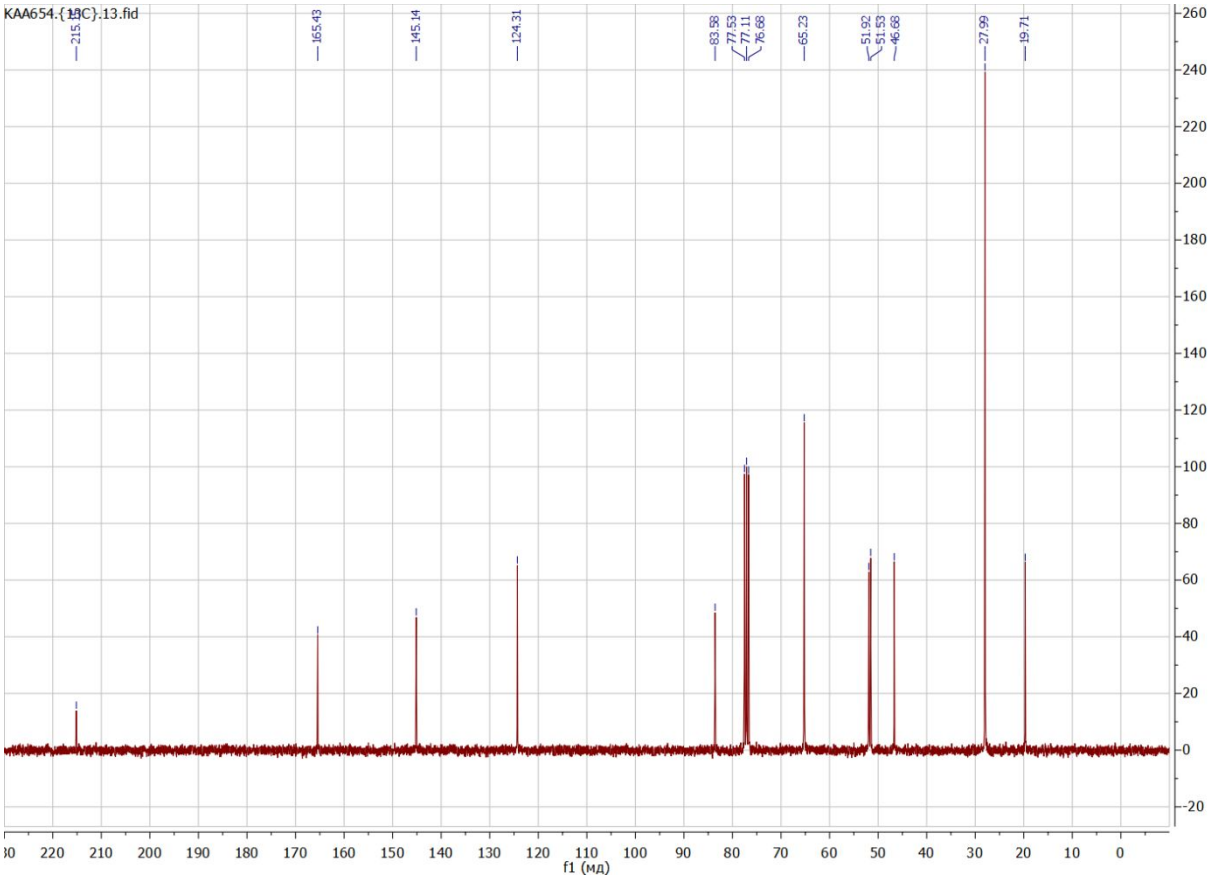

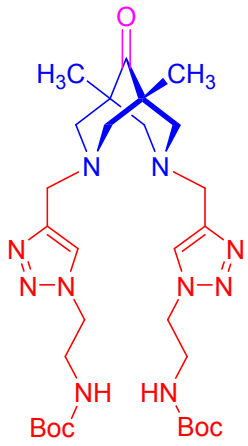

Di-tert-butyl ((((1,5-dimethyl-9-oxo-3,7-diazabicyclo[3.3.1]nonane-3,7-diyl)bis(methylene))bis(1H-1,2,3-triazole-4,1-diyl))bis(ethane-2,1-diyl))dicarbamate) (4q)

White foam. Yield 56%. M.p. 70-72°C Purified with gradient column chromatography eluting from DCM:MeOH 10:1 to DCM:MeOH 3:1 and to DCM:MeOH:25% $NH_3{\cdot}H_2O$ 1:1:0.01. Purity 95% (HPLC).

^{1}H NMR (300 MHz, $CDCl_3$, δ /ppm)0.89 (br. s., 6 H) 1.35 (br. s., 18 H) 2.38 (br. s., 4 H) 3.02 (br. s., 4 H) 3.62 (br. s., 8 H) 4.47 (br. s., 4 H) 5.42 (br. s., 2 H) 7.59 (br. s., 2 H). ^{13}C-NMR (75

MHz, $CDCl_3$, δ /ppm) 19.42, 28.21, 40.49, 46.53, 49.65, 51.59, 65.01, 79.54, 123.53, 144.29, 155.84, 214.90. HRMS-ESI. Calc for [$C_{29}H_{48}N_{10}O_5$+H^+]: 617.3887. Found: 617.3887.

^{1}H NMR spectra of compound **4q** ($CDCl_3$, 300 MHz):

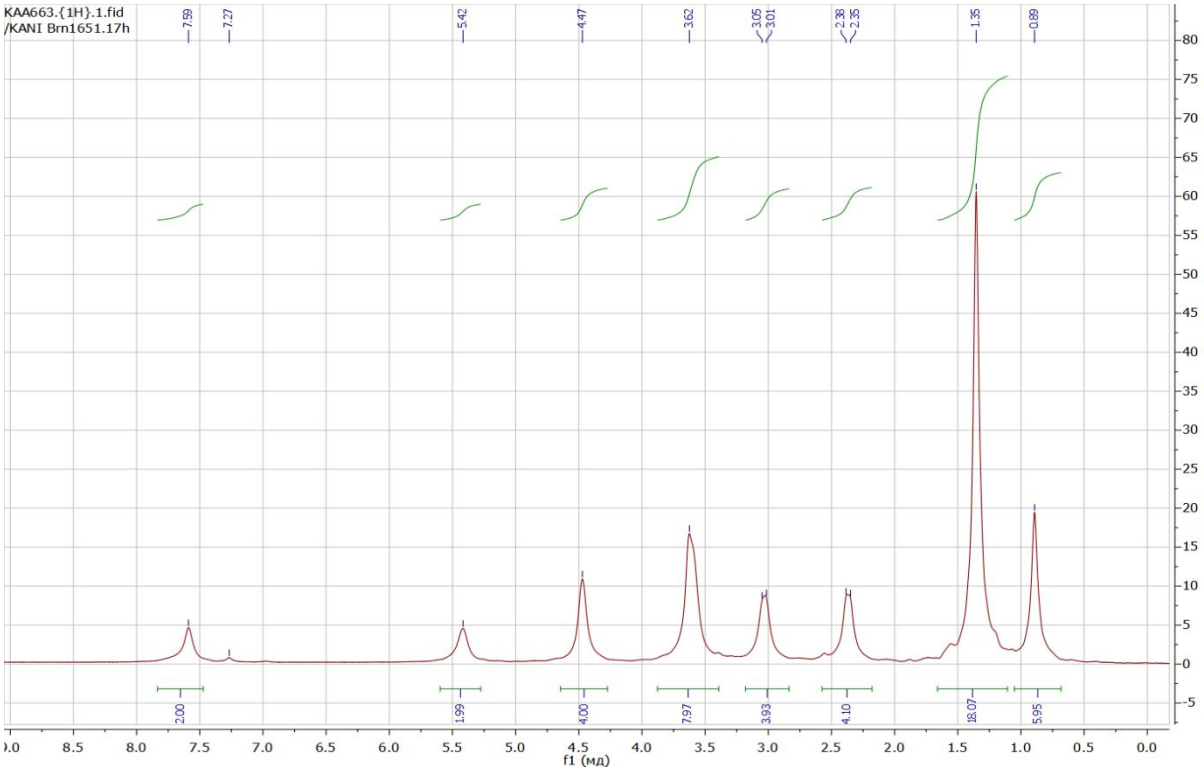

^{13}C NMR spectra of compound **4q** ($CDCl_3$, 75 MHz):

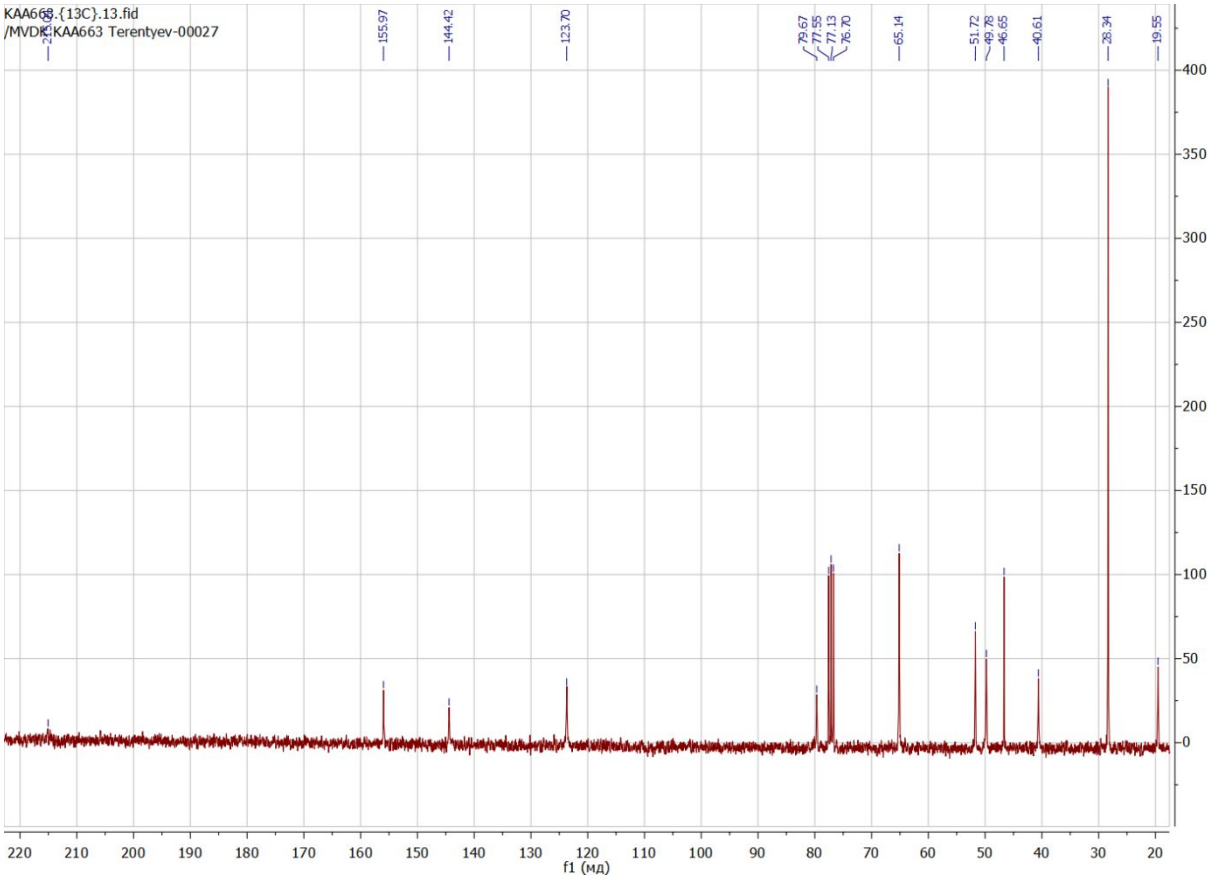

References

(1) Ma, C.; Hu, Y.; Townsend, J. A.; Lagarias, P. I.; Marty, M. T.; Kolocouris, A.; Wang, J. Ebselen, Disulfiram, Carmofur, PX-12, Tideglusib, and Shikonin Are Nonspecific Promiscuous SARS-CoV-2 Main Protease Inhibitors. *ACS Pharmacol. Transl. Sci.* **2020**, *3* (6), 1265–1277. https://doi.org/10.1021/acsptsci.0c00130.

(2) *Schrodinger Small Molecule Drug Discovery Suite*; Schrödinger, LLC: New York, 2016.

(3) Harder, E.; Damm, W.; Maple, J.; Wu, C.; Reboul, M.; Xiang, J. Y.; Wang, L.; Lupyan, D.; Dahlgren, M. K.; Knight, J. L.; Kaus, J. W.; Cerutti, D. S.; Krilov, G.; Jorgensen, W. L.; Abel, R.; Friesner, R. A. OPLS3: A Force Field Providing Broad Coverage of Drug-like Small Molecules and Proteins. *J. Chem. Theory Comput.* **2016**, *12* (1), 281–296. https://doi.org/10.1021/acs.jctc.5b00864.

(4) Dixon, S. L.; Smondyrev, A. M.; Knoll, E. H.; Rao, S. N.; Shaw, D. E.; Friesner, R. A. PHASE: A New Engine for Pharmacophore Perception, 3D QSAR Model Development, and 3D Database Screening: 1. Methodology and Preliminary Results. *J. Comput. Aided. Mol. Des.* **2006**, *20* (10–11), 647–671. https://doi.org/10.1007/s10822-006-9087-6.

(5) Lockbaum, G. J.; Reyes, A. C.; Lee, J. M.; Tilvawala, R.; Nalivaika, E. A.; Ali, A.; Kurt Yilmaz, N.; Thompson, P. R.; Schiffer, C. A. Crystal Structure of SARS-CoV-2 Main Protease in Complex with the Non-Covalent Inhibitor ML188. *Viruses* **2021**, *13* (2), 174. https://doi.org/10.3390/v13020174.

(6) Friesner, R. A.; Murphy, R. B.; Repasky, M. P.; Frye, L. L.; Greenwood, J. R.; Halgren, T. A.; Sanschagrin, P. C.; Mainz, D. T. Extra Precision Glide: Docking and Scoring Incorporating a Model of Hydrophobic Enclosure for Protein−Ligand Complexes. *J. Med. Chem.* **2006**, *49* (21), 6177–6196. https://doi.org/10.1021/jm051256o.

(7) BIOVIA, D. S.; Berman, H. M.; Westbrook, J.; Feng, Z.; Gilliland, G.; Bhat, T. N.; Weissig, H.; Shindyalov, I. N.; Bourne, P. E.; Darden, T.; York, D.; Pedersen, L. G.; Bussi, G.; Donadio, D.; Parrinello, M.; Essmann, U.; Perera, L.; Berkowitz, M. L.; Darden, T.; Lee, H.; Pedersen, L. G.; Parrinello, M.; Rahman, A.; Hornak, V.; Abel, R.; Okur, A.; Strockbine, B.; Roitberg, A.; Simmerling, C.; Abraham, M. J.; Murtola, T.; Schulz, R.; Páll, S.; Smith, J. C.; Hess, B.; Lindah, E.; Berendsen, H. J. C.; Postma, J. P. M.; Van

Gunsteren, W. F.; Dinola, A.; Haak, J. R.; Hockney, R. W.; Goel, S. P.; Eastwood, J. W.; Davey, C. A.; Sargent, D. F.; Luger, K.; Maeder, A. W.; Richmond, T. J. Dassault Systèmes BIOVIA, Discovery Studio Visualizer, v.17.2, San Diego: Dassault Systèmes, 2016. . *J. Chem. Phys.* **2000**. https://doi.org/10.1016/0021-9991(74)90010-2.

(8) Zhu, K.; Borrelli, K. W.; Greenwood, J. R.; Day, T.; Abel, R.; Farid, R. S.; Harder, E. Docking Covalent Inhibitors: A Parameter Free Approach to Pose Prediction and Scoring. *J. Chem. Inf. Model.* **2014**, *54* (7), 1932–1940. https://doi.org/10.1021/ci500118s.

(9) Vuong, W.; Khan, M. B.; Fischer, C.; Arutyunova, E.; Lamer, T.; Shields, J.; Saffran, H. A.; McKay, R. T.; van Belkum, M. J.; Joyce, M. A.; Young, H. S.; Tyrrell, D. L.; Vederas, J. C.; Lemieux, M. J. Feline Coronavirus Drug Inhibits the Main Protease of SARS-CoV-2 and Blocks Virus Replication. *Nat. Commun.* **2020**, *11* (1), 1–8. https://doi.org/10.1038/s41467-020-18096-2.

(10) Genheden, S.; Ryde, U. The MM/PBSA and MM/GBSA Methods to Estimate Ligand-Binding Affinities. *Expert Opinion on Drug Discovery*. Informa Healthcare May 2015, pp 449–461. https://doi.org/10.1517/17460441.2015.1032936.

(11) Dai, W.; Zhang, B.; Jiang, X. M.; Su, H.; Li, J.; Zhao, Y.; Xie, X.; Jin, Z.; Peng, J.; Liu, F.; Li, C.; Li, Y.; Bai, F.; Wang, H.; Cheng, X.; Cen, X.; Hu, S.; Yang, X.; Wang, J.; Liu, X.; Xiao, G.; Jiang, H.; Rao, Z.; Zhang, L. K.; Xu, Y.; Yang, H.; Liu, H. Structure-Based Design of Antiviral Drug Candidates Targeting the SARS-CoV-2 Main Protease. *Science (80-.).* **2020**, *368* (6497), 1331–1335. https://doi.org/10.1126/science.abb4489.

(12) wwPDB: 6WNP.

(13) Hoffman, R. L.; Kania, R. S.; Brothers, M. A.; Davies, J. F.; Ferre, R. A.; Gajiwala, K. S.; He, M.; Hogan, R. J.; Kozminski, K.; Li, L. Y.; Lockner, J. W.; Lou, J.; Marra, M. T.; Mitchell, L. J.; Murray, B. W.; Nieman, J. A.; Noell, S.; Planken, S. P.; Rowe, T.; Ryan, K.; Smith, G. J.; Solowiej, J. E.; Steppan, C. M.; Taggart, B. Discovery of Ketone-Based Covalent Inhibitors of Coronavirus 3CL Proteases for the Potential Therapeutic Treatment of COVID-19. *J. Med. Chem.* **2020**, *63* (21), 12725–12747. https://doi.org/10.1021/acs.jmedchem.0c01063.

(14) Rathnayake, A. D.; Zheng, J.; Kim, Y.; Perera, K. D.; Mackin, S.; Meyerholz, D. K.; Kashipathy, M. M.; Battaile, K. P.; Lovell, S.; Perlman, S.; Groutas, W. C.; Chang, K. O.

3C-like Protease Inhibitors Block Coronavirus Replication in Vitro and Improve Survival in MERS-CoV–Infected Mice. *Sci. Transl. Med.* **2020**, *12* (557). https://doi.org/10.1126/SCITRANSLMED.ABC5332.

(15) Kneller, D. W.; Galanie, S.; Phillips, G.; O'Neill, H. M.; Coates, L.; Kovalevsky, A. Malleability of the SARS-CoV-2 3CL Mpro Active-Site Cavity Facilitates Binding of Clinical Antivirals. *Structure* **2020**, *28* (12), 1313-1320.e3. https://doi.org/10.1016/j.str.2020.10.007.

(16) Zhang, L.; Lin, D.; Sun, X.; Curth, U.; Drosten, C.; Sauerhering, L.; Becker, S.; Rox, K.; Hilgenfeld, R. Crystal Structure of SARS-CoV-2 Main Protease Provides a Basis for Design of Improved α-Ketoamide Inhibitors. *Science* **2020**, *368* (6489), 409–412. https://doi.org/10.1126/science.abb3405.

(17) wwPDB: 7B3E.

(18) wwPDB: 7BE7.

(19) Jin, Z.; Du, X.; Xu, Y.; Deng, Y.; Liu, M.; Zhao, Y.; Zhang, B.; Li, X.; Zhang, L.; Peng, C.; Duan, Y.; Yu, J.; Wang, L.; Yang, K.; Liu, F.; Jiang, R.; Yang, X.; You, T.; Liu, X.; Yang, X.; Bai, F.; Liu, H.; Liu, X.; Guddat, L. W.; Xu, W.; Xiao, G.; Qin, C.; Shi, Z.; Jiang, H.; Rao, Z.; Yang, H. Structure of Mpro from SARS-CoV-2 and Discovery of Its Inhibitors. *Nature* **2020**, *582* (7811), 289–293. https://doi.org/10.1038/s41586-020-2223-y.

(20) Qiao, J.; Li, Y.-S.; Zeng, R.; Liu, F.-L.; Luo, R.-H.; Huang, C.; Wang, Y.-F.; Zhang, J.; Quan, B.; Shen, C.; Mao, X.; Liu, X.; Sun, W.; Yang, W.; Ni, X.; Wang, K.; Xu, L.; Duan, Z.-L.; Zou, Q.-C.; Zhang, H.-L.; Qu, W.; Long, Y.-H.-P.; Li, M.-H.; Yang, R.-C.; Liu, X.; You, J.; Zhou, Y.; Yao, R.; Li, W.-P.; Liu, J.-M.; Chen, P.; Liu, Y.; Lin, G.-F.; Yang, X.; Zou, J.; Li, L.; Hu, Y.; Lu, G.-W.; Li, W.-M.; Wei, Y.-Q.; Zheng, Y.-T.; Lei, J.; Yang, S. SARS-CoV-2 M pro Inhibitors with Antiviral Activity in a Transgenic Mouse Model . *Science (80-.).* **2021**, *371* (6536), 1374–1378. https://doi.org/10.1126/science.abf1611.

(21) Yang, K. S.; Ma, X. R.; Ma, Y.; Alugubelli, Y. R.; Scott, D. A.; Vatansever, E. C.; Drelich, A. K.; Sankaran, B.; Geng, Z. Z.; Blankenship, L. R.; Ward, H. E.; Sheng, Y. J.; Hsu, J. C.; Kratch, K. C.; Zhao, B.; Hayatshahi, H. S.; Liu, J.; Li, P.; Fierke, C. A.; Tseng, C. K.; Xu, S.; Liu, W. R. A Quick Route to Multiple Highly Potent SARS-CoV-2 Main Protease Inhibitors**. *ChemMedChem* **2021**, *16* (6), 942–948. https://doi.org/10.1002/cmdc.202000924.

(22) Günther, S.; Reinke, P. Y. A.; Fernández-García, Y.; Lieske, J.; Lane, T. J.; Ginn, H. M.; Koua, F. H. M.; Ehrt, C.; Ewert, W.; Oberthuer, D.; Yefanov, O.; Meier, S.; Lorenzen, K.; Krichel, B.; Kopicki, J.-D.; Gelisio, L.; Brehm, W.; Dunkel, I.; Seychell, B.; Gieseler, H.; Norton-Baker, B.; Escudero-Pérez, B.; Domaracky, M.; Saouane, S.; Tolstikova, A.; White, T. A.; Hänle, A.; Groessler, M.; Fleckenstein, H.; Trost, F.; Galchenkova, M.; Gevorkov, Y.; Li, C.; Awel, S.; Peck, A.; Barthelmess, M.; Schluenzen, F.; Lourdu Xavier, P.; Werner, N.; Andaleeb, H.; Ullah, N.; Falke, S.; Srinivasan, V.; França, B. A.; Schwinzer, M.; Brognaro, H.; Rogers, C.; Melo, D.; Zaitseva-Doyle, J. J.; Knoska, J.; Peña-Murillo, G. E.; Mashhour, A. R.; Hennicke, V.; Fischer, P.; Hakanpää, J.; Meyer, J.; Gribbon, P.; Ellinger, B.; Kuzikov, M.; Wolf, M.; Beccari, A. R.; Bourenkov, G.; von Stetten, D.; Pompidor, G.; Bento, I.; Panneerselvam, S.; Karpics, I.; Schneider, T. R.; Garcia-Alai, M. M.; Niebling, S.; Günther, C.; Schmidt, C.; Schubert, R.; Han, H.; Boger, J.; Monteiro, D. C. F.; Zhang, L.; Sun, X.; Pletzer-Zelgert, J.; Wollenhaupt, J.; Feiler, C. G.; Weiss, M. S.; Schulz, E.-C.; Mehrabi, P.; Karničar, K.; Usenik, A.; Loboda, J.; Tidow, H.; Chari, A.; Hilgenfeld, R.; Uetrecht, C.; Cox, R.; Zaliani, A.; Beck, T.; Rarey, M.; Günther, S.; Turk, D.; Hinrichs, W.; Chapman, H. N.; Pearson, A. R.; Betzel, C.; Meents, A. X-Ray Screening Identifies Active Site and Allosteric Inhibitors of SARS-CoV-2 Main Protease. *Science (80-.).* **2021**, *372* (6542), eabf7945. https://doi.org/10.1126/science.abf7945.

(23) wwPDB: 7JU7.

(24) wwPDB: 7LTJ.

(25) Zhang, C. H.; Stone, E. A.; Deshmukh, M.; Ippolito, J. A.; Ghahremanpour, M. M.; Tirado-Rives, J.; Spasov, K. A.; Zhang, S.; Takeo, Y.; Kudalkar, S. N.; Liang, Z.; Isaacs, F.; Lindenbach, B.; Miller, S. J.; Anderson, K. S.; Jorgensen, W. L. Potent Noncovalent Inhibitors of the Main Protease of SARS-CoV-2 from Molecular Sculpting of the Drug Perampanel Guided by Free Energy Perturbation Calculations. *ACS Cent. Sci.* **2021**. https://doi.org/10.1021/acscentsci.1c00039.

(26) Dai, W.; Zhang, B.; Su, H.; Li, J.; Zhao, Y.; Xie, X.; Jin, Z.; Liu, F.; Li, C.; Li, Y.; Bai, F.; Wang, H.; Cheng, X.; Cen, X.; Hu, S.; Yang, X.; Wang, J.; Liu, X.; Xiao, G.; Jiang, H.; Rao, Z.; Zhang, L.-K.; Xu, Y.; Yang, H.; Liu, H. Structure-Based Design of Antiviral Drug Candidates Targeting the SARS-CoV-2 Main Protease. *Science (80-.).* **2020**, eabb4489. https://doi.org/10.1126/science.abb4489.

(27) Jin, Z.; Du, X.; Xu, Y.; Deng, Y.; Liu, M.; Zhao, Y.; Zhang, B.; Li, X.; Zhang, L.; Peng, C.; Duan, Y.; Yu, J.; Wang, L.; Yang, K.; Liu, F.; Jiang, R.; Yang, X.; You, T.; Liu, X.; Yang, X.; Bai, F.; Liu, H.; Liu, X.; Guddat, L. W.; Xu, W.; Xiao, G.; Qin, C.; Shi, Z.; Jiang, H.; Rao, Z.; Yang, H. Structure of Mpro from COVID-19 Virus and Discovery of Its Inhibitors. *Nature* **2020**, 1–9. https://doi.org/10.1038/s41586-020-2223-y.

(28) Jin, Z.; Zhao, Y.; Sun, Y.; Zhang, B.; Wang, H.; Wu, Y.; Zhu, Y.; Zhu, C.; Hu, T.; Du, X.; Duan, Y.; Yu, J.; Yang, X.; Yang, X.; Yang, K.; Liu, X.; Guddat, L. W.; Xiao, G.; Zhang, L.; Yang, H.; Rao, Z. Structural Basis for the Inhibition of SARS-CoV-2 Main Protease by Antineoplastic Drug Carmofur. *Nat. Struct. Mol. Biol.* **2020**, *27* (6), 529–532. https://doi.org/10.1038/s41594-020-0440-6.

(29) Pires, D. E. V.; Blundell, T. L.; Ascher, D. B. PkCSM: Predicting Small-Molecule Pharmacokinetic and Toxicity Properties Using Graph-Based Signatures. *J. Med. Chem.* **2015**, *58* (9), 4066–4072. https://doi.org/10.1021/acs.jmedchem.5b00104.

(30) Daina, A.; Michielin, O.; Zoete, V. SwissADME: A Free Web Tool to Evaluate Pharmacokinetics, Drug-Likeness and Medicinal Chemistry Friendliness of Small Molecules. *Sci. Rep.* **2017**, *7* (1), 1–13. https://doi.org/10.1038/srep42717.

(31) Lipinski, C. A.; Lombardo, F.; Dominy, B. W.; Feeney, P. J. Experimental and Computational Approaches to Estimate Solubility and Permeability in Drug Discovery and Development Settings. *Advanced Drug Delivery Reviews*. December 2012, pp 4–17. https://doi.org/10.1016/j.addr.2012.09.019.

(32) Ghose, A. K.; Viswanadhan, V. N.; Wendoloski, J. J. A Knowledge-Based Approach in Designing Combinatorial or Medicinal Chemistry Libraries for Drug Discovery. 1. A Qualitative and Quantitative Characterization of Known Drug Databases. *J. Comb. Chem.* **1999**, *1* (1), 55–68. https://doi.org/10.1021/cc9800071.

(33) Potts, R. O.; Guy, R. H. Predicting Skin Permeability. *Pharm. Res. An Off. J. Am. Assoc. Pharm. Sci.* **1992**, *9* (5), 663–669. https://doi.org/10.1023/A:1015810312465.

(34) Medved'ko, A.; Egorova, B.; Komarova, A.; Rakhimov, R.; Krut'ko, D.; Kalmykov, S.; Vatsadze, S. Copper–Bispidine Complexes: Synthesis and Complex Stability Study. *ACS Omega 1* (5), 854–867. https://doi.org/10.1021/acsomega.6b00237.

(35) Vatsadze, S. Z.; Semashko, V. S.; Manaenkova, M. A.; Krut'Ko, D. P.; Nuriev, V. N.;

Rakhimov, R. D.; Davlyatshin, D. I.; Churakov, A. V.; Howard, J. A. K.; Maksimov, A. L.; Li, W.; Yu, H. New Supramolecular Synthons Based on 3d Transition Metal Complexes with Bidentate Bispidines: Synthesis and Structural, Spectroscopic, and Electrochemical Studies. *Russ. Chem. Bull.* **2014**, *63* (4), 895–911. https://doi.org/10.1007/s11172-014-0526-6.

(36) Vatsadze, S. Z.; Medved'ko, A. V.; Bodunov, A. A.; Lyssenko, K. A. Bispidine-Based Bis-Azoles as a New Family of Supramolecular Receptors: The Theoretical Approach. *Mendeleev Commun.* **2020**, *30* (3), 344–346. https://doi.org/10.1016/j.mencom.2020.05.028.

(37) Dalinger, A. I.; Medved'ko, A. V.; Balalaeva, A. I.; Vatsadze, I. A.; Dalinger, I. L.; Vatsadze, S. Z. Synthesis of Novel Azides and Triazoles on the Basis of 1H-Pyrazole-3(5)-Carboxylic Acids. *Chem. Heterocycl. Compd.* **2020**, *56* (2), 180–191. https://doi.org/10.1007/s10593-020-02643-2.

(38) Tensmeyer, L. G.; Ainsworth, C. Proton Magnetic Resonance Studies of Pyrazoles. *J. Org. Chem.* **1966**, *31* (6), 1878–1883. https://doi.org/10.1021/jo01344a047.

(39) Stempel, G. H.; Cross, R. P.; Mariella, R. P. The Preparation of Acrylyl Chloride. *J. Am. Chem. Soc.* **1950**, *72* (5), 2299–2300. https://doi.org/10.1021/ja01161a527.

(40) Li, B.; Yan, W.; Zhang, C.; Zhang, Y.; Liang, M.; Chu, F.; Gong, Y.; Xu, B.; Wang, P.; Lei, H. New Synthesis Method for Sultone Derivatives: Synthesis, Crystal Structure and Biological Evaluation of S-CA. *Molecules* **2015**, *20* (3), 4307–4318. https://doi.org/10.3390/molecules20034307.

(41) Zimmerman, S. S.; Khatri, A.; Garnier-Amblard, E. C.; Mullasseril, P.; Kurtkaya, N. L.; Gyoneva, S.; Hansen, K. B.; Traynelis, S. F.; Liotta, D. C. Design, Synthesis, and Structure–Activity Relationship of a Novel Series of GluN2C-Selective Potentiators. *J. Med. Chem.* **2014**, *57* (6), 2334–2356. https://doi.org/10.1021/jm401695d.

(42) Aghazadeh Tabrizi, M.; Baraldi, P. G.; Baraldi, S.; Ruggiero, E.; De Stefano, L.; Rizzolio, F.; Di Cesare Mannelli, L.; Ghelardini, C.; Chicca, A.; Lapillo, M.; Gertsch, J.; Manera, C.; Macchia, M.; Martinelli, A.; Granchi, C.; Minutolo, F.; Tuccinardi, T. Discovery of 1,5-Diphenylpyrazole-3-Carboxamide Derivatives as Potent, Reversible, and Selective Monoacylglycerol Lipase (MAGL) Inhibitors. *J. Med. Chem.* **2018**, *61* (3), 1340–1354. https://doi.org/10.1021/acs.jmedchem.7b01845.

(43) Pinna, G. A.; Pirisi, M. A.; Mussinu, J.-M.; Murineddu, G.; Loriga, G.; Pau, A.; Grella, G. E. Chromophore-Modified Bis-Benzo[g]Indole Carboxamides: Synthesis and Antiproliferative Activity of Bis-Benzo[g]Indazole-3-Carboxamides and Related Dimers. *Farm.* **2003**, *58* (9), 749–763. https://doi.org/10.1016/S0014-827X(03)00131-9.